

Aus dem Max-Planck-Institut für Kolloid- und Grenzflächenforschung

**Polymer Self-Assembly:
Adding Complexity to Mesostuctures of
Diblock Copolymers by Specific Interactions**

Habilitationsschrift

zur Erlangung des akademischen Grades

doctor rerum naturalium habilitatus

(Dr. rer. nat. habil.)

in der Wissenschaftsdisziplin Physikalische Chemie

eingereicht an der

Mathematisch-Naturwissenschaftlichen Fakultät

der Universität Potsdam

von

Dr. Helmut Schlaad

geboren am 04.08.1967 in Bad Kreuznach

Potsdam, im Dezember 2003

Meiner Familie

ZUSAMMENFASSUNG

In dieser Arbeit wurde die Rolle selektiver, nicht-kovalenter Wechselwirkungen bei der Selbstorganisation von Diblockcopolymeren untersucht. Durch Einführung elektrostatischer, dipolarer Wechselwirkungen oder Wasserstoffbrückenbindungen sollte es gelingen, komplexe Mesostrukturen zu erzeugen und die Ordnung vom Nanometerbereich auf größere Längenskalen auszuweiten. Diese Arbeit ist im Rahmen von Biomimetik zu sehen, da sie Konzepte der synthetischen Polymer- und Kolloidchemie und Grundprinzipien der Strukturbildung in supramolekularen und biologischen Systemen verbindet.

Folgende Copolymersysteme wurden untersucht: (i) Blockionomere, (ii) Blockcopolymere mit chelatisierenden Acetoacetoxyeinheiten und (iii) Polypeptid-Blockcopolymere.

(i) Das Mischen verdünnter Lösungen (Tetrahydrofuran) entgegengesetzt geladener Blockionomere, Polystyrol-*block*-poly(1-methyl-4-vinylpyridiniumiodid) und Poly(1,2-butadien)-*block*-poly(methacrylsäure Cäsiumsalz), führt zur spontanen Bildung polyionischer Komplexe und dann zu Vesikel. Wegen der Unverträglichkeit der solvatisierenden Blocksegmente weisen die Vesikel eine Membran mit mikrophasenseparierter, asymmetrischer Struktur und damit amphiphilen Charakter auf. Die Struktur der Membran kann durch Änderung der Selektivität des Lösungsmittels invertiert werden.

(ii) Wohldefinierte Homopolymere und Blockcopolymere auf der Basis von 2-(Acetoacetoxy)-ethylmethacrylat können sowohl durch kontrollierte radikalische Polymerisation (RAFT) als auch durch Gruppentransferpolymerisation und nachfolgender azeotroper Acetoacetylierung erhalten werden.

Wasserstoffbrückenbindungen zwischen den Acetoacetoxyseitengruppen in Poly[2-(acetoacetoxy)-ethylmethacrylat] führen zur Bildung von doppelt-helikalen Superhelices in fester Phase. Bei Raumtemperatur kollabiert die helikale Superstruktur innerhalb weniger Tage in kleine, aus einzelnen Polymerketten bestehende Kugeln.

Poly(*n*-butylmethacrylat)-*block*-poly[2-(acetoacetoxy)-ethylmethacrylat] zeigt in verdünnter Cyclohexanlösung das Phasenverhalten eines (super-)stark segregierenden Systems. Das Mizellierungsverhalten und Auftreten sphärischer und zylindrischer Morphologien kann auf der Basis geometrischer Überlegungen hinreichend beschrieben werden. Quellen des aus Poly[2-(acetoacetoxy)-ethylmethacrylat] bestehenden Mizellkerns mit 2,2,2-Trifluoroethanol führt zur Änderung der Form der Aggregate von Kugel über Zylinder zu Vesikel.

Blockcopolymere auf der Basis von Poly[2-(acetoacetoxy)-ethylmethacrylat] dienen der Herstellung von anorganisch-organischen Kolloiden und strukturierten dünnen Filmen.

(iii) Polypeptid-Blockcopolymere werden durch ringöffnende Polymerisation von α -Aminosäure-*N*-carboxyanhydriden (NCA) mit ω -aminofunktionalisierten Makroinitiatoren erhalten. Maskierung der wachstumsaktiven Aminofunktion als Hydrochlorid ermöglicht eine kontrollierte Polymerisation der NCA und Bildung von Blockcopolymeren mit nahezu monodisperser Molekulargewichtsverteilung.

Abhängig von der chemischen Zusammensetzung bilden Poly(1,2-butadien)-*block*-poly(L-glutamat)-Copolymere in verdünnt wässriger Kochsalzlösung sphärische Mizellen oder Vesikel. Die Konformation (Sekundärstruktur) der solvatisierenden Polypeptidsegmente kann über den pH-Wert der Lösung eingestellt werden; der Knäuel-Helix Übergang liegt bei etwa pH 5. Die Konformationsänderung hat keinen Einfluss auf Größe und Morphologie der Aggregate.

Feste Filme von linearen Polystyrol-*block*-poly(Z-L-lysin)-Copolymeren (Knäuel-Stäbchen) weisen eine *hexagonal-in-lamellare* Struktur mit großer langreichweitiger Ordnung auf. Die Bevorzugung dieser Morphologie lässt sich mit starken Dipol-Dipol-Wechselwirkungen und der hexagonalen Packung der Helices innerhalb der Polypeptidschichten erklären. Die Grenzfläche zwischen den Schichten ist dabei nicht planar sondern gekrümmt bzw. unduliert. Diese Ondulationen sind statistische Variationen der Dicke der Polypeptidschichten, welche durch die Kettenlängenverteilung der Helices verursacht werden.

Der Einsatz von linearen und sternförmigen Poly(glutaminsäure Natriumsalz)-Blockcopolymeren als Stabilisatoren in der Heterophasenpolymerisation von Styrol führt zur Produktion elektrosterisch stabilisierter Latices mit Polypeptiddekoration. Die kolloidalen Eigenschaften der Latices hängen stark von der Architektur des polymeren Stabilisators ab. Verzweigte Copolymere führen zu kleineren Latexpartikeln mit breiterer (bimodaler) Größenverteilung und geringerer kritischer Koagulationskonzentration.

Polyethylenoxid-*block*-poly(L-lysin) ist ein geeigneter Träger für *cis*-Dichlorodiamin-platin (II) in der Antikrebs therapie von lymphogen metastasierenden Tumoren der oberen Luft- und Speisewege.

ABSTRACT

In this work, the basic principles of self-organization of diblock copolymers having the inherent property of selective or specific non-covalent binding were examined. By the introduction of electrostatic, dipole–dipole, or hydrogen bonding interactions, it was hoped to add complexity to the self-assembled mesostructures and to extend the level of ordering from the nanometer to a larger length scale. This work may be seen in the framework of biomimetics, as it combines features of synthetic polymer and colloid chemistry with basic concepts of structure formation applying in supramolecular and biological systems.

The copolymer systems under study were (i) block ionomers, (ii) block copolymers with acetoacetoxy chelating units, and (iii) polypeptide block copolymers.

(i) The mixing of dilute tetrahydrofuran solutions of oppositely charged block ionomers, polystyrene-*block*-poly(1-methyl-4-vinyl-pyridinium iodide) and poly(1,2-butadiene)-*block*-poly(cesium methacrylate), led to the spontaneous formation of a polyion complex, which self-assembled into vesicular aggregates. Due to a very high incompatibility of the solvating block segments, vesicles had a microphase-separated, asymmetric membrane and were thus amphiphilic in nature. Inversion of the structure of the membrane could be achieved by a change of the selectivity of the solvent.

(ii) Well-defined homopolymers and block copolymers based on 2-(acetoacetoxy)ethyl methacrylate were prepared by either RAFT radical polymerization or Group Transfer Polymerization / azeotropic acetoacetylation.

Promoted by hydrogen bridging interactions between adjacent acetoacetoxy units, poly[2-(acetoacetoxy)ethyl methacrylate] produced large double-stranded superhelices in the solid state. The helical superstructure was found to collapse within a few days at room temperature, dissociating into small globules of single polymer chains.

Poly(*n*-butyl methacrylate)-*block*-poly[2-(acetoacetoxy)ethyl methacrylate] copolymers in dilute cyclohexane solution were found to exhibit the phase behavior of a (super) strongly segregated system. The micellization behavior and appearance of spherical and cylindrical morphologies could appropriately be described on the basis of geometric considerations. A swelling of the poly[2-(acetoacetoxy)ethyl methacrylate] core with 2,2,2-trifluoroethanol was accompanied by a change of the shape of aggregates from spheres to cylinders to vesicles.

Poly[2-(acetoacetoxy)ethyl methacrylate]-based block copolymers were further used for the fabrication of colloidal organic–inorganic hybrid materials and thin ordered films.

(iii) Polypeptide-based block copolymers were prepared by ring-opening polymerization of α -aminoacid-*N*-carboxyanhydrides (NCA) using ω -primary amino-functional macroinitiators. Screening of the free amine initiating/propagating species as hydrochlorides promoted a well-controlled polymerization of NCA, producing block copolymer samples with a nearly monodisperse distribution.

Depending on chemical composition, poly(1,2-butadiene)-*block*-(L-glutamate) copolymers self-assembled into spherical micelles or vesicles in dilute aqueous NaCl solution. The conformation or secondary structure of the solvating polypeptide segments could be triggered *via* the pH of the solution, the coil–helix transition occurring at pH \sim 5. The dimension and the morphology of aggregates were not affected by the change of conformation.

The solid films of linear polystyrene-*block*-poly(Z-L-lysine) coil-rod copolymers exhibited a *hexagonal-in-lamellar* morphology with high long-range order. The preferential formation of this kind of morphology was attributed to the existence of strong dipole–dipole interactions and a hexagonal packing of α -helices within the polypeptide layers. The interface between the layers was not planar but considerably curved or undulated. Such undulations, i.e. statistical fluctuations in the thickness of the polypeptide layers, were produced in response to the chain length distribution of helices.

Linear and star-shaped poly(sodium glutamate)-based block copolymers were used as stabilizers in the heterophase polymerization of styrene to produce electrosterically stabilized latexes with a polypeptide decoration. The colloidal properties of the latexes were found to depend vastly on the architecture of the block copolymer stabilizer. Branched copolymers yielded smaller latex particles with broader (bimodal) size distribution and lower critical coagulation concentration.

Poly(ethylene oxide)-*block*-poly(L-lysine) was successfully used as a carrier for *cis*-dichlorodiammineplatinum(II) in the anti-cancer therapy of the lymphogenic metastasizing squamous cell carcinomas of the head and neck regions.

TABLE OF CONTENTS

1	Introduction	1
2	Polymer Synthesis and Characterization.....	5
2.1	Block ionomers	7
2.1.1	Conventional anionic polymerization	7
2.1.2	Anionic polymerization and radical addition of mercaptanes.....	10
2.2	Block copolymers with acetoacetoxy chelating units	14
2.2.1	Radical polymerization of 2-(acetoacetoxy)ethyl methacrylate.....	15
2.2.2	Acetoacetylation of poly(2-hydroxyethyl methacrylate)	19
2.3	Polypeptide block copolymers	23
2.3.1	ω -Amino-functional macroinitiators	24
2.3.2	Polypeptide block copolymers	31
3	Block Copolymer Mesostructures.....	45
3.1	Block ionomers and polyion complexes	47
3.2	Chelating block copolymers.....	56
3.2.1	Reverse micellar aggregates.....	56
3.2.2	Superstructures stabilized by hydrogen bridging.....	64
3.3	Polypeptide block copolymers	69
3.3.1	Aggregates in dilute solution.....	70
3.3.2	Solid-state structures	75
4	Functional Colloids	87
4.1	Polymer-metal hybrid materials	88
4.2	Polypeptide-decorated latexes.....	93
4.3	Polypeptide-based drug carriers	98
5	Summary and Outlook	101
6	Experimental Procedures and Methods.....	106
7	Acknowledgments	110
8	References	112
9	List of Publications.....	122

1 INTRODUCTION

Materials science deals increasingly with nanostructures, i.e. structures with a characteristic dimension of 1-100 nm. This particular range of length scale is called the mesoscopic range, as it is located between the microscopic range of atoms and molecules and the macroscopic range of solids. Solid-state physics and electronics have entered the field of nanostructures by making use of lithography and etching processes (“top-down” approach), which enable the fabrication of structures no smaller than ~ 200 nm. Nature, on the other hand, may serve as a model for the building-up of smaller structures. Here, individual molecules are integrated into larger functional units and complex structural hierarchies *via* self-organization (“bottom-up” approach), leading to such advanced materials as wood or bone. It is one of the great challenges in research disciplines like chemistry, physics, or materials science to find ways to structure molecules so as to enable them to produce functional superlattices by self-organization, for example by making use of the self-assembly features of supramolecular chemical devices^{1,2} or block copolymers.³⁻⁵

The micellar aggregates, lyotropic phases, and solid-state mesophases of diblock copolymers are among the best examined supramolecular systems, which is due to the fact that a simple encoding *via* the chemical composition and the overall number of repeating units (N) makes it possible to control both the shape and the size of the resulting superstructures.^{6,7} The phases of amphiphilic diblock copolymers which are most commonly observed in solution are spherical and cylindrical micelles and vesicles, and in the solid state *bcc*-packed spheres (BCC), hexagonally packed cylinders (HEX), lamellae (LAM), and gyroid (Figure 1-1).

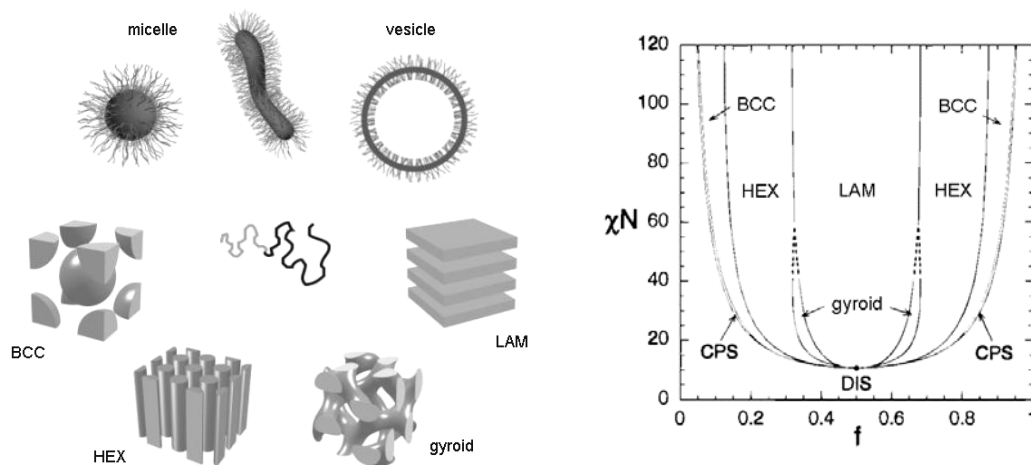


Figure 1-1. Illustration of the “classical” mesophases (left) and theoretical phase diagram (right; f : mole fraction of one comonomer, χ : Flory-Huggins interaction parameter, N : overall number of repeating units; picture taken from ref. ⁸) of non-crystalline linear diblock copolymers.

The origin of structure formation in copolymer systems is the simultaneous establishment of attractive and repulsive forces, i.e. covalent linkage of incompatible block segments A and B. A quantitative measure of the strength of the repulsive interactions between polymer blocks is given by the Flory-Huggins interaction parameter χ . The process of minimizing surface tension at the A–B interface is governed by the counterbalance of thermodynamic demixing and chain elasticity. The volume fraction (or mole fraction f) of comonomers determines the local geometry and thus the interface curvature of the morphology; the dimension of the structure is given by the size of A and B domains.

The free energy of a structure can be calculated by means of self-consistent field theory. The structure with the lowest energy conforms to the equilibrium structure, the stability range of which can be represented in a phase diagram as shown in Figure 1-1. By making use of such a phase diagram, it is possible to purposefully produce different superstructures by variation of the lengths of the blocks A and B. However, this also implies that no other equilibrium structures than the ones included in the diagram can be obtained.

Block copolymer mesostructures with higher complexity are accessible upon increasing the number of incompatible blocks and/or introducing other than linear copolymer architectures.³ Pioneered by the work of Stadler[†] et al.,⁹ ABC triblock copolymers were found to produce a variety of previously unknown morphologies.³ Even a non-centrosymmetric structure could be obtained in the equimolar blend of an ABC and an AC block copolymer (Figure 1-2).¹⁰

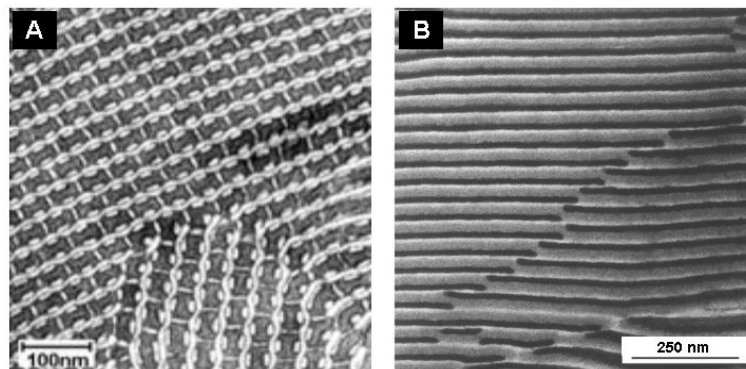


Figure 1-2. TEM micrographs of (A) the “knitting pattern” morphology of a linear ABC triblock copolymer¹¹ and (B) a non-centrosymmetric lamellar structure of an ABC/AC blend (picture taken from ref. ¹⁰).

Another (biomimetic) approach is to introduce additional enthalpic contributions to the mixing free energy in a block copolymer system. Such contributions might originate from non-covalent interactions like van-der-Waals, hydrogen bonding, charge transfer, dipole–dipole, or electrostatic interactions as well as from crystallization processes—like in biological or

supramolecular as well as colloidal systems. Most experimental studies, however, have been focusing on conformationally anisotropic rod–coil block copolymers; this topic has recently been reviewed by Lee et al.¹² Here, the dipole–dipole interactions between rod-like segments may lead to unusual morphologies like the disordered *zigzag lamellar* phase of polystyrene–poly(hexyl isocyanate) block copolymers (Ober et al.^{13,14}; see Figure 1-3). The establishment of additional specific interactions in a rod–coil system, as for example realized in the charged polystyrene–poly(isocyanodipeptide)s, can produce a rich polymorphism of complex mesostructures including filaments or helical superstructures (Nolte et al.^{15,16}; see Figure 1-4).

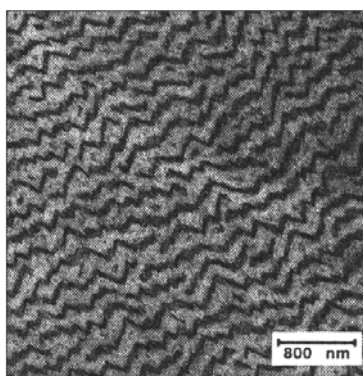


Figure 1-3. TEM micrograph of a disordered *zigzag lamellar* solid-state morphology of a linear polystyrene–poly(hexyl isocyanate) diblock copolymer (picture taken from ref. ¹³).

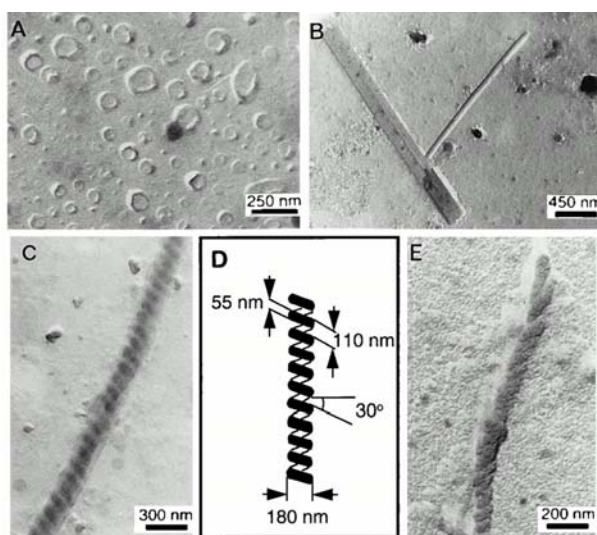


Figure 1-4. TEM micrographs of the morphologies formed by polystyrene–*block*–poly(isocyanodipeptide)s in aqueous solution: (A) vesicles, (B) bilayer filaments, (C) left-handed superhelix (D: schematic representation), and (E) right-handed helical aggregate (pictures taken from ref. ¹⁵).

These two examples may be enough to demonstrate the simplicity of adding complexity to the mesostructures diblock copolymers *via* specific interactions. However, the understanding of the basic principles of structure formation in such systems is not yet complete, making a reliable prediction of the phase behavior and morphologies difficult if not impossible.

The aims of the present work have been to find new, easy-to-prepare systems and biomimetic concepts for the creation of complex mesostructures and to contribute to a better understanding of the phase behavior of block copolymers. Main attention was turned to linear diblock copolymers, i.e. block ionomers (\rightarrow electrostatic interactions), chelating block copolymers (\rightarrow hydrogen bonding and metal ion coordination interactions), and polypeptide-based rod-coil block copolymers (\rightarrow hydrogen bonding and dipole-dipole interactions) (see Chart 1-1). Their synthesis and characterization will be described in chapter 2, including new developments and improvements of experimental techniques. Chapter 3 will summarize the systematic studies on the phase behavior of these block copolymers and the description of novel complex mesostructures. Finally, in chapter 4, the use of block copolymers in the fabrication of functional colloids, i.e. organic-inorganic hybrid materials, latexes, and drug-carrier systems, will be discussed.

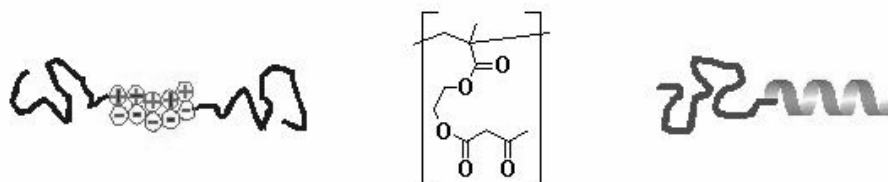


Chart 1-1. Schematic illustrations of the diblock copolymer systems investigated (left to right): block ionomers, chelating block copolymers, and polypeptide-based block copolymers.

2 POLYMER SYNTHESIS AND CHARACTERIZATION

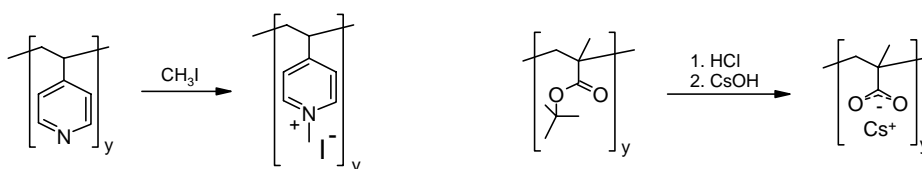
One of the major challenges of this work concerned the synthesis of well-defined functional diblock copolymers, i.e. block ionomers (chapter 2.1), copolymers comprising acetoacetoxy chelating moieties (chapter 2.2), and hybrid block copolymers with a synthetic block segment and a polypeptide segment (“molecular chimeras”,¹⁷ chapter 2.3). The synthetic techniques of choice were ANIONIC POLYMERIZATION and RAFT RADICAL POLYMERIZATION. Any of the procedures described in the following chapters are considerable improvements of current state-of-the-art techniques or are new developments as in the case of chelating polymers. A controlled polymerization of 2-(acetoacetoxy)ethyl methacrylate, which is a commercially available monomer, has so far not been described. However, as will be seen later, it is possible to synthesize well-defined homopolymer and copolymers of this special monomer *via* RAFT radical polymerization. This very simple approach might open new possibilities in the fields of organic–inorganic colloids, polymer–metal coatings, and fabrication of ordered metal arrays on surfaces, to mention just a few.

Lots of efforts went into the synthesis and characterization of polypeptide block copolymers. The characterization of products obtained by ring-opening polymerization of amino acid-*N*-carboxyanhydrides (2,5-dioxo-4-*R*-tetrahydro-oxazol, *Leuchs* anhydride) turned out to play a key role when trying to optimize the reaction conditions. For whatever reason, no adequate procedures have so far been reported that allow a determination of absolute molecular weight distributions of synthetic polypeptide block copolymers. However, SIZE EXCLUSION CHROMATOGRAPHY (SEC) can provide this information without even referring to any kind of calibration curve or molar mass-sensitive detecting devices. The newly developed data evaluation method is based on the established procedure to determine the molecular weight of a diblock copolymer from its chemical composition and the molar mass of the first block segment (precursor), applied on an ensemble of monodisperse SEC fractions. The molecular weight averages and distributions obtained by this very simple and straight-forward approach were found to be in reasonable good agreement with the ones determined by NMR, osmometry, and SEC with on-line viscometry or multiangle laser light scattering. Having access to this information made it finally possible to optimize the reaction conditions in a way that polypeptide block copolymers with a Poisson molecular weight distribution were produced. A higher level of control of polypeptide synthesis can, however, only be achieved with solid-phase synthesis.

For the synthesis of block ionomers, which are asymmetric block copolymers with a low content of ionic residues, the established recipes of sequential anionic polymerization were employed. However, the functional monomer is usually second in the sequence of monomer addition, which can make characterization and purification of the copolymer products very difficult. It would be desirable if the minority species could be polymerized first. As will be shown in the next subchapter, polybutadiene-based copolymers can be easily transformed into well-defined block ionomers *via* radical addition of ω -functional mercaptanes. This approach combines the advantageous features of anionic polymerization with the versatility of radical addition reactions.

2.1 Block ionomers

Block ionomers are segmented copolymers with an electrolyte content of less than 15 mol %.¹⁸ The preparation of well-defined ionomer samples requires the application of living/controlled polymerization techniques, usually followed by a chemical modification step to produce the polyelectrolyte block segment.⁷ Ionomers of choice were polystyrene-*block*-poly(1-methyl-4-vinyl-pyridinium iodide) (PS-*b*-PVP⁺I⁻) and polybutadiene-*block*-poly(cesium methacrylate) (PB-*b*-PMA⁻Cs⁺), which can be prepared by living ANIONIC POLYMERIZATION and subsequent chemical modification (quaternization and ester hydrolysis, see Scheme 2-1). Recipes were adopted from literature,¹⁹⁻²¹ and the synthesis and characterization of ionomer samples shall therefore just very briefly be described here (chapter 2.1.1).



Scheme 2-1. Quaternization of P4VP with methyl iodide (left) and hydrolysis/neutralization of PtBMA (right).

However, due to the different reactivities of propagating anionic species and monomers, the sequence of monomer addition in anionic polymerization must follow the following order: dienes, styrenes, acrylates, methacrylates, vinylpyridines, ethylene oxide.²² It is therefore inevitable that the synthesis of the above mentioned block copolymers starts with the major component (styrene or butadiene), followed by polymerization of the functional monomer (4-vinylpyridine or *tert*-butyl methacrylate). As a matter of fact, block copolymer and precursors might exhibit very similar hydrodynamic volumes and solubility characteristics, making the characterization with SIZE EXCLUSION CHROMATOGRAPHY (SEC) and purification very difficult. It would be therefore desirable if polyvinyl-based block ionomers could be prepared starting with the short functional (ionic) segment. A very promising approach, which will be described in chapter 2.1.2, is the free-radical addition of functional mercaptanes to the double bonds in polybutadiene-based block copolymers.²³

2.1.1 Conventional anionic polymerization

2.1.1.1 Polystyrene-*block*-poly(1-methyl-4-vinyl-pyridinium iodide)

First, PS-*b*-P4VP copolymers were synthesized by a sequential anionic polymerization of styrene and 4-vinylpyridine (4VP) in tetrahydrofuran (THF) at -78 °C.¹⁹ Polymerizations were initiated by *sec*-butyl lithium employing LiCl as an additive in a six-fold excess with

respect to the initiator. In order to avoid side reactions during the crossover step, the living polystyryl lithium was endcapped with 1,1-diphenylethylene prior to the addition of 4-vinylpyridine. ^1H NMR confirmed the chemical structure (spectra not shown), and SEC indicated a monomodal molecular weight distribution of the PS-*b*-P4VP copolymer products (cf. Figure 2-1). Note that under the supposedly best experimental conditions for fractionation in the SEC mode (mobile phase: DMA + 0.5 wt % LiBr at 70 °C; stationary phase: SDV, polystyrene gel), adsorption of copolymer chains in the pores of the stationary phase could not completely be avoided, as indicated by the strong tailing of chromatographic peaks. Since fractions of copolymer chains were eluting after the precursor (cf. Figure 2-1), it was hardly possible to decide whether or not samples were contaminated with traces of PS. A clear separation of homopolymer and copolymer fractions should be achieved with LIQUID ADSORPTION CHROMATOGRAPHY AT CRITICAL CONDITIONS (LACCC, see also chapter 2.3.1.2).

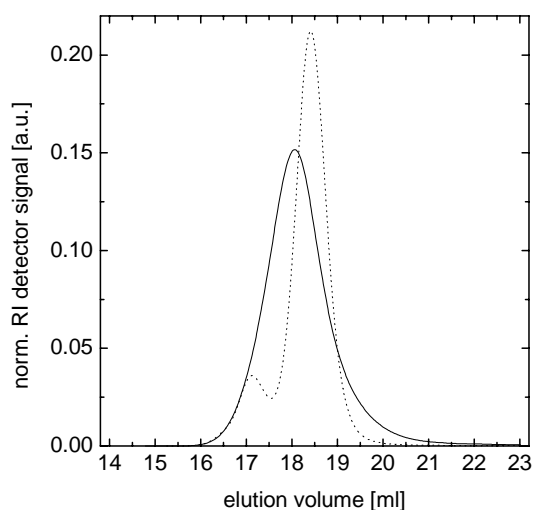
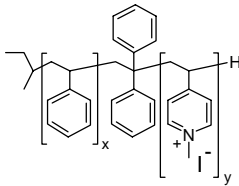


Figure 2-1. SEC chromatograms (eluent: DMA+0.5 wt % LiBr, flow rate: 1.0 mL min⁻¹; columns: 300 x 8 mm, 5 μm MZ-SDplus, 10³, 10⁵, 10⁶ Å; 70 °C; detector: RI) of PS-*b*-P4VP (precursor of sample SP2, cf. Table 2-1) (solid line) and the corresponding PS precursor (dashed line).

For the subsequent quaternization of pyridine residues,¹⁹ PS-*b*-P4VP precursor polymers were dissolved in a THF/nitromethane (~1:2 w/w) mixture and stirred with a 10-fold excess of methyl iodide at room temperature for 4 days. As indicated by ^1H NMR analysis (DMF-*d*₇), considering the signals of protons next to the nitrogen atom arising at $\delta \sim 8.4$ (4VP) and 9.0 ppm (4VP⁺), quaternization of the P4VP segment is achieved in virtually quantitative yield. The molecular characteristics of the synthesized PS-*b*-P4VP⁺T⁻ copolymer samples are summarized in Table 2-1.

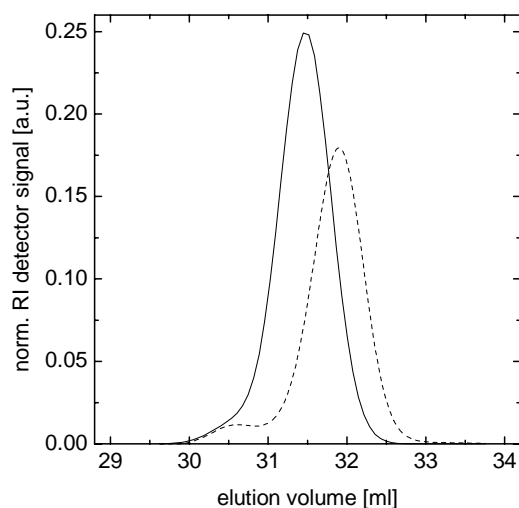
Table 2-1. Molecular characteristics of PS-*b*-P4VP⁺I⁻ cationomers prepared by sequential anionic polymerization of styrene and 4-vinylpyridine and subsequent quaternization with methyl iodide.

chemical structure	entry	precursor	x^{\S}	$y^{\#}$	PDI [§]	degree of quaternization ^{&}
	SP1	PS- <i>b</i> -P4VP	211	12	(1.3)	quantitative
	SP2	PS- <i>b</i> -P4VP	211	33	(1.2)	quantitative

[§] Number-average degree of polymerization of PS; SEC analysis (eluent: THF at 25 °C; stationary phase: SDV; detector: RI/UV; calibration: PS) of the PS precursor, which was isolated prior to the addition of the second monomer. [#] Number-average degree of polymerization of P4VP; ¹H NMR (400.1 MHz, CDCl₃, 25 °C). [§] Polydispersity index; SEC (eluent: DMA + 0.5 wt % LiBr at 70 °C; stationary phase: SDV; detector: RI; calibration: PS). [&] ¹H NMR (400.1 MHz, DMF-d₇, 25 °C)

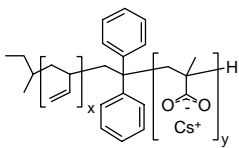
2.1.1.2 Poly(1,2-butadiene)-*block*-poly(cesium methacrylate)

1,3-Butadiene was polymerized at -78 °C in THF with *sec*-butyl lithium as the initiator in the presence of LiCl (see above). The living polybutadienyl lithium was end-capped with 1,1-diphenylethylene and then *tert*-butyl methacrylate (*t*BMA) was added as the second monomer to yield PB-*b*-*Pt*BMA copolymers.²⁰ The chemical structure of copolymers was confirmed by ¹H NMR analysis (microstructure of PB: 93% 1,2 and 7% *trans*-1,4; spectra not shown). SEC analyses indicate that copolymer products have a narrow molecular weight distribution (apparent polydispersity index, PDI < 1.1) and should be free of PB homopolymer impurities (cf. Figure 2-2).

**Figure 2-2.** SEC chromatograms (eluent: THF, flow rate: 1.0 mL min⁻¹; columns: 300 x 8 mm, 5 μm MZ-SDplus, 10³, 10⁵, 10⁶ Å; 25 °C; detector: RI) of PB-*b*-*Pt*BMA (precursor of sample BM2, cf. Table 2-2) (solid line) and the corresponding PB precursor (dashed line). Note that the RI trace of the copolymer sample was corrected with respect to the comonomer-specific detector response.

The PB-*b*-PtBMA precursor polymers were transformed into PB-*b*-PMA⁻Cs⁺ by an HCl-catalyzed hydrolysis of ester groups in dioxane²¹ and subsequent neutralization with CsOH. The quantitative modification of methacrylate units was confirmed by ¹H and ¹³C NMR and FT-IR analysis (spectra not shown). The molecular characteristics of the PB-*b*-PMA⁻Cs⁺ copolymers prepared are listed in Table 2-2.

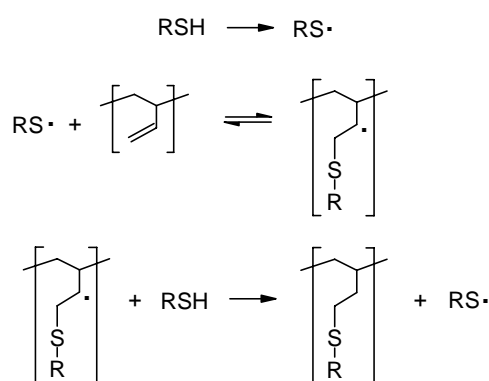
Table 2-2. Molecular characteristics of PB-*b*-PMA⁻Cs⁺ anionomers prepared by sequential anionic polymerization of 1,3-butadiene and *tert*-butyl methacrylate and subsequent hydrolysis of ester residues.

chemical structure	entry	precursor	x^{\S}	$y^{\#}$	PDI [§]	degree of hydrolysis ^{&}
	BM1	PB- <i>b</i> -PtBMA	216	9	1.09	quantitative
	BM2	PB- <i>b</i> -PtBMA	216	29	1.07	quantitative

[§] Number-average degree of polymerization of PB; SEC analysis (eluent: THF at 25 °C; stationary phase: SDV; detector: RI; calibration: PB-1,2) of the PB precursor, which was isolated prior to the addition of the second monomer. [#] Number-average degree of polymerization of PtBMA; ¹H NMR (400.1 MHz, CDCl₃, 25 °C). [§] Polydispersity index; SEC. [&] NMR and FT-IR.

2.1.2 Anionic polymerization and radical addition of mercaptanes

The free-radical addition of mercaptanes (RSH) to unsaturated substrates is a valuable tool in synthetic organic chemistry for the synthesis of functional thioethers.²⁴ Like in other free-radical processes, the addition of thiyl radicals to unsymmetrically substituted multiple bonds occurs in an anti-Markownikoff orientation (cf. Scheme 2-2) and tolerates the presence of most functional groups (–OH, –NH₂, –COOH, etc.).



Scheme 2-2. Functionalization of unsaturated polymers *via* radical addition of mercaptanes.

However, this reaction has not extensively been used for modification of unsaturated polymers. The only examples reported in the literature are—to the best of our knowledge—the

hydroxylation of telechelic polybutadienes²⁵ and the carboxylation of SBR rubbers.²⁶ For whatever reason, modification yields were always less than 50%. Nevertheless, the addition of commercial ω -amino- or ω -carboxy-functional mercaptanes to PB-based block copolymers would be a convenient route towards block ionomers (see below). The precursor block copolymers are available by living sequential ANIONIC POLYMERIZATION in a high quality, i.e. free of homopolymer contaminants and with narrow molecular weight distribution.²⁷ The subsequent modification reaction should then satisfy the following two basic requirements: (i) the addition of thiyl radicals should be quantitative and (ii) cross-linking of the PB segment must be avoided.

The poly(1,2-butadiene)-*block*-poly(ethylene oxide) (PB₂₅-*b*-PEO₇₅; subscripts denote the number-average degrees of polymerization) used throughout these studies was prepared in two steps. First, a PB₂₅-OH (PDI = 1.08) was prepared by the anionic polymerization of 1,3-butadiene in THF using *s*BuLi as an initiator and ethylene oxide as a quenching agent.²⁸ According to ¹H NMR analysis, the end-capping of chains was quantitative and the PB microstructure was 97% 1,2 and 3% *trans*-1,4. Then, the phosphazene base *t*-BuP₄ was used to deprotonate the PB₂₅-OH macroinitiator to initiate the polymerization of ethylene oxide in THF (T = +50 °C, 3 days). Polymerization was quenched with acetic acid, and the product was precipitated in cold acetone, re-dissolved in water, and freeze-dried.²⁹ The chemical structure of the copolymer was confirmed by ¹H NMR analysis. As indicated by SEC (cf. Figure 2-4), the product had a narrow molecular weight distribution (apparent PDI = 1.07) and did not contain any homopolymer impurities.

The ω -functional mercaptanes used for the modification of PB-PEO were methyl 3-mercaptopropionate (MMP), 3-mercaptopropionic acid (MPA), and 2-mercaptopethylamine (MEA). In a typical procedure, the radical addition of the mercaptanes to PB₂₅-*b*-PEO₇₅ was performed as follows (cf. Table 2-3, entry DM1): PB₂₅-*b*-PEO₇₅ (1.0 g, 0.213 mmol) and AIBN (0.254 g, 1.62 mmol) were dissolved in dry THF (30 mL) to give a ~3 wt % solution. After addition of MMP (6.1 g, 53.3 mmol), the solution was degassed and then refluxed for 24 hours under a dry argon atmosphere. The crude product was precipitated into cold hexane, filtered, re-dissolved in water, and dialyzed (molecular weight cut-off: 1 kDa) against bi-distilled water. After freeze-drying, the modified copolymer sample DM1 was isolated as a colorless fluffy material in a 55% yield. The sample did not contain detectable amounts of mercaptane, as indicated by GAS CHROMATOGRAPHY (GC) (and smelling).

Table 2-3. Experimental conditions for the radical addition of the ω -functionalized mercaptanes MMP, MPA, and MEA to PB₂₅-*b*-PEO₇₅ (initiator: AIBN, solvent: THF, temperature: 65 °C) and molecular characteristics of modified products.

entry	mercaptane	[C=C] ₀ /[RSH] ₀ /[AIBN] ₀	time (h)	$x_{C=C}$ ^{&}	PDI [§]
DM1	MMP	1 : 10 : 0.30	24	1.0	1.05
DM2	MPA	1 : 10 : 0.31	24	0.6	–
DM3	MEA	1 : 10 : 0.64	24	0.8	–

[&] Conversion of C=C double bonds; ¹H NMR analysis (400.1 MHz, CDCl₃, 25 °C). [§] Polydispersity index; SEC (eluent: THF at 25 °C; stationary phase: SDV; detector: RI; calibration: PS).

¹H NMR was applied to confirm the chemical structures of the modified copolymer samples DM1-3; the exemplary spectrum of DM1 bearing ester functional groups is shown in Figure 2-3. The characteristic signals of the newly formed thioether linkage (–CH₂SCH₂–) could be observed at $\delta \sim 2.6$ and 2.8 ppm. Evidently, the spectrum of DM1 did not reveal any trace of unsaturated PB units ($\delta = 4.8$ -5.6 ppm), indicating that the addition of MMP to the PB block segment had been achieved in a quantitative yield. In the case of the polyelectrolyte block copolymers DM2 (–COOH) and DM3 (–NH₂), however, about 40% and 20% of PB double bonds remained untouched (spectra not shown) (see Table 2-3). Anyway, modification yields achieved were higher than the ones reported earlier in the literature (see above).

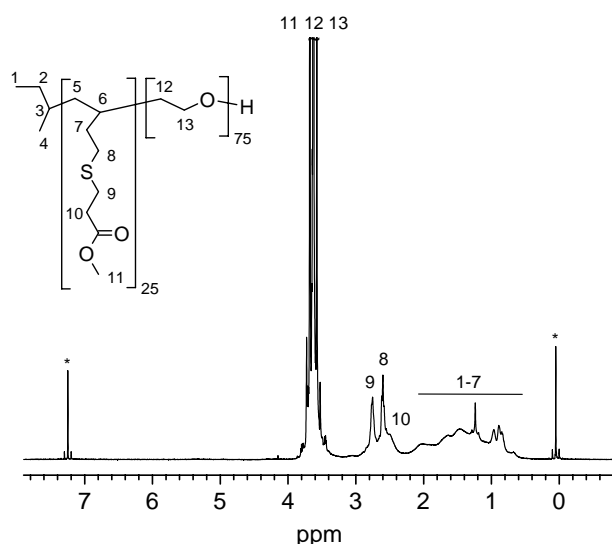


Figure 2-3. ¹H NMR spectrum (400.1 MHz) of MMP-modified PB-*b*-PEO sample DM1 in CDCl₃ at 25 °C.

As shown by SEC analysis (see Figure 2-4), sample DM1 and the PB₂₅-*b*-PEO₇₅ precursor exhibited virtually the same molecular weight distribution (PDI < 1.1). From this it was concluded that under the chosen experimental conditions an intermolecular radical cross-linking

of the PB segments had been avoided. Due to the somewhat larger hydrodynamic size of ester-functional units, DM1 was eluting somewhat faster than the parent copolymer ($\Delta V \sim 0.1$ mL). It is noteworthy that the DM1 sample showed a distinct UV absorption at $\lambda = 260$ nm, which supposedly originated from the ($n \rightarrow \sigma^*$) transition of the thioether moieties. However, a characterization of DM2 and DM3 with SEC could not be achieved yet.

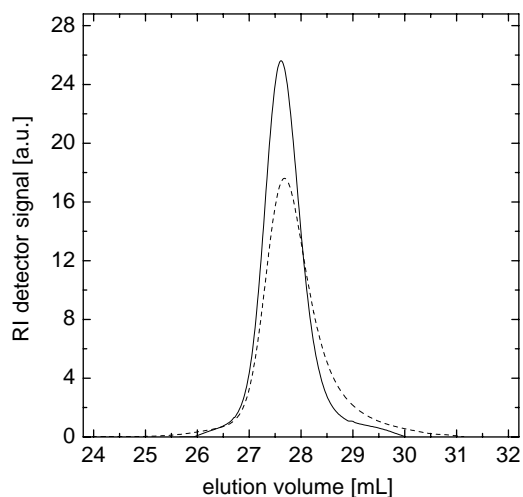
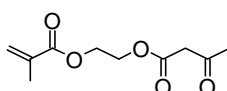


Figure 2-4. SEC chromatograms (eluent: THF, flow rate: 1.0 mL min^{-1} ; columns: $300 \times 8 \text{ mm}$, $5 \mu\text{m}$ MZ-SDplus, 10^3 , 10^5 , 10^6 \AA ; $25 \text{ }^\circ\text{C}$; detector: RI) of the PB₂₅-b-PEO₇₅ precursor (dashed line) and the functional block copolymer DM1 (solid line; methyl 3-mercaptopropionate, MMP).

Building on the very promising results obtained with MMP, the methodology of the radical addition of mercaptanes to PB-based block copolymers shall be used to generate a “library” of functional block copolymers.

2.2 Block copolymers with acetoacetoxy chelating units

Polymers with chelating β -dicarbonyl residues, like the ones based on 2-(acetoacetoxy)ethyl methacrylate (AEMA) (the chemical structure is shown in Scheme 2-3), have so far only been available as homopolymers, random copolymers, and resins.³⁰ Advantageously, acetoacetoxy groups are tolerated by radicals and need not to be masked or protected (see below), but nevertheless the resulting products are chemically disperse and therefore less or not suited for systematic studies on colloidal and materials properties. Information on the chemical and physical properties of poly(AEMA) (in the following abbreviated as PAEMA) are not existing in the literature.



Scheme 2-3. Chemical structure of 2-(acetoacetoxy)ethyl methacrylate (AEMA) (keto tautomer).

A way to circumvent this major drawback is to use one of modern techniques of controlled radical polymerization, for instance ATOM TRANSFER RADICAL POLYMERIZATION (ATRP) or REVERSIBLE ADDITION-FRAGMENTATION CHAIN TRANSFER (RAFT) RADICAL POLYMERIZATION.³¹ Both these methods are designed to produce poly(meth)acrylates with predetermined molecular weight and narrow molecular weight distribution. However, as will be shown in the following subchapter 2.2.1, ATRP does not promote a controlled polymerization of AEMA. By the RAFT process, on the other hand, well-defined PAEMA homopolymers and block copolymers could be prepared.³²

A synthesis of copolymers based on AEMA *via* anionic polymerization techniques would require a suitable masking of the CH-acidic acetoacetoxy group. However, all attempts to prepare a ketal derivative of AEMA with a sufficiently high purity were not successful. It was therefore decided to employ an indirect route to prepare PAEMA, namely the acetoacetylation of a poly(2-hydroxy-ethyl methacrylate) (PHEMA). Precursor polymers were synthesized in a separate step by GROUP TRANSFER POLYMERIZATION (GTP).³³ This procedure is experimentally more demanding than the previous one, but it can provide materials of better quality regarding purity and molecular weight distribution.³⁴ A description of this approach will be given in subchapter 2.2.2.

2.2.1 Radical polymerization of 2-(acetoacetoxy)ethyl methacrylate

As seen from the SEC trace A shown in Figure 2-5, the free radical polymerization of AEMA initiated by 2,2'-azobis(isobutyronitrile) (AIBN) yields an ill-defined product with a multimodal molecular weight distribution. Also, as expected, the molecular weight of the final product is much higher than calculated from the monomer/initiator ratio.

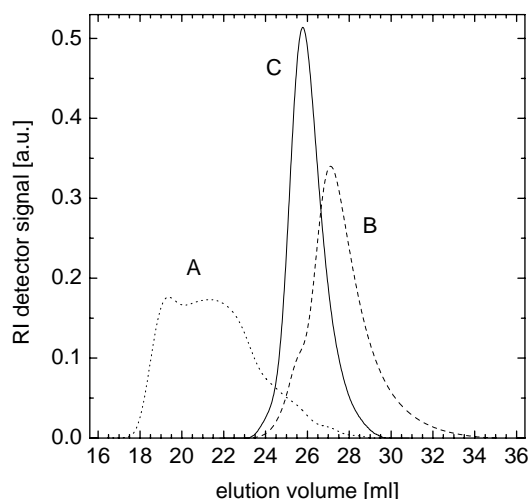
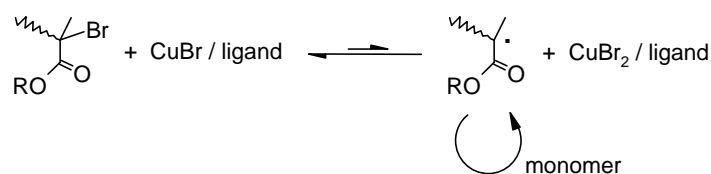


Figure 2-5. SEC chromatograms (eluent: THF; flow rate: 1.0 mL min⁻¹; columns: 300 x 8 mm, 5 μ m MZ-SDplus, 10³, 10⁵, 10⁶ Å; 25 °C; detector: RI) of PAEMA obtained by (A) free radical polymerization, (B) ATRP, and (C) RAFT radical polymerization. Experimental conditions: A: [AEMA]₀ = 2.1 M, [AIBN]₀ = 10.0 mM, solvent: ethyl acetate, temperature: 60 °C, time: 20 h. B: [AEMA]₀ = 2.1 M, [α BiB]₀ = 10.5 mM, [CuBr]₀ = 7.4 mM, [CuBr₂]₀ = 0.4 mM, [dNbpy]₀ = 14.7 mM, methyl ethyl ketone, 90 °C, 80 min; C: [AEMA]₀ = 5.2 M, [CPDB]₀ = 0.0264 M, [AIBN]₀ = 4.9 mM, ethyl acetate, 60 °C, 18 h.

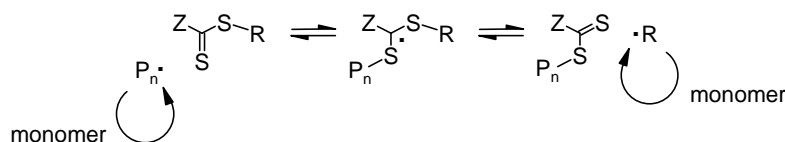
The radical polymerization of AEMA via ATRP using *tert*-butyl α -bromoisobutyrate (α BiB) as the initiator and CuBr/4,4'-dinonyl-2,2'-bipyridine (dNbpy) as the catalyst complex³⁵ gives considerably better results. SEC analysis (trace B in Figure 2-5) reveals that the resulting PAEMA, however, has a bimodal and moderately broad molecular weight distribution (apparent PDI \sim 1.5). Noteworthy that in the early stages of polymerization the color of the reaction mixture turned from red-brown to yellow could be observed, pointing to a structural change of the catalyst complex. Presumably, the dNbpy ligand was replaced by the growing multi-dentate AEMA chains. As a matter of the changed structure of catalyst complex, the position of the equilibrium between dormant covalent species and propagating radicals (see Scheme 2-4) might have been shifted to the right, thus promoting side reactions like the recombination of polymer chains. Also, a decrease of the rate of exchange between different species could be a reason for the broadening of the molecular weight distribution.



Scheme 2-4. Dynamic equilibrium between covalent dormant species (left) and propagating radicals (right) in Atom Transfer Radical Polymerization (ATRP).

In order to avoid ligand exchange in the course of polymerization, a more effective ligand than dNbipy was used, namely tris[2-(dimethylamino)ethyl]amine (Me_6TREN).³⁶ However, polymerization in the presence of Me_6TREN produced an insoluble polymer gel. It is assumed that Me_6TREN as a base is sufficiently strong to abstract CH-acidic protons of AEMA, thus promoting an aldol-type cross-linking of the polymer chains. Apparently, a controlled polymerization of AEMA via ATRP may only be achieved when acetoacetoxy groups are suitably masked, for example as ketals, to reduce their ligating capability (\rightarrow dNbipy) and chemical reactivity (\rightarrow Me_6TREN).

RAFT radical polymerization is performed in the presence of a highly efficient chain transfer agent, such as 2-cyano-prop-2-yl dithiobenzoate (CPDB), metal ion salt catalysts are not involved. The controlled character of polymerization is maintained by a reversible addition-fragmentation process, in which the dithiocarbonyl moiety is transferred between active and dormant chains (see Scheme 2-5).³⁷



Scheme 2-5. Reversible addition-fragmentation equilibrium between active and dormant chains in the presence of a chain transfer agent (CPDB: $\text{Z} = -\text{C}_6\text{H}_5$, $\text{R} = -\text{C}(\text{CN})\text{CH}_3$).

Following a standard recipe described in literature,^{37,38} polymerization of AEMA was performed in the presence of CPDB as the chain transfer agent and AIBN as the radical source in ethyl acetate at 60 °C. Experimental details and molecular characteristics of the PAEMA samples obtained in different entries are summarized in Table 2-4.

Under the given reaction conditions, virtually quantitative monomer conversion was reached within 15 to 20 hours. Initial kinetic experiments indicate that polymerization follows first-order kinetics with respect to monomer. In addition it was found that the molecular weight of polymers was increasing linearly with conversion. The final products usually exhibited a monomodal and narrow molecular weight distribution (apparent PDI < 1.2) (cf. the SEC chro-

matogram of sample A5 in Figure 2-5, trace C). These results suggested that RAFT radical polymerization promoted a controlled synthesis of PAEMA. However, the experimental molecular weights were always found to be considerably higher as calculated from the ratio $[AEMA]_0/[CPDB]_0$, the efficiency of CPDB being in the range of 35-70%. The reason for the partial deactivation of the chain transfer agent is not known yet.

Table 2-4. Experimental conditions and molecular characteristics of PAEMA homopolymers obtained by RAFT radical polymerization (initiator: AIBN, chain transfer agent: CPDB, solvent: ethyl acetate, temperature: 60 °C).

entry	$[AEMA]_0/[CPDB]_0/[AIBN]_0$ (M)	time (h)	x_p^+	$n^\#$	PDI §
A1	5.2 / 0.271 / 0.037	20	> 0.99	30 (19)	1.16
A2	2.6 / 0.132 / 0.020	n.d.	0.82	44 (16)	1.17
A3	5.2 / 0.072 / 0.020	15	> 0.99	106 (72)	1.16
A4	3.7 / 0.052 / 0.007	20	0.96	145 (69)	1.15
A5	5.2 / 0.026 / 0.005	18	0.39	177 (77)	1.13
A6	2.6 / 0.021 / 0.004	46	0.85	176 (105)	1.13

$^+$ Monomer conversion; gravimetric analysis. $^\#$ Number-average degree of polymerization; 1H NMR endgroup analysis (cf. Figure 2-6), values in brackets correspond to the theoretical degree of polymerization as calculated by $x_p \cdot [AEMA]_0/[CPDB]_0$. § Polydispersity index; SEC (eluent: THF at 25 °C; stationary phase: SDV; detector: RI; calibration: PBMA).

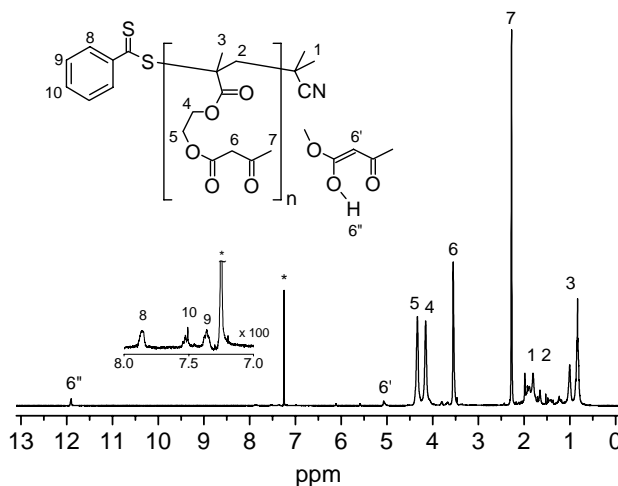


Figure 2-6. 1H NMR spectrum (400.1 MHz) of PAEMA sample A1 in $CDCl_3$ at 25 °C.

The 1H NMR spectrum of sample A1 in $CDCl_3$, shown in Figure 2-6, confirmed the expected chemical structure of PAEMA. The spectrum showed the characteristic signals of both acetoacetoxy tautomers (keto: $\delta = 2.3$ ppm; enol: $\delta = 5.1$ and 11.9 ppm, two possible enol forms), the first being the preferred structure (~92%). Virtually the same amount of keto/enol was found in polar aprotic solvents like $DMF-d_7$. The signals at $\delta = 0.8-1.2$ ppm arising from the

protons of the α -methyl groups of the backbone were used to determine the triad tacticity of the polymer:³⁹ $mm = 0.13$, $mr = 0.27$, and $rr = 0.60$ ($m = \text{meso}$, $r = \text{racemic}$).

Note that well-defined samples of PAEMA are available for the first time. Some of physical properties and a list of solvents and non-solvents are summarized in Table 2-5.

Table 2-5. Selected physical properties of PAEMA and list of solvents and non-solvents.

		sample	method
Density	1.2632 g cm ⁻³	A1	DENSITY OSCILLATION TUBE
Dipole moment	$\sim 8.1 \cdot 10^{-30}$ C m (2.4 D) per unit	A1	DIELECTRIC RELAXATION SPECTROSCOPY*
Glass Transition Temperature	276.1 ($\Delta c_p = 0.269$ J g ⁻¹ K ⁻¹)	A1	DIFFERENTIAL SCANNING CALORIMETRY
	276.5 ($\Delta c_p = 0.306$ J g ⁻¹ K ⁻¹)	A3	DIELECTRIC RELAXATION SPECTROSCOPY*
	274 K	A1	DIELECTRIC RELAXATION SPECTROSCOPY*
Thermal stability	up to ~ 460 K	A1, A3	THERMOGRAVIMETRIC ANALYSIS
Solubility parameter	21.2 (MPa) ^{1/2}		GROUP CONTRIBUTION METHOD (SMALL)
Solvents	chloroform, tetrahydrofuran, dioxane, methyl ethyl ketone, acetone, ethyl acetate, dimethyl formamide, dimethyl sulfoxide, trifluoroethanol, trifluoroacetic acid		
Non-solvents	cyclohexane, benzene, methanol, water		

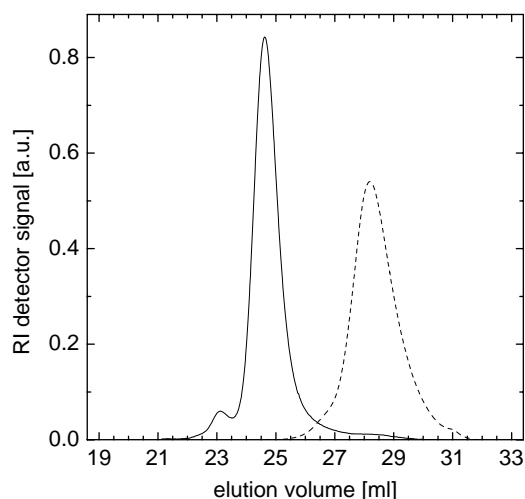
* P. Frübing, Applied Condensed-Matter Physics, University of Potsdam, Germany.

RAFT radical polymerization further promises to produce a large variety of block copolymers based on AEMA. Synthesized PAEMA samples carrying 2-cyano-prop-2-yl dithiobenzoyl endgroups were used as chain transfer agents for RAFT radical polymerization of a second monomer, namely methyl methacrylate (MMA), *n*-butyl (meth)acrylate (BMA and BA), and *N*-isopropylacrylamide (NiPAM).³² Among all these block copolymers synthesized, only the PAEMA-*b*-PBMA was used for further investigations on supramolecular assembly. Polymerization of BMA was carried out in the presence of PAEMA A1 using AIBN as the initiator in ethyl acetate at 60 °C. Experimental conditions and molecular characteristics of the isolated product are listed in Table 2-6. The SEC chromatogram of the copolymer and that of the corresponding PAEMA precursor are shown in Figure 2-7.

Table 2-6. Molecular characteristics of the PAEMA-*b*-PBMA copolymer, synthesized by RAFT radical polymerization of BMA using PAEMA sample A1 as chain transfer agent.

entry	[BMA] ₀ /[1] ₀ /[AIBN] ₀ (M)	time (h)	x_p^+	$f_{\text{BMA}}^{\&}$	$n^{\#}$	$m^{\$}$	PDI [§]
BA1	6.3 / 0.156 / 0.031	18	0.84	0.87	30	206	1.15

⁺ Monomer conversion; gravimetric analysis. [&] Mole fraction of BMA in the copolymer; ¹H NMR (400.1 MHz, CDCl₃, 25 °C). [#] Number-average degree of polymerization of PAEMA; ¹H NMR. ^{\$} Number-average degree of polymerization of PBMA; ¹H NMR. [§] Polydispersity index; SEC (eluent: THF at 25°C; stationary phase: SDV; detector: RI; calibration: PBMA).

**Figure 2-7.** SEC chromatograms (eluent: THF; flow rate: 1.0 mL min⁻¹; columns: 300 x 8 mm, 5 μm MZ-SDplus, 10³, 10⁵, 10⁶ Å; 25 °C; detector: RI) of PAEMA-*b*-PBMA sample BA1 (solid line) and the corresponding PAEMA precursor A1 (dashed line), as obtained by RAFT radical polymerization.

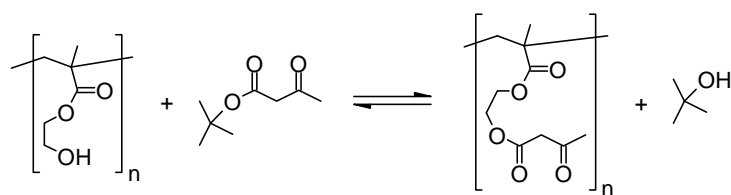
SEC results indicate that the PAEMA-*b*-PBMA product contains traces of unreacted PAEMA precursor (< 3 wt %; fraction eluting from 27 to 31 mL) and ~6 wt % of presumably recombined polymer chains (fraction eluting at ~23 mL), i.e. the purity of the diblock copolymer is greater than 93 %.

2.2.2 Acetoacetylation of poly(2-hydroxyethyl methacrylate)

The alternative method to prepare well-defined block copolymers based on AEMA was the transesterification or acetoacetylation of PHEMA segments with *tert*-butyl acetoacetate (*t*BAA), as illustrated in Scheme 2-6. The PBMA-*b*-PHEMA precursor polymers were synthesized by GTP of BMA and TMSHEMA (the trimethylsilyl-protected derivative of HEMA) and subsequent hydrolysis of the TMS group. Following a standard procedure described in the literature,⁴⁰ sequential polymerizations of BMA and TMSHEMA were performed at room temperature in tetrahydrofuran (THF) with 1-methoxy-1-trimethylsilyloxy-2-methyl-prop-1-ene (MTS) as the initiator and tetrabutylammonium bibenzoate (TBABB) as a nucleophilic

catalyst. ^1H NMR was used to confirm the chemical structure of the isolated products and to determine the mole fraction of comonomers. According to SEC, all block copolymers exhibit a monomodal and narrow molecular weight distribution ($\text{PDI} = 1.03\text{--}1.09$; cf. Table 2-7). TMS residues were then quantitatively removed by HCl-catalyzed hydrolysis at room temperature, as shown by the disappearance of $\text{Si}(\text{CH}_3)$ signals at $\delta = 0.1$ ppm in ^1H NMR spectra. Note that the triad tacticity of PHEMA prepared under GTP conditions is $mm = 0.14$, $mr = 0.41$, and $rr = 0.45$ (^1H NMR, DMSO-d_6).

Regarding the acetoacetylation of PBMA-*b*-PHEMA copolymers it has to be taken into consideration that these are equilibrium reactions (cf. Scheme 2-6). In order to achieve high yields of acetoacetylated HEMA (AEMA) units, the released *tert*-butyl alcohol should be removed from the reaction mixture. Performing the reaction in toluene at $130\text{ }^\circ\text{C}$ and distilling off the alcohol, a procedure first reported by Witzeman and Nottingham,⁴¹ 69-97% of HEMA units were acetoacetylated. Another method developed by us employed the removal of the *tert*-butyl alcohol within a ternary azeotrope with benzene and water. The azeotrope has a boiling point of $67.3\text{ }^\circ\text{C}$, and the acetoacetylation reaction can therefore be carried out at much milder conditions. In a typical procedure, a mixture of *t*BAA and PBMA-*b*-PHEMA ($[\textit{t}\text{BAA}]/[\text{HEMA}] \sim 1.5$) in benzene was stirred for 1 h at room temperature. Then, water was added and the solution was refluxed (usually overnight) in a liquid-liquid extraction apparatus to remove the aqueous phase (water + *tert*-butyl alcohol). The acetoacetylated products were finally isolated by precipitation into hexane.



Scheme 2-6. Transesterification of PHEMA segments with *tert*-butyl acetoacetate (*t*BAA).

As shown by ^1H NMR analysis (comparing the signal intensities of $-\text{OCH}_2-$ protons of BMA and AEMA units arising at $\delta = 3.92$ and $4.14/4.32$ ppm, respectively; cf. Figure 2-8), the degree of acetoacetylation of HEMA residues was always greater than 95%. SEC indicates that the narrow molecular weight distribution of PBMA-*b*-PHEMA copolymers was maintained during the acetoacetylation. As further seen from the chromatograms in Figure 2-9, the PBMA-*b*-PAEMA products elute faster in the SEC mode than the hydroxylated precursors, which is due to the somewhat larger hydrodynamic volume of the derivatized functional seg-

ment. The molecular characteristics of the PBMA-*b*-PAEMA copolymers obtained by GTP and subsequent azeotropic acetoacetylation are listed in Table 2-7.

It should be mentioned that PAEMA homopolymers cannot be prepared by this method as both the PHEMA precursor as well as the acetoacetylated product are not soluble in benzene solution.

Table 2-7. Molecular characteristics of PBMA-*b*-PAEMA copolymers, synthesized by sequential Group Transfer Polymerization (GTP) of BMA and TMSHEMA and subsequent acetoacetylation of HEMA residues.

entry	$f_{\text{BMA}}^{\&}$	m^{\S}	$n^{\#}$	PDI §	residual HEMA units (mol %)
BA2	0.90	342	39	1.05	< 5
BA3	0.85	58	10	1.07	< 5
BA4	0.78	80	22	1.03	< 5
BA5	0.55	76	60	1.09	< 5

$\&$ Mole fraction of BMA in the copolymer; ^1H NMR analysis (400.1 MHz, CDCl_3 , 25 °C) of PBMA-*b*-PTMSHEMA. § Number-average degree of polymerization of PBMA; SEC analysis (eluent: THF at 25°C; stationary phase: SDV; detector: RI; calibration: PBMA) of the PBMA precursor, which was isolated prior to the addition of the second monomer. $^{\#}$ Number-average degree of polymerization of PAEMA; ^1H NMR. § Polydispersity index; SEC.

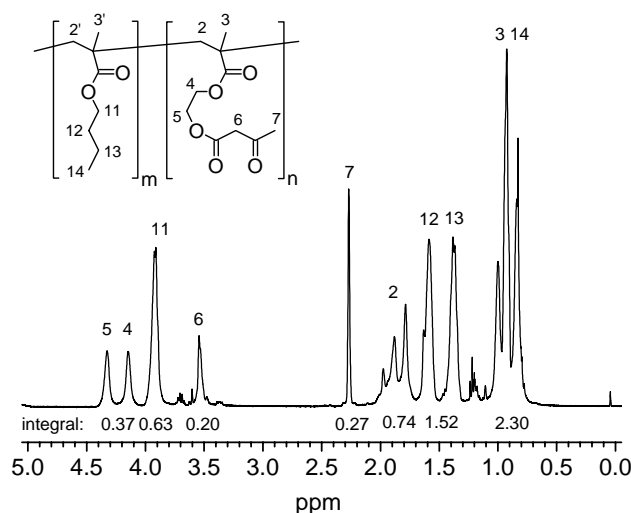


Figure 2-8. ^1H NMR spectrum (400.1 MHz) of PBMA-*b*-PAEMA sample BA4 in CDCl_3 at 25 °C.

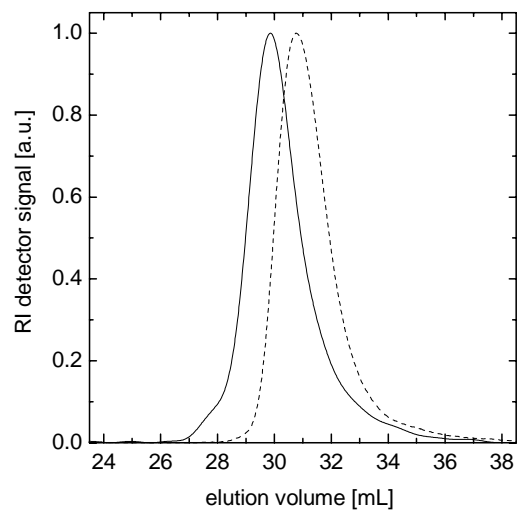


Figure 2-9. SEC chromatograms (eluent: DMA + 0.5 wt % LiBr; flow rate: 1.0 mL min⁻¹; columns: 300 x 8 mm, 10 μ m PSS-GRAM, 30, 30, 100, 3000 \AA ; 70 $^{\circ}$ C; detector: RI) of PBMA-*b*-PAEMA BA4 (solid line) obtained by the azeotropic acetoacetylation of PBMA-*b*-PHEMA (dashed line) with *t*BAA.

2.3 Polypeptide block copolymers

Linear polypeptide block copolymers can be obtained via (i) a SOLID-STATE PEPTIDE SYNTHESIS (Merrifield synthesis) and subsequent coupling with a carboxylated polymer⁴² or (ii) a RING-OPENING POLYMERIZATION of α -amino acid *N*-carboxyanhydrides (NCA) initiated by a primary amino-functional macroinitiator⁴³ or a transition metal-based system.^{44,45} The first method enables one to synthesize very well-defined samples with a perfectly monodisperse polypeptide segment. Disadvantageously, it is a costly and time-consuming process producing polypeptides in rather low yields. The primary amine-initiated polymerization of NCA, on the other hand, is experimentally less demanding and allows one to synthesize polymer materials on a several gram scale. Due to the rather complex mechanism of the reaction (see chapter 2.3.2), the resulting polypeptides sometimes exhibit a very broad molecular weight distribution ($PDI > 2$).⁴⁶ A careful fractionation of crude products is therefore required in order to obtain copolymer fractions with a narrow distribution. With transition metal complex initiators, which are rather difficult to handle compounds, polypeptides with $PDI < 1.2$ can be obtained.⁴⁴

Note that it was a goal to synthesize not only linear but also hetero star-shaped samples of the AB_y type (B denoting the polypeptide segment). For obvious reasons, copolymers of the latter structure are not accessible by a solid-state synthesis and coupling on a solid support. The method of choice is the grafting of polypeptide arms from an ω -polyamino-functional macroinitiator *via* NCA polymerization. Due to expected experimental problems, transition metal complex macroinitiators were not investigated.

In the following chapter 2.3.1 will first be described the anionic synthesis and characterization of mono- and polyamino-functional polymers,⁴⁷ which served as the macroinitiators for the polymerization of NCAs. Most polypeptide block copolymers were prepared according to a standard recipe from literature,⁴⁸⁻⁵⁰ synthetic procedures will briefly be described in the first part of chapter 2.3.2. More emphasis will lie on the complete molecular characterization of (linear) copolymer samples.⁵¹ Note that no adequate procedures have so far been reported that allow determination of absolute molecular weight distributions.¹⁷ As will be shown, advanced SIZE EXCLUSION CHROMATOGRAPHY (SEC) can provide this information, making it possible to evaluate the level of control in NCA polymerization. In the last part of the chapter will be described a novel approach for a controlled polymerization of NCAs, by which nearly monodisperse block copolymers can be obtained.^{51,52}

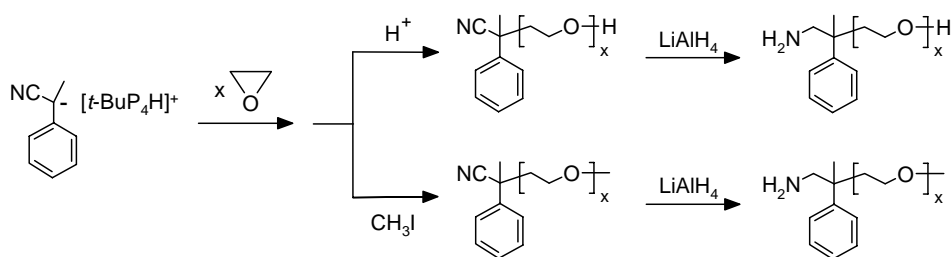
2.3.1 ω -Amino-functional macroinitiators

Various ω -amino-functional polymers based on ethylene oxide,²⁹ styrene, and butadiene⁴⁷ were prepared employing living ANIONIC POLYMERIZATION techniques. The synthetic procedures, which will be described in the following subchapters, are significant improvements of existing procedures. Not included in this work is the first synthesis of primary amino-end-functionalized polyacrylates by RAFT RADICAL POLYMERIZATION.⁵³

2.3.1.1 Monoamino-functional poly(ethylene oxide)s

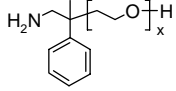
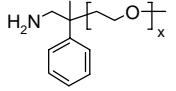
The preferred route for the preparation of functionalized poly(ethylene oxide)s (PEO) is the anionic ring-opening polymerization of ethylene oxide using suitable initiators or terminating agents.⁵⁴ Note that the controlled polymerization of oxiranes requires larger counterions than lithium, and thus potassium alkoxides and amides are the most commonly employed initiators.²² Other effective initiating systems are metalloporphyrins⁵⁵ as well as carbanions^{27,56} and alkoxides⁵⁷ with bulky organic counterions generated from the phosphazene *t*-BuP₄. Note that *t*-BuP₄ is a very strong base with $pK_a = 30.2$ (DMSO), which upon protonation gives a very soft and bulky cation of ~ 14 Å in diameter.⁵⁸ It might therefore be used to prepare a variety of novel metal-free anionic initiators with diverse functionalities from readily available protic and CH-acidic compounds. Also, due to the known counterion effects on ion pair association and reactivity,²² the use of [*t*-BuP₄H]⁺ instead of smaller metal counterions should lead to considerably higher polymerization rates.

A novel route towards primary amino-endfunctional PEOs is shown in Scheme 2-7.²⁹ The initiating system of choice was α -methylbenzyl cyanide/*t*-BuP₄ to produce an α -cyano-PEO in the first step. Subsequent reduction of the cyano group with lithium aluminiumhydride led to the primary amino-functional group.⁵⁹ Depending on whether acetic acid or methyl iodide was used to quench ethylene oxide polymerization, the PEO chains carried either a hydroxyl or a methoxy group at the ω -chain end.⁶⁰ Results are summarized in Table 2-8.



Scheme 2-7. Synthesis of primary amino-endfunctional (heterotelechelic) poly(ethylene oxide)s.

Table 2-8. Molecular characteristics of primary amino-functional PEO samples, as prepared by anionic ring-opening polymerization of ethylene oxide with α -methylbenzyl cyanide/*t*-BuP₄ and subsequent reduction of α -terminal cyano groups with LiAlH₄.

chemical structure	entry	$x^{\#}$	PDI [§]	$f_{\text{amino}}^{\&}$
	E1	53	1.04	1.0
	E2	109	1.06	1.0

[#] Number-average degree of polymerization; SEC (eluent: CHCl₃ at 25 °C; stationary phase: SDV; detectors: RI/UV; calibration: PEO). [§] Polydispersity index; SEC. [&] Degree of amino-functionalization; SEC; ¹³C NMR (100.6 MHz, CDCl₃, 25 °C), considering the signal at 123 ppm of residual cyano moieties.

The synthetic procedure was as follows: α -methylbenzyl cyanide was added to a solution of *t*-BuP₄ in tetrahydrofuran (THF) at -70 °C. Then, ethylene oxide was condensed into the reactor. The reaction solution was stirred for 1 hour at -70 °C, then slowly warmed to $+45$ °C and kept at this temperature for 20 hours under a dry argon atmosphere. The reaction was quenched by the addition of either acetic acid (\rightarrow sample E1') or methyl iodide (\rightarrow sample E2'). In the latter case, a 20-fold excess of the terminating agent with respect to the initiator was employed, and the solution was stirred for three days at room temperature.⁶⁰ The solvent was then evaporated to dryness, and the residue was re-dissolved in water. The aqueous polymer solution was washed three times with the strongly acidic cation exchanger DOWEX 50WX4-100 (Sigma) to extract protonated phosphazene, ultrafiltered with bi-distilled water (molecular weight cut-off: 1 kDa), and freeze-dried.

Gravimetric analyses indicated that after 20 hours a monomer conversion was greater than 90%. Note that with K⁺ as the counterion, reaction times would have been in the range of days.⁶⁰ According to SEC, samples E1' and E2' had a very narrow molecular weight distribution (polydispersity index, PDI < 1.1, see Table 2-8 and Figure 2-10). Molecular weights were close to the calculated ones, indicating a high efficiency of the α -methylbenzyl cyanide initiator. Quantitative analysis of UV and RI detector traces also suggested that the average number of aromatic initiator units per polymer chain was equal to unity (see Figure 2-10). ¹³C NMR analyses (100.6 MHz, CDCl₃, 25 °C) confirmed the expected chemical structure of the samples; characteristic signals of terminal functional groups were observed at $\delta/\text{ppm} = 123.0$ ($-\text{C}\equiv\text{N}$), 72.5, 61.8 ($-\text{CH}_2\text{CH}_2\text{OH}$) (E1') and 124.4 ($-\text{C}\equiv\text{N}$), 73.0, 59.4 ($-\text{CH}_2\text{CH}_2\text{OCH}_3$) (E2').^{54,59} It should be emphasized that the NMR spectrum of E2' did not reveal any trace of

hydroxyl chain ends. These results were further supported by MATRIX-ASSISTED LASER DESORPTION/IONIZATION TIME-OF-FLIGHT MASS SPECTROMETRY (MALDI-TOF MS)⁶¹. In the mass spectrum of E2', just a single homologous series with $\Delta m = 44.0$ Da (molar mass of an ethylene oxide repeating unit) could be observed. The residual mass (*r.m.*) of PEO chains was found to be 144.8 Da, almost exactly matching the calculated molar mass of cyano and methyl endgroups ($m(\text{C}_9\text{H}_8\text{N}) + m(\text{CH}_3) = 145.11$ Da).

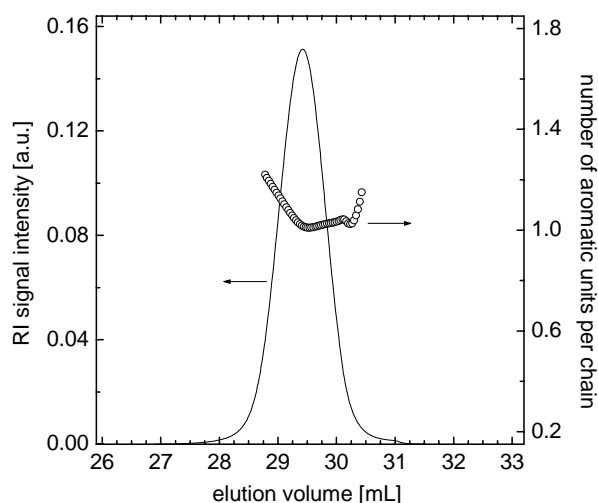


Figure 2-10. SEC chromatogram (eluent: CHCl_3 ; flow rate: 1.0 mL min^{-1} ; columns: $300 \times 8 \text{ mm}$, $5 \mu\text{m}$ MZ-SDplus, 10^3 , 10^5 , 10^6 \AA ; $25 \text{ }^\circ\text{C}$; detector: UV and RI) of PEO sample E1' (line: normalized RI signal intensity; circles: average number of aromatic initiator units per PEO chain). The absolute concentration of aromatic units in an SEC slice was determined applying Lambert-Beer's law from the UV detector output and a detector calibration constant; the detector was calibrated with an α -methylbenzyl cyanide standard solution. The concentration of polymer chains was calculated from the ratio of the normalized RI signal intensity over the molecular weight of the eluting PEO fraction.

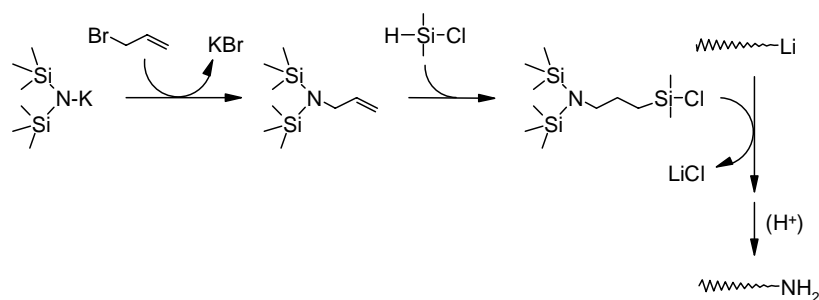
For the preparation of primary amino-terminal PEOs, solutions of E1' (\rightarrow E1) and E2' (\rightarrow E2) in THF were slowly added to a stirred suspension of lithium aluminumhydride in THF ($[\text{LiAlH}_4]/[-\text{CN}] \sim 20$). Mixtures were heated to reflux and stirred for 2 hours under an argon atmosphere.⁵⁹ After cooling to room temperature, the reaction mixture was quenched with water, ultrafiltrated, and freeze-dried. The ^{13}C NMR spectra of samples E1 and E2 did not show a signal at $\delta \sim 123.0$ ppm, indicating quantitative reduction of the cyano group. The signal of the methylene carbon atom next to the amino functional group was observed at $\delta = 51.4$ and 54.4 ppm, respectively. However, sample E2 was found to contain ~ 30 mol % of hydroxylated PEO chains (additional signals arising at $\delta = 72.3$ and 62.0 ppm, see above), which had not been observed for the precursor polymer E2'. A reasonable explanation for the occurrence of ether cleavage cannot be given at the moment.

Since alcohols are known as slow initiators for NCA polymerization,⁶² samples E1 and E2 were not suited for the preparation of PEO-polypeptide diblock copolymers. Instead it was used a commercial α -methoxy- ω -amino-PEO sample (Aldrich, product # M4147) with MW \sim 5 kg/mol (\rightarrow sample EL1 and EG1, Table 2-11).

2.3.1.2 Monoamino-functional polystyrenes and polybutadienes

In order to prepare well-defined polymers with a high degree of functionalization, living anionic polymerization was usually applied using either functionalized initiators or termination agents.⁶³⁻⁶⁷ It should be emphasized that any of these reactions demands high-purity experimental conditions and a suitable masking of the functional groups.²² The most general and efficient procedures for the ω -endfunctionalization of polystyrenes and polydienes include the capping of living polymeric anions with 1,1-diphenylethylene derivatives⁶⁸ or the termination with ω -functional- α -haloalkanes⁶⁹ or ω -chlorosilanes.⁷⁰ Here, the latter was the methodology of choice.

Chlorosilane derivatives bearing a bis(trimethylsilyl)amino group have so far been prepared in a three-step procedure in less than 40% yield.⁷⁰ It was possible to modify the process and to obtain 1-(chlorodimethylsilyl)-3-[*N,N*-bis(trimethylsilyl)amino]-propane (CAP) from readily available reagents in just two steps in a 46% yield (cf. Scheme 2-8).⁴⁷



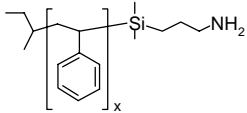
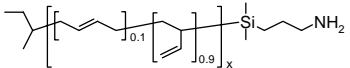
Scheme 2-8. Synthesis of 1-(chlorodimethylsilyl)-3-[*N,N*-bis(trimethylsilyl)amino]-propane (CAP) used to prepare ω -primary amino-functional polystyrenes and polybutadienes.

In the first step, 3-[*N,N*-bis(trimethylsilyl)amino]-1-propene was synthesized by nucleophilic substitution of allyl bromide with potassium *N,N*-bis(trimethylsilyl)amide (yield: 66%; colorless liquid; bp 82 °C at 30 mbar; ¹H NMR: δ /ppm = 0.0-0.3 (m, 18H, $-\text{Si}(\text{CH}_3)_3$), 3.44 (d, $J = 4.6$, 2H, $-\text{CH}_2\text{N}-$), 5.04 (dd, $J = 10.1, 17.2$, 2H, $\text{CH}_2=$), 5.78 (m, 1H, $=\text{CH}-$)).⁷¹ The *N*-allyl disilazane intermediate was then hydrosilylated with chlorodimethylsilane using chloroplatinic acid as the catalyst to afford CAP as a colorless liquid (bp 104 °C at 1 mbar) in 69 % yield.⁷⁰ The chemical structure of CAP was confirmed by ¹H NMR: δ /ppm = 0.0-0.3 (m, 18H,

–NSi(CH₃)₃), 0.43 (s, 6H, ClSiCH₃), 0.72 (m, 2H, ClSiCH₂–), 1.45 (m, 2H, –CH₂–), 2.75 (m, 2H, –CH₂N–).

A series of ω-amino-endfunctional polystyrenes (PS) and polybutadienes (PB) was prepared by quenching the solutions of either polystyryl lithium (~20 wt % in cyclohexane) or polybutadienyl lithium (~2 wt % in tetrahydrofuran, THF) with a solution of the freshly distilled CAP (1.2 mol equiv with respect to lithiated chain ends, + 5 mol % *s*BuLi to remove last traces of impurities) in THF. Subsequent removal of the trimethylsilyl (TMS) protecting group was achieved by HCl-catalyzed hydrolysis at room temperature. ¹H NMR spectra of the final products were in accordance with the expected chemical structure (PB; microstructure: 90% 1,2 and 10% *trans*-1,4), and the lack of TMS signals at δ ~ 0.2 ppm confirmed the complete removal of the protecting groups. According to ¹H NMR analysis, considering the areas beneath the signals of end groups at δ = 0.5–1.0 (*s*-butyl, 8H) and –0.2–0.1 ppm (–Si(CH₃)₂CH₂–, 8H), and LACCC measurements (LACCC = LIQUID ADSORPTION CHROMATOGRAPHY AT CRITICAL CONDITIONS,⁷² cf. Figure 2-11), the degree of functionalization of the samples was usually greater than 90%. The molecular characteristics of ω-amino-functional polymer samples are summarized in Table 2-9.

Table 2-9. Molecular characteristics of ω-amino-functional PS and PB^s samples, as prepared by anionic polymerization and termination with CAP.

chemical structure	entry	$x^{\#}$	PDI [§]	$f_{\text{amino}}^{\&}$	method
	S1	57	1.04	0.94 >0.95	¹ H NMR LACCC*
	S2	217	1.03	0.90	LACCC*
	B1	27	1.10	0.95	¹ H NMR
	B2	85	1.08	0.87	¹ H NMR
	B3	119	1.08	0.95	¹ H NMR

^s Microstructure: 90% 1,2 and 10% *trans*-1,4; ¹H NMR (400.1 MHz, CDCl₃, 25 °C). [#] Number-average degree of polymerization; SEC (eluent: THF at 25 °C; stationary phase: SDV; detectors: RI/UV; calibration: PS and PB-1,2, respectively). [§] Polydispersity index; SEC. [&] Degree of amino-functionalization; ¹H NMR, LACCC (eluent: THF/*n*-hexane 60/40 (w/w) at 45 °C; stationary phase: SGX NH₂; detector: ELSD). * Dr. J. Falkenhagen, Bundesanstalt für Materialforschung und –prüfung (BAM), Berlin, Germany.

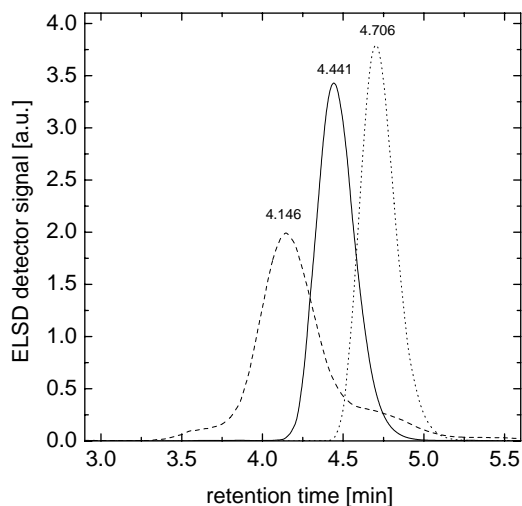
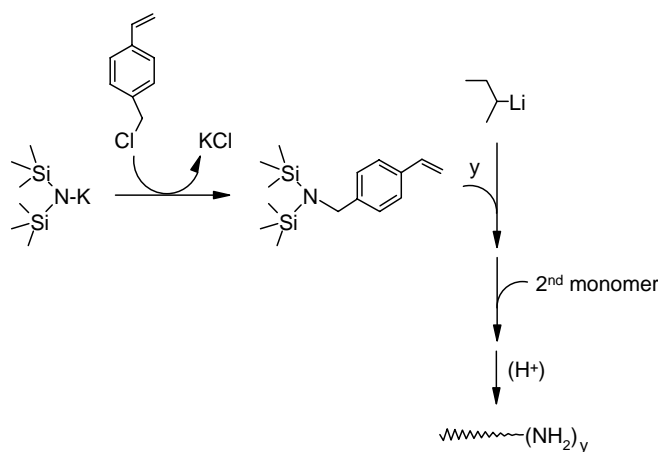


Figure 2-11. LACC chromatograms (eluent: THF/*n*-hexane 60/40 (w/w); flow rate: 0.5 mL min⁻¹; column: 250 x 4 mm, 7 μm SGX NH₂, 120 Å; 45 °C; detector: ELSD) of ω-amino-functional PS samples S1 (solid line) and S2 (dashed line). Note that under the critical conditions established for the H-terminated PS precursors (dotted line), any fraction of non-functionalized polymer chains elute at 4.7 minutes independent of molecular weight, whereas the ones carrying an amino functional group elute faster in the SEC mode.

2.3.1.3 Polyamino-functional polystyrenes

There are two different ways to synthesize polyamino-endfunctional polymers *via* ANIONIC POLYMERIZATION, namely (i) the initiation or termination of the polymerization with reagents carrying more than one masked amino group and (ii) the sequential copolymerization of an amino-functional monomer (see Scheme 2-9). The latter method is the preferred one because it is experimentally much less demanding. However, the better availability of block copolymers is at the expense of perfect control of the degree of amino-functionalization, i.e., macro-initiators exhibit an average number of amino endgroups with a Poisson distribution at the best.

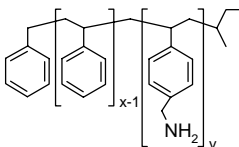


Scheme 2-9. Synthesis of 4-[*N,N*-bis(trimethylsilyl)aminomethyl]-styrene (TMSAMS) used to prepare ω-polyamino-functional polystyrenes.

The functional monomer of choice was 4-[*N,N*-bis(trimethylsilyl)aminomethyl]-styrene (TMSAMS), which can be readily prepared by nucleophilic substitution of 4-chloromethylstyrene with potassium *N,N*-bis(trimethylsilyl)amide in hexamethyldisilazane (see Scheme 2-9).⁴⁷ The product was isolated as a clear, colorless liquid in a 43 % yield (bp 72 °C at 0.05 mbar), ¹H NMR: δ /ppm = 0.07 (s, 18H, –Si(CH₃)₂), 4.08 (s, 2H, –CH₂N–), 5.18, 5.70 (2d, J = 11, 18 Hz, 2H, –CH₂=), 6.69 (dd, –CH=), 7.20, 7.33 (dd, 4H, CH-phenyl). It should be emphasized that this reaction pathway considerably facilitates the synthesis of amino-functional monomers. TMSAMS had so far been prepared in a three-step reaction from chloromethyl methyl ether, lithium *N,N*-bis(trimethylsilyl)amide, and 4-vinylphenyl magnesiumchloride.⁷³

Four samples of PAMS-*b*-PS copolymers were prepared by sequential anionic polymerization of TMSAMS and styrene in THF at –78 °C using *s*BuLi as the initiator⁷³—their molecular characteristics are listed in Table 2-10. The TMS protecting groups were removed by HCl-catalyzed hydrolysis as described above. ¹H NMR confirmed the expected chemical structure of copolymers, δ /ppm = 0.5-1.0 (m, CH₂, CH₃, *s*-butyl), 1.3-2.4 (m, CH, CH₂), 3.8-4.2 (m, –NCH₂–), 6.2-6.9 (m, *m*-CH, phenyl), 6.9-7.3 (m, *o/p*-CH, phenyl). SEC analysis showed that the (TMS-protected) block copolymers have a narrow molecular weight distribution (PDI = 1.08-1.14) and are free of PAMS precursor. MALDI-TOF mass spectrometric measurements enabled the determination of the absolute number-average degree of polymerization of the PAMS homopolymer precursors ($\Delta m = 133.4$ Da, *r.m.* = 58.3 Da, expected: 133.1 and 58.0 Da, respectively; cf. Figure 2-12), which is equal to the average amino-functionality of the copolymer.

Table 2-10. Molecular characteristics of PAMS-*b*-PS copolymers (ω -polyamino-functional PS), as prepared by sequential anionic polymerization of TMSAMS and styrene.

chemical structure	entry	$x^{\#}$	$y^{\&}$	PDI [§]
	S4	182	4.3	1.13
	S5	63	8.0	1.08
	S6	193	7.7	1.14
	S7	188	12.6	1.14

[#] Number-average degree of polymerization of the PS block; ¹H NMR (400.1 MHz, CDCl₃, 25 °C). [&] Number-average degree of polymerization of PAMS (precursor sample was isolated prior to the addition of the second monomer); MALDI-TOF MS (matrix: 2,5-dihydroxy benzoic acid, cation: Ag⁺). [§] Polydispersity index; SEC analysis (eluent: THF at 25 °C; stationary phase: SDV; calibration: PS) of TMS-protected block copolymers.

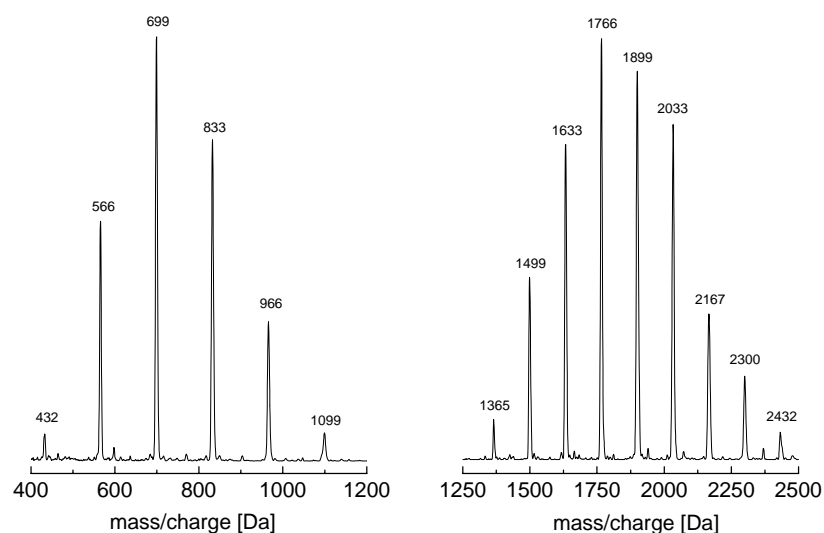


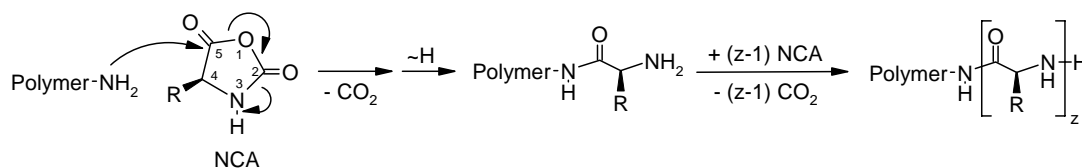
Figure 2-12. MALDI-TOF mass spectra (N_2 laser operating at 337 nm; linear mode; matrix: 2,5-dihydroxy benzoic acid; cation source: silver trifluoroacetate; calibration: bovine insulin) of the PAMS precursors ($[M-Ag]^+$) of copolymers S4 (left), and S7 (right).

However, all attempts failed to achieve a living/controlled polymerization of 1,3-butadiene as the second monomer.

2.3.2 Polypeptide block copolymers

2.3.2.1 Conventional synthesis and characterization

For a synthesis of polypeptide-based block copolymers, the polymerization of an *N*-carboxyanhydride (NCA) should proceed *via* the nucleophilic ring-opening of the NCA at the C-5 position. This process, which is called the “amine” mechanism, is depicted in Scheme 1.⁶² Linear or star-shaped block copolymers are obtained depending on whether monoamino- or polyamino-endfunctional polymers were used to initiate the polymerization of the NCA.



Scheme 2-10. Ring-opening polymerization of an NCA *via* the “amine” mechanism.

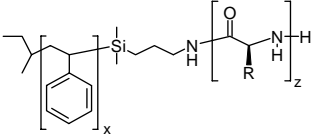
The NCAs of *N*^ε-benzyloxycarbonyl (*Z*)-L-lysine (ZLLys) and γ -benzyl-L-glutamate (BLGlu) were prepared by the Fuchs-Farthing method using bis(trichloromethyl)carbonat (triphosgene) as the phosgenation agent.⁷⁴ The reaction was performed in THF as the solvent at 40 °C. The crude products were purified by repeated re-crystallization from a THF/petrolether 1:2 (v/v) mixture prior to use and were dried in high vacuum at room temperature. The chemical structure and purity of NCAs was checked by ¹H NMR and measurement of melting points.

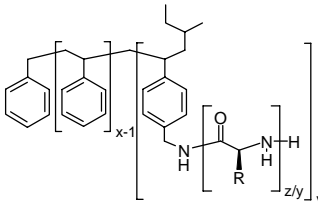
The primary amino-functional macroinitiator (see Table 2-9 and Table 2-10) and the NCA were placed in separate flasks and dried in high vacuum for 1 hour at room temperature. *N,N*-dimethylformamide (DMF) was then cryo-distilled from CaH₂ into the flasks (chloroform was used to dissolve PB macroinitiators), and the two solutions were combined *via* a transfer needle to give a ~8 wt % reaction mixture. Polymerizations were performed at 40 °C for at least 2 days under a dry argon atmosphere. After evaporation of the solvent in high vacuum, the residual solid was dissolved in CHCl₃ and precipitated in either petrolether or methanol. Macroinitiator contaminants in the copolymer samples were removed by the extraction with cyclohexane (→ PS) or petrolether (→ PB). Finally, block copolymers were dried in vacuum at 35-40 °C to constant weight.

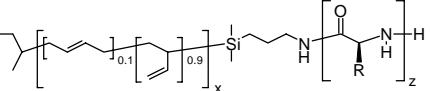
A list of linear and star-shaped block copolymers prepared by this procedure is provided in Table 2-11. As indicated by SEC and ANALYTICAL ULTRACENTRIFUGATION (AUC) (selected samples), samples were free of any homopolymer contaminants. ¹H NMR was applied to confirm the chemical structure (see Figure 2-13) and to determine the absolute number-average degree of polymerization or molecular weight (M_n) of the block copolymers. Note that under the chosen conditions, samples were dissolved on a molecular level and were not forming aggregates. The spectra of star-shaped copolymer samples did not show a signal of residual benzyl amino groups at $\delta \sim 4$ ppm (see Figure 2-13) indicating that the number of polypeptide grafts should be equal to the functionality of the corresponding macroinitiator. However, it cannot completely be excluded that residual benzyl amine signals were buried under some signals of the polypeptide backbone.

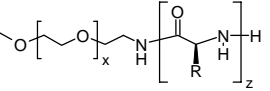
According to a standard SEC analysis (eluent: DMA + 0.5 wt % LiBr at 70 °C, stationary phase: PSS-GRAM polyester gel) applying a calibration recorded with PS standards, the samples exhibited a rather broad molecular weight distribution with apparent PDI values in the range of 1.2-1.8. It was, however, not possible to characterize the PB-containing block copolymers by SEC employing either THF or CHCl₃ as a common solvent (stationary phase: SDV). Assumably due to a large effective dipole moment arising from the polypeptide α -helix ($\mu = 3.5$ D per monomer unit),⁷⁵ samples were quantitatively adsorbed onto the SDV columns.

Table 2-11. Molecular characteristics of the linear and star-shaped polypeptide block copolymers, as prepared by “conventional” ring-opening polymerization of the *N*-carboxyanhydride of Z-L-lysine (ZLLys) or γ -benzyl-L-glutamate (BLGlu) using the ω -primary amino-functional macroinitiators listed in Table 2-9 (\rightarrow linear) and Table 2-10 (\rightarrow star-shaped).

chemical structure	sample	$x^{\#}$	z^{\S}	$y^{\&}$	PDI §
 R = (CH ₂) ₄ NHC(O)OBzl; ZLLys (SL1-SL3) R = (CH ₂) ₂ C(O)OBzl; BLGlu (SG1-SG2)	SL1	52	69	1	1.4
	SL2	52	111	1	1.4
	SL3	217	93	1	1.3
	SG1	52	104	1	1.3
	SG2	57	274	1	1.5

 R = (CH ₂) ₄ NHC(O)OBzl; ZLLys (SL1*-SL6*) R = (CH ₂) ₂ C(O)OBzl; BLGlu (SG1*-SG2*)	SL*1	182	243	(4)	1.8 ^a
	SL*2	193	65	(8)	1.3
	SL*3	193	255	(8)	1.6 ^a
	SL*4	188	54	(12)	1.2
	SL*5	188	123	(12)	1.4
	SL*6	188	227	(12)	1.5 ^a
	SG*1	63	176	(8)	1.4
	SG*2	63	293	(8)	1.6 ^a

 R = (CH ₂) ₂ C(O)OBzl; BLGlu (BG1-BG4)	BG1	27	64	1	–
	BG2	85	75	1	–
	BG3	85	55	1	–
	BG4	119	24	1	–

 R = (CH ₂) ₄ NHC(O)OBzl; ZLLys (EL1) R = (CH ₂) ₂ C(O)OBzl; BLGlu (EG1)	EL1	114	40	1	1.2
	EG1	114	31	1	1.2

[#] Number-average degree of polymerization of the first block segment (macroinitiator). [&] Number of polypeptide arms of the block copolymer (\equiv amino functionality of the macroinitiator). [§] Number-average degree of polymerization of the polypeptide segment; ¹H NMR (400.1 MHz, DMF-d₇ (SL), CDCl₃ (SG, BG), DMSO-d₆ (EL) 25 °C). [§] Polydispersity index; SEC (eluent: DMA + 0.5 wt % LiBr at 70 °C, stationary phase: PSS-GRAM, calibration: PS), ^a multimodal.

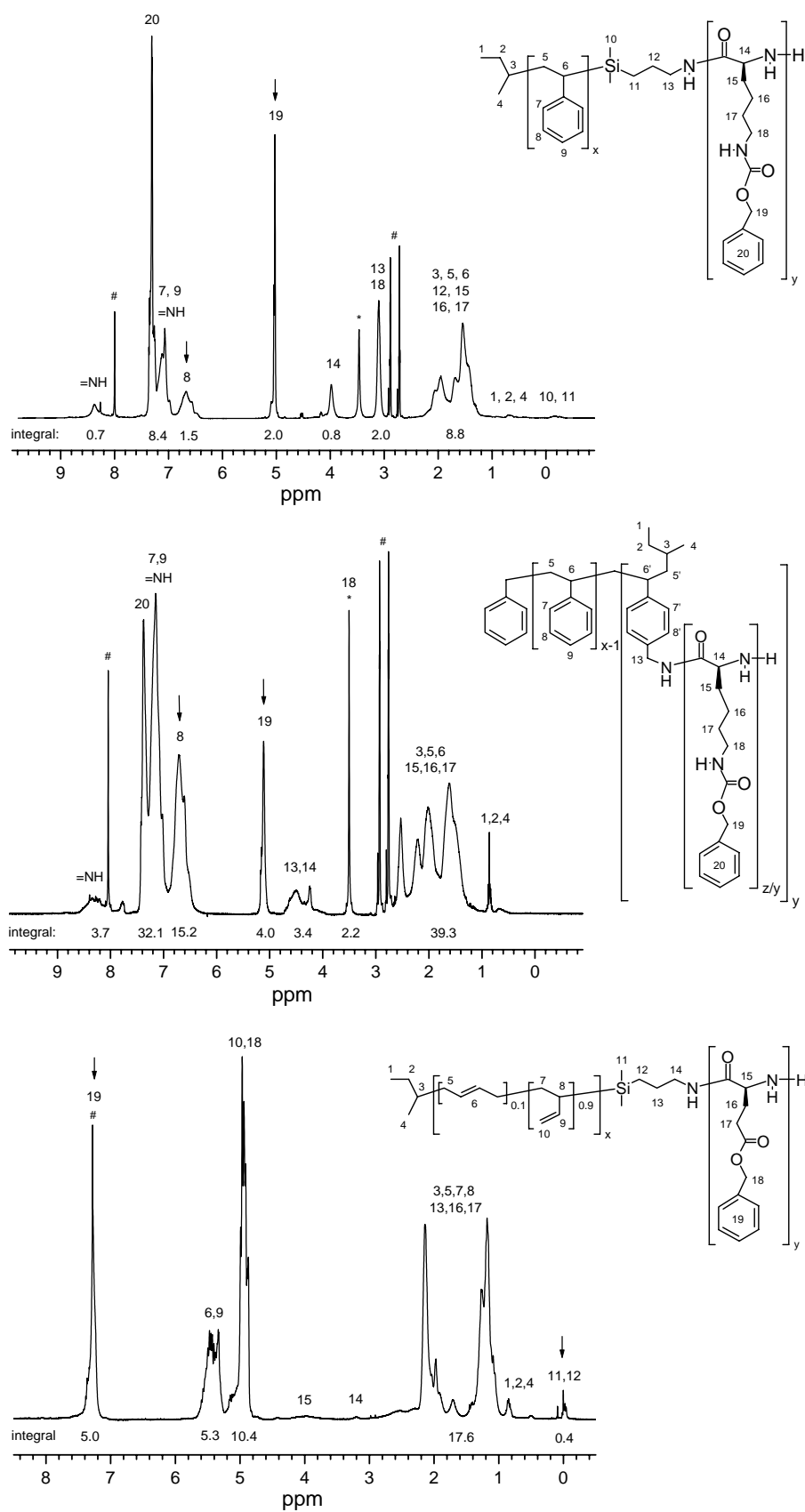


Figure 2-13. ^1H NMR spectra (400.1 MHz) of PS-*b*-PZLLys samples SL1 and SL*4 (DMF- d_7 , 25 °C) and PB-*b*-PBLGlu sample BG4 (CDCl $_3$, 25 °C) (top to bottom). Signals denoted with # and * correspond to protonated solvent and water traces, respectively. Signals marked with ↓ were used to determine the molar ratio of comonomers.

2.3.2.2 Advanced characterization of block copolymers

The linear block copolymer samples exhibited all monomodal distributions (see Figure 2-16) and showed the expected elution behavior in an SEC mode. In the case of star-shaped samples, chromatograms were only monomodal when the number of peptide units was less than 200 (see Table 2-11). Above this limit, bimodal or even multimodal chromatograms were obtained (see Figure 2-14). Additionally, some fraction of polymer chains was eluting after the corresponding macroinitiator. It is therefore evident that fractionation was not only driven by size exclusion but also by adsorption phenomena.

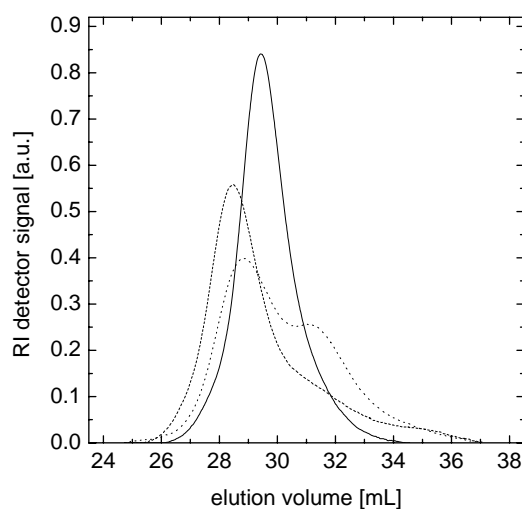


Figure 2-14. SEC chromatograms (eluent: DMA + 0.5 wt % LiBr at 70 °C, stationary phase: PSS-GRAM, detector: RI) of the star-shaped PS-*b*-PZLLys samples SL*4 (solid line), SL*6 (dashed line), and SL*1 (dotted line).

One should take into consideration that the samples might not only be polydisperse with respect to molecular weight but also with respect to conformation or secondary structure. Since polypeptide β -sheets are usually less soluble than α -helices,⁶² a β -sheet containing polymer fraction might rather elute in the adsorption than in the size exclusion mode. Also the hydrodynamic properties of polypeptides might depend very much on their secondary structure. In order to examine the secondary structure of different chromatographic fractions, the bimodal sample SG*2 was analyzed by SEC with a FOURIER TRANSFORM-INFRARED SPECTROSCOPY (FT-IR) device (see Figure 2-15).⁷⁶ Indeed, the faster eluting fraction was found to contain exclusively α -helical polypeptide chains ($\tilde{\nu}_{\text{C=O, amide I}} = 1651 \text{ cm}^{-1}$), whereas in the second fraction α -helices and β -sheets ($\tilde{\nu}_{\text{C=O, amide I}} = 1625 \text{ cm}^{-1}$) could be identified.^{77,78}

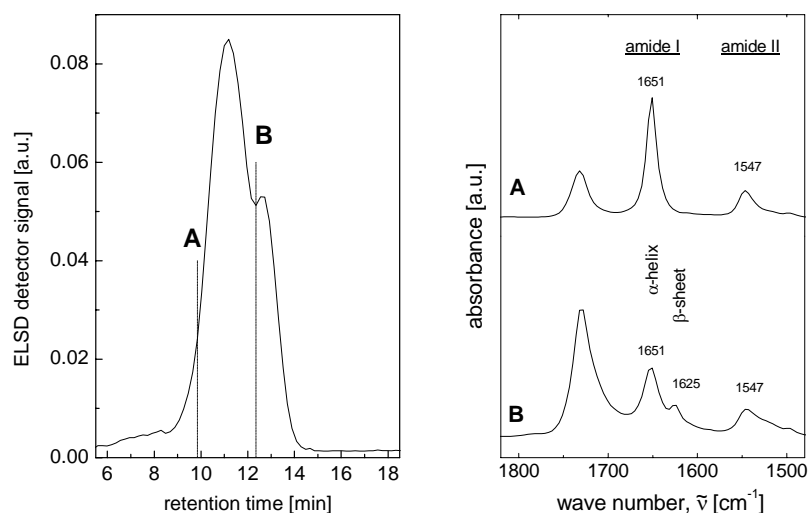


Figure 2-15. SEC chromatogram (eluent: DMA/*iso*-propanol 90:10 (v/v), stationary phase: RP 18, 65 °C) (left) of the PS-*b*-PBLGlu sample SG*2 and FT-IR spectra (right) of the fractions eluting at 9.84 (A) and 12.35 minutes (B).

Due to a superposition of two different distributions, molecular weight and conformation, the true molecular weight distribution of block copolymer samples cannot be determined by a conventional SEC analysis. In principle, 2D-CHROMATOGRAPHY (i.e. coupling of LACCC and SEC) would be suited to treat such a problem,^{79,80} but so far it was not possible to establish critical conditions allowing to separate polypeptide β -sheets from α -helices. It was therefore attempted to racemize peptide units, aiming to convert the secondary structure of the polypeptide chains into a random coil. Indeed, as shown by CIRCULAR DICHROISM SPECTROSCOPY (CD), treatment with lithium diisopropylamide (LDA) or phosphazene base *t*-BuP₄ afforded racemization of L-peptides and thus destruction of α -helical or β -sheet secondary structures. However, reaction was sometimes accompanied by a partial hydrolysis of the protecting groups. Note that this side reaction must strictly be avoided because the SEC elution behavior might then be affected by the presence of free amino (Lys) or carboxyl groups (Glu). So far, it was not possible to isolate the pure racemic isomers of polypeptide block copolymers. At this point, however, it seemed not reasonable to continue SEC analysis of the star-shaped copolymer samples.

Secondary structure effects seemed not to play an important role for the SEC fractionation of the linear block copolymers. It was therefore decided to focus on the characterization of the samples SL1-3. Two different SEC methods were employed to determine absolute molecular weight averages and molecular weight distributions: (i) SEC with on-line differential viscosity (DV) detection applying universal calibration (UC) (SEC-DV/UC)⁸¹⁻⁸³ and (ii) SEC with on-line tracing of the copolymer composition (SEC-UV/RI).⁸⁴ The first method is well

established in the literature and does not need further explanation. It should be emphasized that the concept of universal calibration has successfully been applied to polypeptides.⁸¹ The second method allows determination of molecular weight distributions of diblock copolymers without referring to any kind of calibration curve or molar mass-sensitive device. It is based on the standard procedure to calculate number-average molecular weights (M_n) from the chemical composition of a copolymer and the molar mass of the first block segment, applied on an ensemble of monodisperse copolymer fractions. In general, the chemical composition of diblock copolymer fractions is accessible by a quantitative analysis of two independent detector traces (for example UV and RI). The M_n value of the precursor is taken as the molar mass of the first block (Table 2-9). From this set of data, molecular weight distributions and molecular weight averages can be calculated. Since the distribution of the first block was neglected, results are only apparent. However, the less disperse the first block and the broader the distribution of the second block, the better should be the agreement with the true molecular weight distribution of the sample.⁸⁴

The SEC chromatograms of the samples SL1-3 including specific viscosity (measured with a Viscotek model H502B on-line viscometer) and composition traces (calculated from UV and RI signal intensities) are shown in Figure 2-16. In SEC, it is expected that copolymer fractions elute faster the higher the mole fraction of ZLLys. Indeed, samples SL1 and SL2 show such an elution behavior but SL3 does not. The chemical gradient along the chromatogram observed for SL3 indicates that the late copolymer fractions were passing too slowly through the stationary phase. Due to adsorption, fractions with a ZLLys content of 40-60 mol % were detected at the same elution volume as the corresponding macroinitiator. Also, there was a considerable shift between the maximums of RI and specific viscosity traces of ~0.7 mL, which was not observed for samples SL1 and SL2 (see Figure 2-16).

The results of SEC-DV/UC and SEC-UV/RI analyses for samples SL1-3 are summarized in Table 2-12. It can be seen that there is very good agreement between the number-average molecular weights obtained by NMR (Table 2-13) and SEC-DV/UC, deviations are usually less than 10%. Results of SEC-UV/RI are also in reasonable agreement with NMR (deviations < 20%). Polydispersity indexes were found to be in the range of 1.4-1.7 (SEC-DV/UC) or 1.2-1.6 (SEC-UV/RI). It should be noted that the best agreement between methods was obtained for sample SL1 with the lowest molecular weight (69 ZLLys units, Table 2-11).

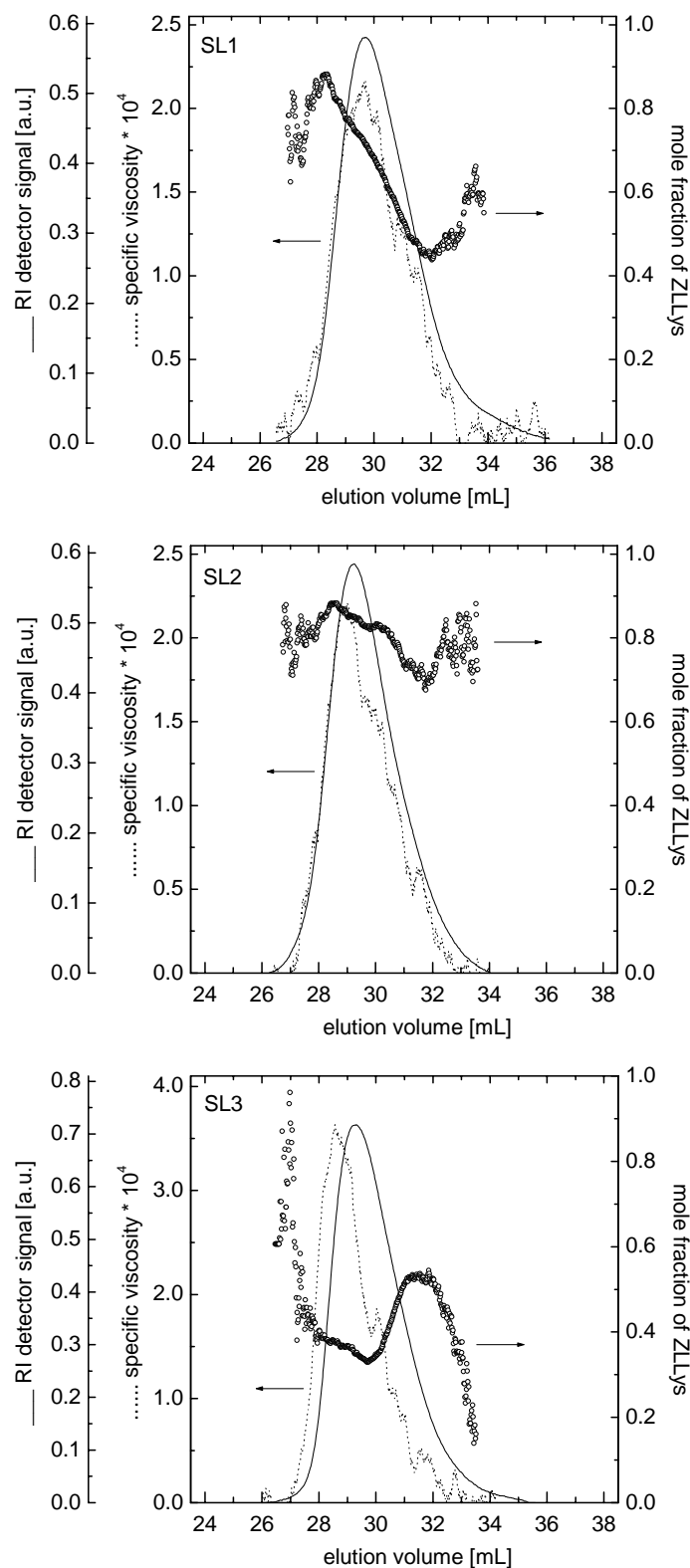


Figure 2-16. SEC chromatograms (eluent: DMA + 0.5 wt % LiBr at 70 °C, stationary phase: PSS-GRAM, detectors: UV, RI, DV) of the linear PS-*b*-PZLLys samples SL1-3 (top to bottom). Solid lines: RI, dotted lines: specific viscosity, open circles: mole fraction of ZLLys in the copolymer.

Table 2-12. Number-average molecular weights (M_n) and polydispersity index (PDI) values of the linear PS-*b*-PZLLys samples SL1-3 as determined by SEC-DV/UC and SEC-UV/RI.

sample	M_n (kg·mol ⁻¹)		PDI	
	SEC-DV/UC ^{&##}	SEC-UV/RI ^{&*}	SEC-DV/UC ^{&##}	SEC-UV/RI ^{&*}
SL1	21.7	23.6	1.7	1.6
SL2	35.8	41.4	1.6	1.2
SL3	51.0	54.6	1.4	1.3

[&] Eluent: DMA + 0.5 wt % LiBr at 70 °C, stationary phase: PSS-GRAM. [#] Universal calibration curve was recorded with PS standards. ^{*} Signal of the RI detector was corrected according to the comonomer-specific detector response.

The samples SL1-3 were further analyzed by means of MEMBRANE OSMOMETRY (MO) and AUC SEDIMENTATION EQUILIBRIUM runs, which are standard methods for the determination of absolute number- and weight-average molecular weights (M_w), respectively. Results are summarized in Table 2-13. Regarding M_n values, there is good agreement between NMR, MO, and SEC results. Again, deviations are smallest for the sample SL1. AUC, on the other hand, provided values for M_w which were about two times smaller than the ones obtained from SEC analyses. At a first glance, this result suggested that results from SEC were wrong. However, AUC values for M_w were even smaller than the corresponding M_n values determined by NMR or MO, thus making rather AUC results doubtful. At the present, a conclusive explanation for the failure of AUC in the determination of M_w cannot be given. It should be noted that NMR, IR, and UV SPECTROSCOPY, ELEMENTAL ANALYSIS, AUC, and conventional SEC were the methods used by others to determine the molecular weights of polypeptide block copolymers.^{48,49,85-90} A comparison of results obtained by different methods has not been done yet.

Table 2-13. Comparison between values of number- (M_n) and weight-average molecular weight (M_w) obtained by NMR, Membrane Osmometry (MO), Analytical Ultracentrifugation (AUC), and Size Exclusion Chromatography (SEC).

sample	M_n (kg·mol ⁻¹)			M_w (kg·mol ⁻¹)	
	NMR [§]	MO [#]	SEC ^{&}	AUC [§]	SEC ^{&}
SL1	23.7	27.6	21.7	19.0	36.6
SL2	34.7	27.6	35.8	18.8	57.5
SL3	47.2	31.5	51.0	43.0	73.2

[§] Frequency: 400.1 MHz (¹H), solvent: DMF-d₇, 25 °C. [#] Membrane: regenerated cellulose (molecular weight cut-off: 20 kDa, Gonotec GmbH), solvent: DMF, 25 °C. [&] Eluent: DMA + 0.5 wt % LiBr at 70 °C, stationary phase: PSS-GRAM, universal calibration. [§] Sedimentation equilibrium: 0.1-0.6 wt % polymer solutions in DMF, 25 °C, 20K rpm.

However, although M_w values could not yet be confirmed, it is believed that the two SEC procedures used provide reliable information about the true molecular weight distribution of linear PS-*b*-PZLLys copolymers. SEC-UV/RI is much easier to apply and enables a quick evaluation of a large number of chromatograms, produced for example in screening experiments to find best conditions for a controlled polymerization.

2.3.2.3 Advanced polymerization of amino acid-*N*-carboxyanhydrides

The broad distributions of samples SL1-3 (PDI \sim 1.5) indicate that the so far applied recipe did not promote a well-controlled polymerization of the NCA. For the following series of experiments, the same initial monomer and initiator concentrations were used as for the synthesis of SL1, i.e., $[\text{ZLLys-NCA}]_0 \sim 8$ wt % and $[\text{ZLLys-NCA}]_0/[\text{S1}]_0 = 31$. Polymerizations were conducted for 3 days in DMF as the solvent under a dry argon atmosphere. Conversion of the NCA always went to completion as indicated by SEC analysis of the crude reaction mixtures. Products were precipitated in methanol/water 70:30 (v/v) and extracted with cyclohexane to remove any residual PS precursor. The number-average molecular weights (M_n) and distributions (PDI) of the PS-*b*-PZLLys copolymer samples were determined by means of NMR and SEC-UV/RI, respectively.

It is well known that acidic or other contaminants in the NCA sample can have severe impact on the distribution of polypeptide products.⁶² Recently, Poché et al.⁹¹ reported an advanced procedure that allows preparation of NCAs in a very high purity. Accordingly, ZLLys-NCA was prepared from ZLLys and triphosgene in ethyl acetate (instead of THF) as the solvent. The crude product was then successively washed with cold water and aqueous NaHCO_3 , precipitated from petrolether, and dried in high vacuum. Polymerization of the so obtained NCA with S1 the macroinitiator in DMF at 40 °C yielded sample SL4, which had a monomodal molecular weight distribution with PDI = 1.2 (see Figure 2-17 and Table 2-14). It is evident that this PDI value is considerably smaller than that of reference sample SL1 (PDI = 1.6). An even narrower distribution could be obtained upon increasing polymerization temperature: the sample SL5 produced at 80 °C under otherwise identical conditions exhibited a distribution with PDI = 1.1. It should further be noted that the efficiency of the macroinitiator, as calculated from the ratio of the targeted molecular weight over the experimental molecular weight (NMR), was not affected by neither the purity of the NCA nor the polymerization temperature (\sim 0.64, see Table 2-14.)

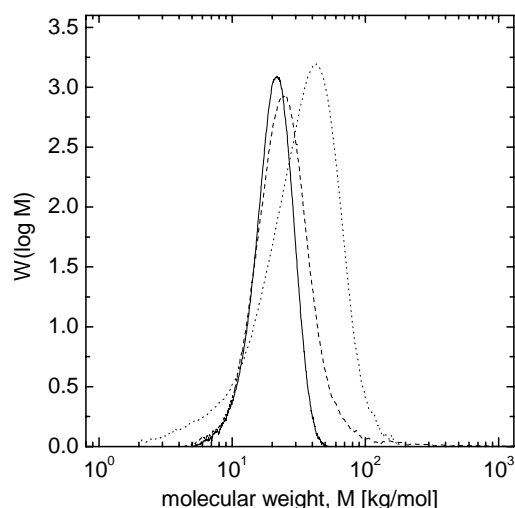


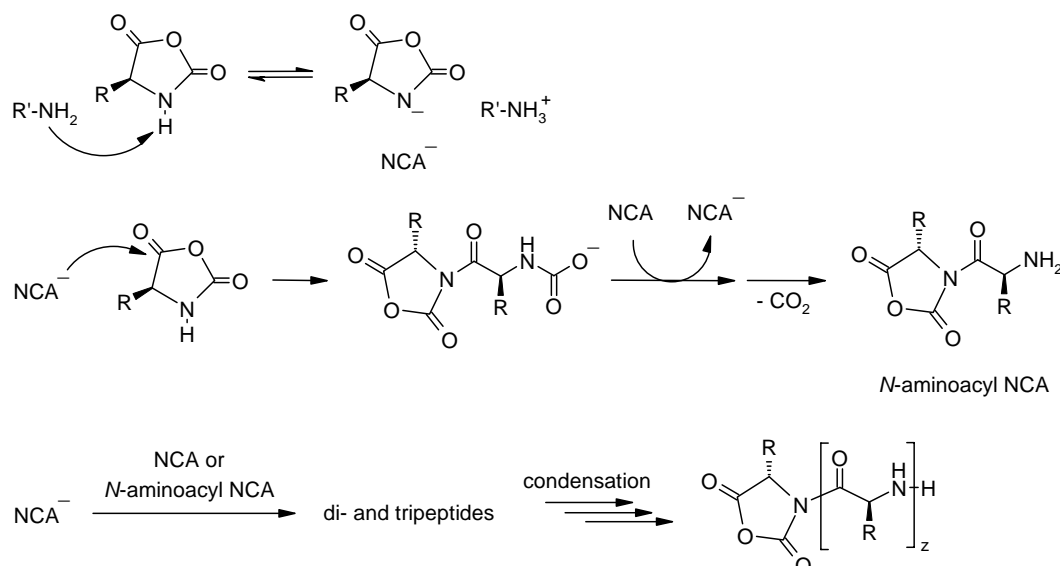
Figure 2-17. Mass distribution (SEC-UV/RI) of the linear PS-*b*-PZLLys samples SL1 (dotted line), SL4 (dashed line) and SL5 (solid line) obtained for different reaction conditions (see text).

Table 2-14. Experimental results for the polymerization of ZLLys-NCA, prepared by two different methods,^{74,91} employing macroinitiator S1 in DMF at 40-80 °C ($[ZLLys-NCA]_0/[S1]_0 = 31$, $[ZLLys-NCA]_0 \sim 8$ wt %).

sample	method of NCA preparation	T (°C)	M_n (kg·mol ⁻¹) [#]	PDI ^{&}	initiator efficiency [§]
SL1	ref. ⁷⁴	40	21.7	1.6	0.63
SL4	ref. ⁹¹	40	21.4	1.2	0.64
SL5	ref. ⁹¹	80	20.8	1.1	0.66

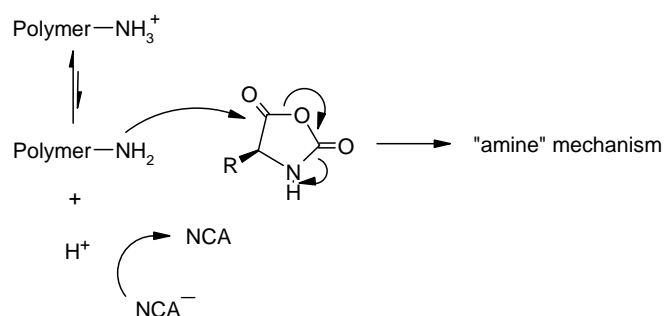
[#] ¹H NMR (400 MHz, DMF-*d*₇, 25 °C). [&] SEC-UV/RI (eluent: DMA + 0.5 wt % LiBr at 70 °C, stationary phase: PSS-GRAM, detectors: UV, RI). [§] $M_n^{\text{targeted}}/M_n^{\text{experimental}}$, quantitative conversion of ZLLys-NCA.

A second reason for a non-controlled polymerization of NCAs is the occurrence of side reactions, the most likely one being the so-called “activated monomer” process.⁶² Whereas the key step in the “amine” mechanism is the nucleophilic opening of the NCA ring at the C-5 position (see Scheme 2-10), it is the deprotonation of an NCA molecule that initiates the “activated monomer” process. The NCA anion (NCA⁻) is a sufficiently strong nucleophile to initiate the oligomerization of NCAs, and the produced *N*-aminoacyl NCA compounds can then undergo condensation to yield high-molecular weight products (Scheme 2-11). Note that the propagating primary amine can act as both a nucleophile and a base, thus polymerization will always switch back and forth between the “amine” and “activated monomer” mechanism.



Scheme 2-11. Polymerization (condensation) of NCAs via the “activated monomer” mechanism.

One way to avoid the “activated monomer” process is to use metal-amine complex catalysts instead of primary amine initiators.^{44,92} Polymerization then proceeds in a controlled manner via a “coordination” polymerization process to yield polypeptide block copolymers with PDI < 1.2 (determined by SEC with on-line MALLS detection using 0.1 M LiBr in DMF as the eluent at 60 °C). However, as seen from Scheme 2-11, it would just need protons to re-protonate eventually formed NCA⁻ and thus to avoid the “activated monomer” pathway. For this reaction to be successful, re-protonation of NCA⁻ must be faster than a nucleophilic attack of another NCA molecule. It was therefore decided to use the hydrochloride of a free primary amine macroinitiator for NCA polymerization. Note, the hydrochloride is a dormant species, and the growing free primary amine and H⁺(Cl⁻) is released upon dissociation. This process is illustrated in Scheme 2-12.



Scheme 2-12. Tentative mechanism of the ring-opening polymerization of NCAs using primary amine hydrochlorides (chloride ions omitted).

It has to be mentioned that a screening of primary amines as hydrochlorides had successfully been applied for the synthesis of α -aminoacyl compounds.^{93,94} It was emphasized that the

reactions proceeded smoothly without producing polymeric by-products. Interestingly, also the anilide from phenylalanine-NCA and *p*-chloroaniline hydrochloride could be obtained in a high yield, although the free amine is known for its poor aminolytic power and its ability to initiate NCA polymerization (presumably *via* an “activated monomer” route).⁹³

The hydrochloride of S1 (S1·HCl) was obtained by treating a solution of the polymer in THF with aqueous HCl. The product was precipitated and dried in vacuum at 40 °C to constant weight. All block copolymers prepared (SL6-9) with the S1·HCl macroinitiator in DMF at 40-80 °C exhibited very a narrow molecular weight distribution, close to a Poisson distribution (see Table 2-15, Figure 2-18, and Figure 2-19). These results seem to confirm the novel concept described above for achieving a controlled polymerization of NCAs. According to SEC and AUC analyses (Figure 2-19), sample were free of PZLLys homopolymer, which might have eventually been formed by a chloride-initiated polymerization of the NCA.⁶² In addition, initiator efficiencies were found to be ~0.8, somewhat higher as for the free amine initiating system (~0.65).

Table 2-15. Experimental results for the polymerization of ZLLys-NCA (prepared according to ref. ⁹¹) employing the hydrochloride of S1 in DMF at 40-80 °C ($[ZLLys-NCA]_0/[S1]_0 = 31$, $[ZLLys-NCA]_0 \sim 8$ wt %, * 20 wt %).

sample	T (°C)	M_n (kg·mol ⁻¹) [#]	PDI ^{&}	initiator efficiency [§]
SL6	40	17.9	(1.01)	0.78
SL7*	40	18.5	(1.01)	0.74
SL8	60	18.0	(1.01)	0.77
SL9	80	16.3	(1.01)	0.84

[#] ¹H NMR (400 MHz, DMF-d₇, 25 °C). [&] SEC-UV/RI (eluent: DMA + 0.5 wt % LiBr at 70 °C, stationary phase: PSS-GRAM, detectors: UV, RI). [§] $M_n^{\text{targeted}}/M_n^{\text{experimental}}$, quantitative conversion of ZLLys-NCA.

However, kinetic studies have not yet been performed to confirm the mechanism depicted in Scheme 2-12. It is expected that the rate of polymerization depends on the position of the hydrochloride/amine equilibrium and thus on the polarity of the reaction medium and on the temperature. It should be mentioned that BLGlu-NCA did not undergo polymerization with primary amine hydrochlorides when the same experimental conditions as for the ZLLys-NCA were applied. It seems that in this case the hydrochloride/amine equilibrium is too far shifted to the left hand side, thus inhibiting polymerization.

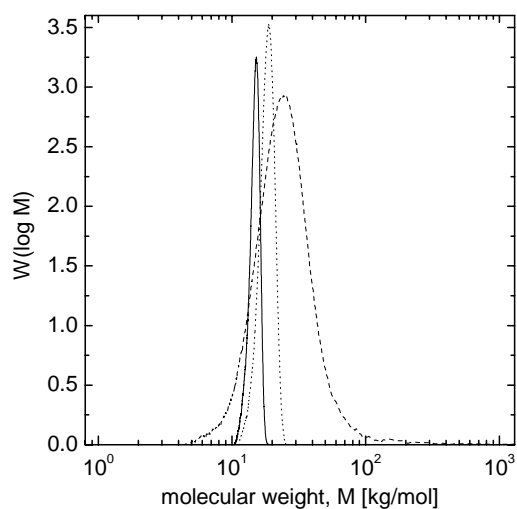


Figure 2-18. Mass distribution (SEC-UV/RI) of the linear PS-*b*-PZLLys samples SL6 (dashed line) and SL9 (solid line) obtained by polymerization of ZLLys-NCA with S1·HCl in DMF at 40 or 80 °C. For comparison, the distribution of SL5 (dotted line) prepared with S1 is also included in the plot.

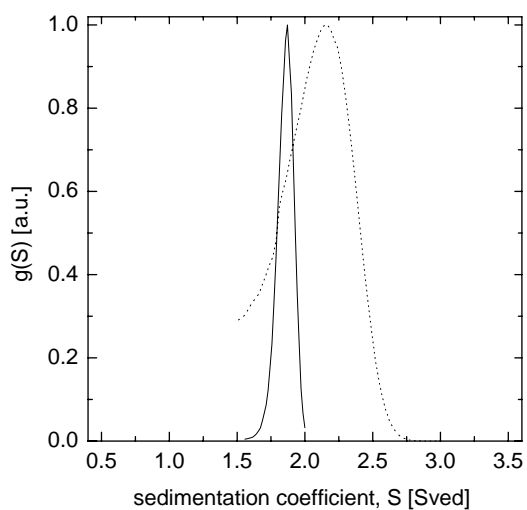


Figure 2-19. Sedimentation coefficient distributions (AUC) of the linear PS-*b*-PZLLys samples SL5 (dotted line) and SL9 (solid line) obtained by polymerization of ZLLys-NCA with S1 and S1·HCl, respectively, in DMF at 80 °C.

3 BLOCK COPOLYMER MESOSTRUCTURES

The following part of the work is devoted to the formation of mesophases with diblock copolymers, the synthesis and characterization of which has been described in chapter 2. Any of the copolymer systems examined has the inherent ability to establish specific interactions *via* electrostatic interactions (block ionomers), dipole–dipole interactions (polypeptide block copolymers), or hydrogen bonding (chelating polymers/polypeptide block copolymers). As will be seen, such specific interactions can introduce a higher order of complexity and hierarchy in the resulting mesostructures as well as make them able to respond to an external stimulus.

Regarding the formation of polyion complexes by mixing oppositely charged block ionomers (chapter 3.1), attractive electrostatic forces alone might not be sufficient to add complexity to a mesostructure. It is evident that additional repulsive forces are needed, which for example originate from the strong segregation of the two solvating block segments. In fact, following this rule, vesicles with an asymmetric membrane could be obtained from a pair of block ionomers. This is a first step in the generation of aggregates with a reduced or broken symmetry and finally exhibiting chirality.

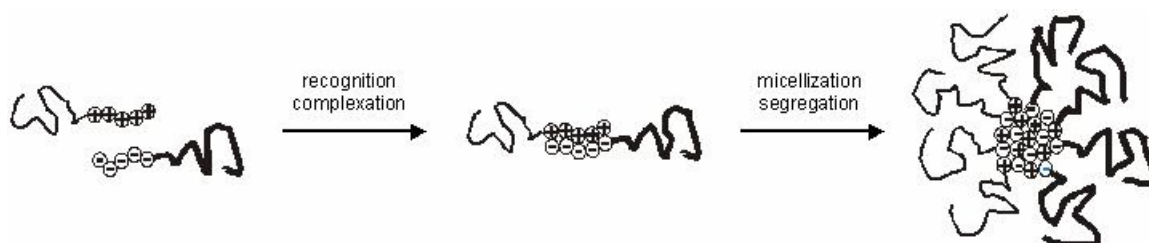
The polymers referred to as chelating polymers are homopolymers and block copolymers based on 2-(acetoacetoxy)ethyl methacrylate (chapter 3.2). There are several aspects making this polymer system very attractive for colloid chemistry and structural investigations, among them the ability to coordinate to metal ions and metals and to establish hydrogen bridges between adjacent acetoacetoxy units. Hydrogen bonding certainly is one of the most important motifs promoting the formation of secondary, tertiary, and quaternary structures in biological and supramolecular systems. Poly[2-(acetoacetoxy)ethyl methacrylate] might therefore be considered as a “supramolecular polymer”, which combines the advantageous features of a synthetic polymer (e.g. facile synthesis and processing) with the ability to form ordered structures on a higher level (chapter 3.2.2).

Also, poly[2-(acetoacetoxy)ethyl methacrylate] block copolymers might exhibit features of strongly segregating systems, the hydrogen bonding interactions between acetoacetoxy units contributing to a high incompatibility of block segments. Poly(*n*-butyl methacrylate)-*block*-poly[2-(acetoacetoxy)ethyl methacrylate]s, for example, were found to self-assemble into reverse micellar aggregates with an unusually high grafting density. Depending on experimental conditions, either spherical or cylindrical micelles or vesicles could be observed (chapter 3.2.1).

Last but not least, the formation of aggregates and solid-state structures using polypeptide block copolymers (“molecular chimeras”) will be described in chapters 3.3.1 and 3.3.2. Polypeptides are highly attractive building blocks because of many reasons, the most important one being their ability to establish a well-defined secondary structure of either an α -helix or a β -sheet *via* hydrogen bonding. The conformation of the polypeptide can be easily triggered by an external stimulus like temperature or the pH of the medium. The polypeptides investigated here are the helix-forming poly(L-glutamate) and poly(Z-L-lysine), which can be regarded as rod-like mesogens. As a matter of the large dipole moments, structure formation in the solid state (or lyotropic phases) is governed by the strong dipole-dipole interactions between the α -helices, which can lead to substantial deviations from the “classical” phase behavior of block copolymers (cf. chapter 1). Indeed, polystyrene-*block*-poly(Z-L-lysine) copolymers almost exclusively form a lamellar superstructure or, being more accurate, an *undulated* or *zigzag lamellar* phase. Such undulations, i.e. statistical fluctuations in the thickness of polypeptide layers, are due to the packing of a polydisperse ensemble of helices (chapter 3.3.2). The chain length distribution of rod-like segments, however, is usually not considered when regarding the phase behavior of rod-coil block copolymers, thus making a comparison between theory and experiment very difficult if not impossible. Thanks to the earlier described advances in the synthesis and characterization of polystyrene-*block*-poly(Z-L-lysine)s (chapter 2.3.2), the impact of polydispersity on the properties of the resulting solid-state structures could for the time be examined in a systematic way.

3.1 Block ionomers and polyion complexes

The basic idea of this project was to employ a modular approach to generate a “library” of mesostructures in dilute solution, just by mixing two different diblock copolymers. By bringing together competing repulsive and attractive forces, it was hoped that the self-assembly process could be directed towards superstructures with a higher complexity. Suitable systems are pairs of strongly segregating block copolymers carrying complementary recognition sites in one block segment, like positively and negatively charged block ionomers. Harada and Kataoka were the first to employ oppositely charged double-hydrophilic block copolymers, namely poly(ethylene oxide)-*block*-poly(L-Lysine) (PEO-*b*-PLLys) and poly(ethylene oxide)-*block*-poly(L-aspartate) (PEO-*b*-PLAsp), for generation of monodisperse spherical “polyion complex (PIC) micelles” in aqueous media (see Scheme 3-1).^{88,95} Interestingly, PIC micelle formation was only observed for pairs of block copolymers with a matching length of the charged segment (“chain length recognition”).⁹⁶ Note that the solvating corona or shell of PIC micelles consisted of PEO chains only. If the shell were consisting of two segregating components, one might have expected the formation of for example a spherical micelle with a corona being divided into two compartments, a so-called “Janus micelle” (named after the two-faced Roman god Janus).⁹⁷⁻⁹⁹ Such micelle exhibits a broken symmetry, and thus a higher complexity than a conventional core-shell aggregate.



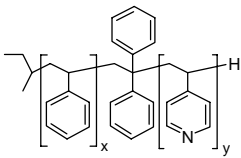
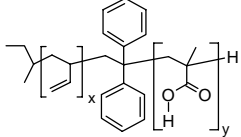
Scheme 3-1. Modular approach for the generation of a library of block copolymer superstructures (here: formation of a PIC micelle, Harada and Kataoka⁹⁶).

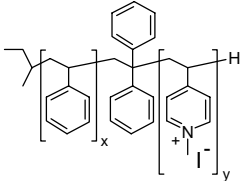
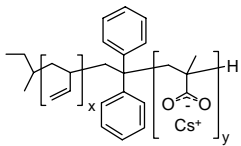
Very recently, Luo and Eisenberg described a one-step procedure to obtain block copolymer vesicles with preferentially segregated acidic and basic corona chains.¹⁰⁰ The system investigated was a mixture of polystyrene-*block*-poly(acrylic acid) (PS₃₀₀-*b*-PAA₁₁) and polystyrene-*block*-poly(4-vinylpyridine) (PS₃₁₀-*b*-P4VP₃₃) ionomers (the subscripts denoting the number of repeating units) in *N,N*-dimethylformamide (DMF)/water 50:50 (w/w) at pH ~ 3. As a matter of different block lengths and thus different space filling requirements or curvature, PAA chains were segregated into the inside of the vesicles, while the outside corona consisted of P4VP chains. This is the first example of a vesicular aggregate with an asymmetric mem-

brane made by diblock copolymer self-assembly. As reported by Stoenescu and Meier, asymmetric vesicles could also be obtained from poly(ethylene oxide)-*block*-poly(dimethyl siloxane)-*block*-poly(methyl oxazoline) (PEO-*b*-PDMS-*b*-PMOXA) amphiphilic triblock copolymers in aqueous media.¹⁰¹ The location of the hydrophilic PEO and PMOXA domains within the vesicle membrane was determined by the relative block length or volume fraction of the two block segments.

A list of amphiphilic block ionomers based on polystyrene-*block*-poly(4-vinylpyridine) (SP': PS-*b*-P4VP, SP: PS-*b*-P4VP^{+I}⁻, Table 2-1) and polybutadiene-*block*-poly(methacrylic acid) (BM': PB-*b*-PMAA, BM: PB-*b*-PMA⁻Cs⁺, Table 2-2) used in this work is given in Table 3-1. Dilute solutions (0.003-0.25 wt %) of block ionomers were obtained by dissolution of the dry powders in tetrahydrofuran (THF). PIC samples were prepared by mixing block ionomer solutions. Since THF is a selective solvent for PS and PB block segments, reverse aggregates with a PS/PB corona and an ionic core should be formed. The length of the solvating blocks was ~200 in order to satisfy the $\chi N \gg 10$ criteria for strong segregation (χ : Flory-Huggins interaction parameter, $\chi_{PS-PB} \sim 0.13$ at 295 K,¹⁰² $N = N_{PS} + N_{PB}$: degree of polymerization).⁶ Ionic segments consisted of about 10 or 30 repeating units.

Table 3-1. Molecular characteristics of diblock copolymers used for the generation of polyion complex aggregates (cf. Scheme 3-1).

chemical structure	sample	x	y	$f_y^{\#}$	ϕ_y^{\S}
	SP'1	211	12	0.054	0.057
	SP'2	211	33	0.135	0.144
	BM'1	216	9	0.040	0.059
	BM'2	216	29	0.118	0.167

	SP1	211	12	0.054	0.075
	SP2	211	33	0.135	0.183
	BM1	216	9	0.040	0.058
	BM2	216	29	0.118	0.164

[#] Mole fraction of ionic block. [§] Volume fraction of the ionic block, densities used for calculation: $\rho / \text{g cm}^{-3} = 1.04$ (PS), 0.96 (PB), 0.98 (4VP), 1.02 (MAA), 1.72 (4VP^{+I}), 2.64 (MA⁻Cs⁺).

As indicated by low scattering intensities in DYNAMIC LIGHT SCATTERING (DLS), samples of the SP' and BM' series (see Table 3-1) and the corresponding pyridine-carboxylic acid complexes did not form stable aggregates in THF solution.¹⁰³ Evidently, the volume fractions of functional repeating units were chosen too small and/or the segregation between electrolyte and solvating segments was too weak to cross the disorder–order phase boundary (cf. Figure 1-1). In the case of the SP and BM samples carrying permanent positive or negative charges, respectively, incompatibility of the solvating and functional segments was much higher, thus forcing the formation of aggregates. In fact, the scattering intensities observed for SP and BM solutions were several orders of magnitude higher (>120 kHz for 1 wt % polymer solutions, laser power: ~ 35 mW) than for SP' and BM'. Also, compared to the corresponding pyridine-carboxylic acid complex, a PIC made from pyridinium (P4VP⁺ Γ) and carboxylate polyions (PMA⁻Cs⁺) should have a much lower solubility product and thus a higher stability in THF solution. For these reasons, the block ionomers SP2 and BM2 with the highest amount of ionic block (~ 17 mol %, Table 3-1) were chosen as model systems for the following studies.¹⁰⁴

Dilute THF solutions of samples SP2 and BM2 and the corresponding stoichiometric PIC ([+]/[-] = 1) were first analyzed at room temperature by means of DLS and STATIC LIGHT SCATTERING (SLS). It is known that the analysis of the aggregation behavior of ionomers with LIGHT SCATTERING is complicated, often producing difficult to evaluate data. The size of the aggregates and aggregation numbers (Z = average number of ionomer chains per aggregate) obtained from DLS and SLS measurements were therefore considered as rough estimates. Accordingly, the values of the ratio of the radius of gyration over the hydrodynamic radius (R_g/R_h) loose significance in the determination of the structure of aggregates.

At 25 °C, the 0.003–0.25 wt % solutions of SP2 and BM2 in THF contained aggregates with $R_h \sim 50$ nm and 75 nm, respectively (DLS, see Figure 3-1). Sample BM2, which was rather poorly soluble in THF (less than 0.8 mg/mL), seemed to form stable aggregates only when the concentration was less than 0.02 wt %. At higher concentrations, the hydrodynamic radius of aggregates was steeply increasing above 100 nm, indicating coagulation of aggregates or formation of some kind of cluster. In the case of SP2, on the other hand, the size of aggregates remained the same in the whole concentration range investigated. Noteworthy, there was no evidence for a dissociation of aggregates nor of a polyelectrolyte effect. Aggregation numbers were in the order of $Z \sim 700$ (SP2) and 1000 (BM2) (SLS).¹⁰⁴ Evidently, the dimensions of SP2 and BM2 aggregates were larger as expected for an ordinary spherical micelle.¹⁰⁵⁻¹⁰⁷

Additional SMALL-ANGLE NEUTRON SCATTERING (SANS) experiments suggested that in a 1 wt % solution of SP2 in THF- d_8 vesicles were present. The hydrodynamic radius of SP2 vesicles was found to be $R_h = 59$ nm and the thickness of the membrane was $\Delta R = 17$ nm. For the ~ 0.8 wt % solution of BM2, it was observed a mixture of large vesicles ($R_h = 124$ nm, $\Delta R = 66$ nm) and micelles ($R_h = 23$ nm). However, as mentioned above, THF solutions of BM2 were not stable when the polymer content was greater than 0.02 wt %, making these results rather doubtful. However, it is fact that the hydrodynamic radius of BM2 aggregates, as determined by DLS, exceeded the contour length of a single polymer chain. A hollow vesicular structure therefore appeared more likely than a compact core-shell structure of a micelle.

Upon mixing the solutions of oppositely charged block ionomers SP2 and BM2 so that $[-]/[+] = 1.0$, a neutral PIC (SP2:BM2) should be formed, accompanied by the release of cesium iodide. Note that cesium iodide to a certain extent is soluble in THF. First DLS measurements indicated that in 0.01–0.25 wt % solutions of SP2:BM2 in THF aggregates with $R_h = 65$ –80 nm were present (see Figure 3-1). Although the CONTIN analysis¹⁰⁸ of DLS data provided monomodal particle size distributions, diffusion coefficients showed a non-linear dependence on the scattering vector. This indicates that the sample exhibits a considerable polydispersity. The aggregation number was estimated to be $Z \sim 1200$,¹⁰⁴ somewhat higher than for the aggregates of the pure block ionomers.

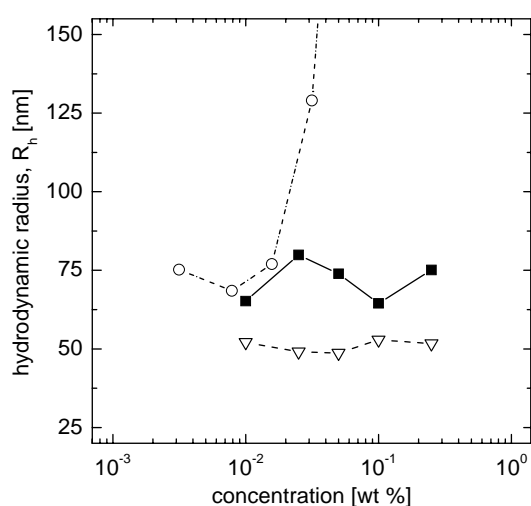


Figure 3-1. Concentration dependence of hydrodynamic radii (DLS) of aggregates formed by PS-*b*-P4VP⁺I⁻ sample SP2 (triangles), PB-*b*-PMA⁻Cs⁺ sample BM2 (circles), and the mixed sample SP2:BM2 ($[+]/[-] = 1$) (squares) in THF at 25 °C.

In order to show that a PIC had been formed in the mixed SP2 and BM2 ionomer solution, samples were analyzed by means of ANALYTICAL ULTRACENTRIFUGATION (AUC). Sedimen-

tation-velocity runs were applied to fractionate the 0.1 wt % THF solutions of SP2, BM2, and SP2:BM2. The sedimentation coefficient distributions (see Figure 3-2) of aggregates of SP2 and BM2 were very broad with a peak value of the sedimentation coefficient (S) of ~ 1590 and 270 Sved, respectively. The distribution, which was obtained for the mixed sample SP2:BM2, was considerably narrower and exhibited a maximum at $S \sim 600$ Sved. These results confirm that the mixing of oppositely charged block ionomers produced a novel PIC species, which again was forming stable aggregates in dilute THF solution. It is evident that the steric stabilization by the hydrophobic corona chains could not prevent the ionomer aggregates from coalescence followed by polyion complexation.

Knowing the sedimentation coefficient and the hydrodynamic radius allowed determination of the density (ρ) of aggregates (hard-sphere model).¹⁰⁹ For the PIC aggregates, $\rho = 0.922 \text{ g cm}^{-3}$ was obtained, a value ranging between the density of the solvent (0.889 g cm^{-3}) and the bulk densities of PB (0.96 g cm^{-3}) and PS (1.04 g cm^{-3}). This result was a first hint that the PIC aggregates had a hollow vesicular structure, which later could be confirmed by SANS and TRANSMISSION ELECTRON MICROSCOPY (TEM). It further suggested that the cesium iodide ($\rho = 4.51 \text{ g cm}^{-3}$) released during polyion complexation was partly if not completely extracted from the polymer and transferred into the THF phase, thus fixing the structure of aggregates.¹⁰⁴

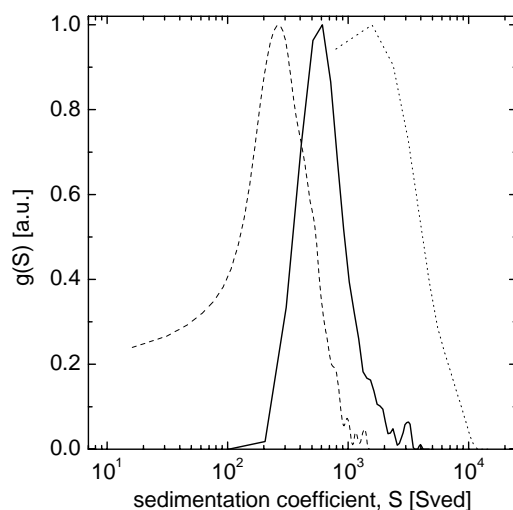


Figure 3-2. Sedimentation coefficient distributions $g(S)$ obtained for the aggregates in 0.1 wt % solutions of PS-*b*-P4VP⁺T⁻ sample SP2 (dashed line), PB-*b*-PMA⁻Cs⁺ sample BM2 (dotted line), and the mixed sample SP2:BM2 ([+]/[-] = 1) (solid line) in THF at 25 °C.

The TEM image shown in Figure 3-3 was obtained by drying a 0.01 wt % solution of PIC aggregates in THF on a carbon-coated grid. The contrast in the micrograph was due to small amounts of cesium iodide in the original solution, giving a negative staining of the particles.

Note that all attempts to selectively stain the PB segments by exposing the specimen to OsO_4 vapor were not successful. However, it can be clearly seen spherical vesicles, which are about 100-200 nm in diameter. This is in reasonable agreement with the results obtained from DLS indicating that the original dimension of aggregates had been well preserved during the preparation of the TEM specimen. The thickness of the collapsed polymer membrane, which in TEM shows as a bright layer between the dark regions, was estimated to be ~ 30 nm.¹⁰⁴

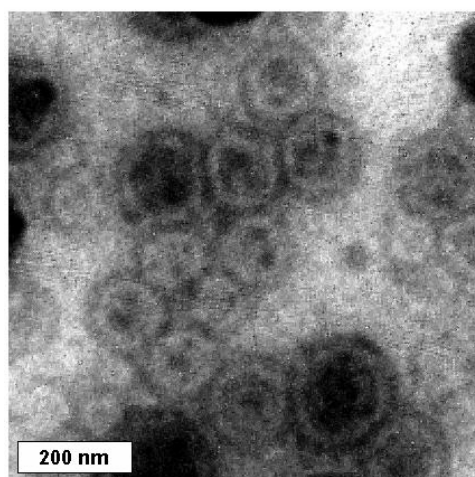


Figure 3-3. TEM micrograph of negatively stained aggregates of the PIC SP2:BM2 ([+]/[-] = 1), as prepared by fast drying of a 0.01 wt % THF solution.

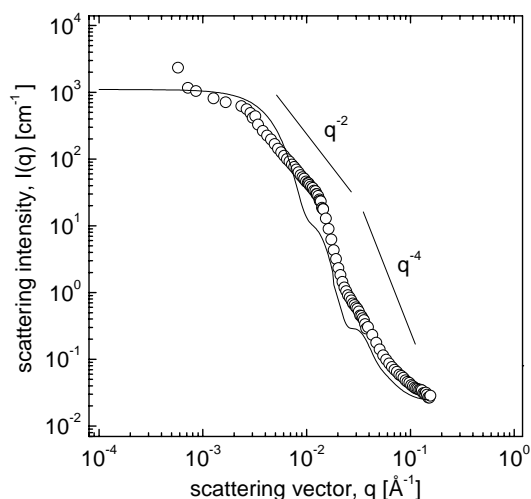


Figure 3-4. LS/SANS curve of a 0.7 wt % solution of the PIC SP2:BM2 ([+]/[-] = 1) in THF- d_8 at 25 °C. The solid line is the result of fitting the data to the form factor of a polydisperse hollow sphere.^{110,111}

The LS/SANS scattering curve, which was obtained for a ~ 0.7 wt % solution of the PIC in THF- d_8 , is shown in Figure 3-4. It is characteristic for vesicles as scattering objects and exhibits the expected scaling laws for the scattering intensity, i.e. $I(q) \propto q^{-2}$ at intermediate values of the scattering vector q and $I(q) \propto q^{-4}$ at high values of q . However, presumably due to

the contributions of a structure factor, the best possible fit of the data to the form factor of a polydisperse hollow sphere¹¹⁰ was less than perfect. Nevertheless, it was found that the hydrodynamic radius of the PIC vesicles should be $R_h \sim 50$ nm, which is in reasonable agreement with TEM results. The thickness of the membrane should be $\Delta R \sim 5$ nm, which is considerably less than the ~ 30 nm estimated by TEM. It is a working hypothesis that the ΔR value obtained from SANS is not a measure of the thickness of the complete polymer membrane but of the PIC layer (cf. Chart 3-1).

Regarding the inner structure of the vesicle membrane, it seemed reasonable that the insoluble $[P4VP^+ : PMA^-]$ layer was covered by two solvating PS/PB layers. However, as the solvating segments were strongly segregating ($\chi N \gg 10$), the membrane should have an asymmetric structure (cf. the work of Meier et al.).¹⁰¹ Due to the different volumes and thus space filling requirements of the PS and PB segments ($\phi_{PS}/\phi_{PB} \sim 1.8$), PS was expected to form the outer layer of the membrane and PB the inner one (see the illustration in Chart 3-1). Such a micro-phase-separated structure of the membrane would explain the unsuccessful attempts to stain the vesicles for TEM analysis (see above), the PS outer layer shielding the PB from the OsO_4 vapor.

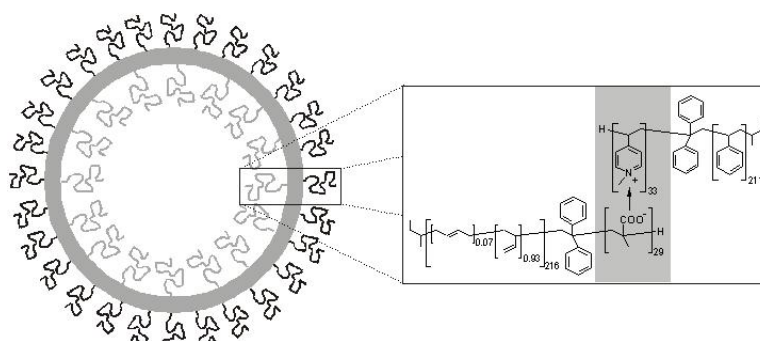


Chart 3-1. Structure of PIC vesicles having an asymmetric membrane.

TEM analysis of a cryo-microtomed (-20 °C) and selectively stained (OsO_4) polymer film, prepared by slowly evaporating a 0.1 wt % THF solution of PIC vesicles, provided further evidence for the proposed structure. The obtained micrograph shown in Figure 3-5 revealed a rather regular pattern of spherical PB domains (dark) in a PS matrix (bright) and nothing like a lamellar morphology, which one might have expected regarding the mole fractions of the two hydrophobic segments ($f_{PS}/f_{PB} \sim 1$, cf. Figure 1-1). The occurrence of a “cubic” morphology could only be explained assuming that the PIC vesicles originally had a phase-separated microstructure, as shown in Chart 3-1, and maintained their structure during the preparation of the specimen. Of course, due to shrinkage, PB domains should be smaller than the original

size of the inner PIC vesicle compartment. However, the diameter of PB spheres observed in TEM was only ~ 25 nm, which is considerably smaller than the 36 nm calculated for a PB sphere containing 1200 chains (= aggregation number, SLS), each having 216 repeating units.¹⁰⁷ Either the true aggregation number of PIC vesicles is smaller than estimated by SLS and/or domains were further shrinking upon lowering the temperature below the glass transition temperature of PB ($T_g \sim -14$ °C) for microtoming.

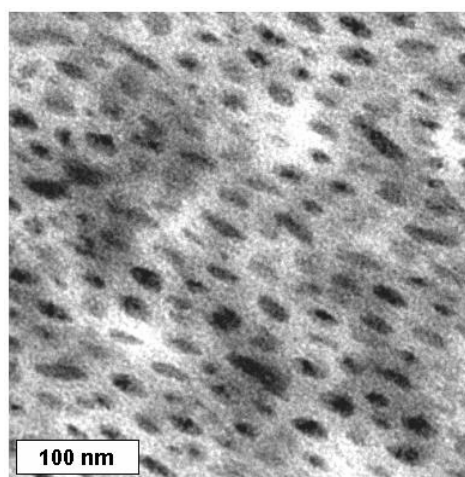


Figure 3-5. TEM micrograph of a cryo-microtomed and OsO₄-stained polymer film, prepared by solvent casting from a 0.1 wt % solution of the PIC SP2:BM2 ([+]/[-] = 1) in THF (dark: PB, bright: PS). Note that some deformation of the specimen occurred during microtoming.

Evidently, a microscopic technique like TEM cannot provide a picture of the asymmetric PIC membrane in its original state. Also, none of the scattering and fractionation methods used in the characterization of colloidal systems could reveal to the inner structure of PIC vesicles. Asymmetry in the membrane might be recognized in SANS contrast variation experiments by an apparent decrease of the thickness of the membrane. Note that the form factor of the PIC vesicle is the same as that of an “ordinary” vesicle. Future investigations shall therefore be extended to a spectroscopic analysis of PIC structures in solution with NMR and SURFACE-ENHANCED RESONANCE RAMAN SPECTROSCOPY (SERR).

Note that the PIC vesicles should exhibit stimulus-responsive features, which shall be examined in greater detail in the future. Since polyion complexation is a reversible process, PIC vesicles might disintegrate upon the addition of a low-molecular weight acid or base, and thus release molecules entrapped in the inner compartment. Also, PIC vesicles are amphiphilic in nature and should therefore change morphology when exposed to different solvents. For example, the addition of hexane, a non-solvent for PS, to the solution of PIC vesicles in THF might induce an inversion of the membrane structure. ATOMIC FORCE MICROSCOPY (AFM) studies on thin films prepared from dilute solutions of PIC vesicles in THF and THF/hexane

1:1 (v/v) seemed to confirm this expectation, see the AFM phase images shown in Figure 3-6. The mechanism and the dynamics of the PIC vesicle membrane shall in the future be investigated in detail using spectroscopy, especially SERR.

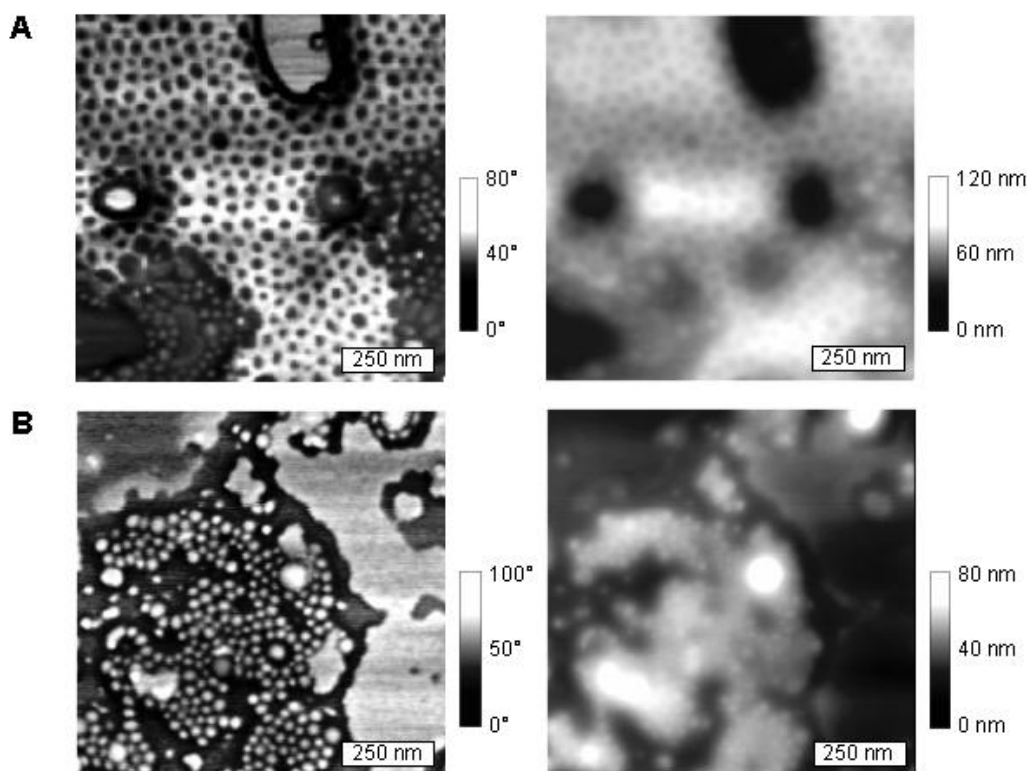


Figure 3-6. AFM micrographs (tapping mode; left: phase, right: height) of the collapsed vesicular aggregates of the PIC SP2:BM2 ([+]/[-] = 1), obtained by spin-coating of a 0.1 wt % THF solution (A) and THF/hexane 1:1 (v/v) (B) on mica. Note that in both phase images the substrate appears bright, showing that the phase contrast should be the same in both pictures—dark: PB, bright: PS.

In summary, it was possible to generate a novel complex, stimulus-responsive morphology *via* a modular approach, just by mixing oppositely charged block ionomers with a most simple chemical structure. Here, electrostatic interactions were employed to control the formation of the superstructure, but other specific interactions like hydrogen bonding, donor–acceptor interactions, or stereocomplex formation could also be applied. A library of block copolymers with different molecular weights, compositions and recognition sites shall be prepared using the methodology described in chapter 2.1.2, i.e. functionalization of PB-based block copolymers with ω -functional mercaptanes. Having such a library in hand, it would be possible to produce series of complex superstructures with adjustable or tunable properties for special applications.

3.2 Chelating block copolymers

Homopolymers and block copolymers based on 2-(acetoacetoxy)ethyl methacrylate (AEMA) are interesting materials in various aspects. First coming into one's mind is the high affinity of β -dicarbonyl chelates towards metals and metal ions.¹¹² Polymers of this kind have therefore a great application potential in the field of organic-inorganic hybrid materials.³⁰ Furthermore, β -dicarbonyl compounds are commonly involved in hydrogen bonding motifs,¹¹³ for example in biological macromolecules (uracil or thymine in nucleic acids)¹¹⁴ or synthetic supramolecular assemblies,¹ and can produce highly ordered superstructures like double helices, tubes, or ribbons. Accordingly, on a less sophisticated level, block polymers with PAEMA segments might exhibit some kind of secondary structure, which should affect the phase behavior and add complexity to the resulting structures. Indeed, PAEMA was found to form large helical superstructures with a persistence length of several hundreds of nanometers—this will be described in the second part of this chapter (3.2.2).¹¹⁵

Regarding the solubility parameters of PAEMA ($\delta = 21.2 \text{ MPa}^{0.5}$, Table 2-5) and of *n*-butyl isobutyrate ($\delta = 16.6 \text{ MPa}^{0.5}$)¹⁰² reveals another very interesting property of PBMA-PAEMA (PBMA = poly(*n*-butyl methacrylate)) copolymers. Using these solubility parameters for the estimation of the Flory-Huggins interaction parameter yields $\chi_{\text{PBMA-PAEMA}} \sim 0.8$, a value being substantially larger than the ones reported for other non-ionic block copolymer systems like polystyrene-*block*-poly(4-vinylpyridine) (~ 0.35)¹¹⁶ or polystyrene-*block*-poly(ethylene oxide) (~ 0.28)¹¹⁷. Such a high value of χ indicates that PAEMA and PBMA are highly incompatible and further suggests that PBMA-PAEMA copolymers might exhibit a phase behavior which is referred to as the *super strong segregation limit* (SSSL).¹¹⁸ This system would therefore be well suited to evaluate theoretical models and predictions about the size and shape of micellar aggregates.¹⁰⁷ The following chapter 3.2.1 is devoted to fundamental studies on the micellization behavior of PAEMA-PBMA block copolymers in dilute organic solution.¹¹⁹

3.2.1 Reverse micellar aggregates

Initial SEC and NMR studies suggested that chloroform (CHCl_3) and tetrahydrofuran (THF) are non-selective solvents for PBMA-*b*-PAEMA, i.e. aggregation does not occur in these solvents. Cyclohexane and dimethyl sulfoxide (DMSO), on the other hand, were found to solvate selectively one or the other block segment. In cyclohexane, only the ^1H NMR signals of PBMA and none of PAEMA could be observed (see Figure 3-7), suggesting the presence of aggregates with a PBMA solvating corona and a PAEMA core. Aggregates with the inverse

structure are formed in DMSO (spectrum not shown). In the following part, the focus will be on the aggregation behavior of PBMA-*b*-PAEMA copolymers in dilute cyclohexane solution at room temperature; a list of copolymer samples (BA1-5) is given in Table 3-2. Note that the glass transition of core-forming PAEMA should occur at about +3 °C (Table 2-5), and the aggregates can therefore be considered as equilibrium structures.

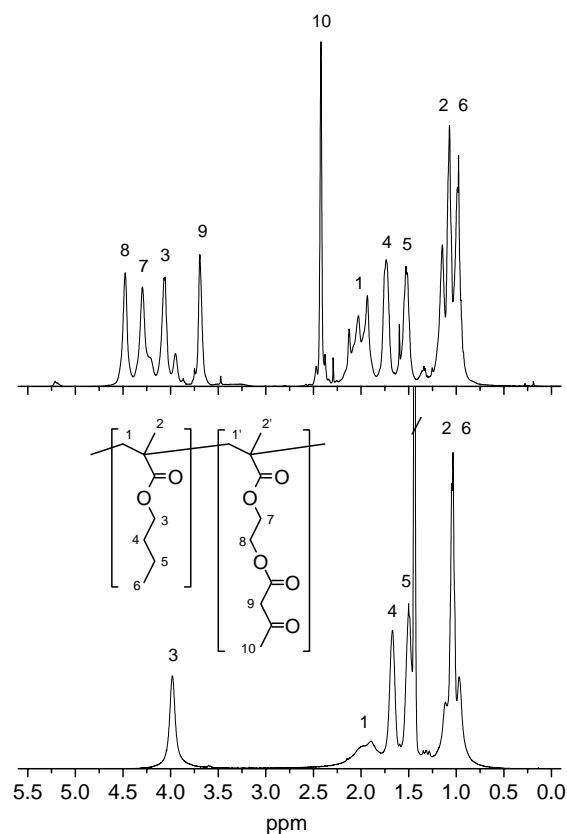


Figure 3-7. ^1H NMR spectra (400.1 MHz) of PBMA-*b*-PAEMA sample BA5 (see Table 3-2) in CDCl_3 (top) and cyclohexane- d_{12} (bottom) at 25 °C ($\prime =$ solvent).

Table 3-2. Molecular characteristics of the PBMA-*b*-PAEMA copolymers examined with respect to the aggregation behavior in dilute cyclohexane solution.

chemical structure	sample	$m (N_B)$	$n (N_A)$	$f_n^\#$
	BA2	342	39	0.10
	BA1	206	30	0.13
	BA3	58	10	0.15
	BA4	80	22	0.22
	BA5	74	60	0.45

$^\#$ Mole fraction of AEMA units.

DYNAMIC LIGHT SCATTERING (DLS) analysis was performed on 0.1-0.4 wt % solutions of BA1-4 in cyclohexane. In the case of BA5, the copolymer sample with the highest mole frac-

tion of AEMA (see Table 3-2), the concentration had to be lowered to 0.005-0.00625 wt % in order to avoid precipitation. DLS showed the presence of aggregates with hydrodynamic radii $R_h = 10$ -50 nm. All measured particle size distributions were found to be monomodal. It is noteworthy that virtually identical values of R_h were obtained at any scattering angle and concentration examined, indicating a nearly monodisperse size distribution of the aggregates. The results also suggest that the polymer concentration had been chosen well above the critical micellization concentration (cmc; not determined).

STATIC LIGHT SCATTERING (SLS; standard Zimm analysis) provided information on the radius of gyration (R_g), the second virial coefficient (A_2), and the aggregation number (Z) of the aggregates BA1-5 in dilute cyclohexane solution; data are summarized in Table 3-3. The values obtained for R_g/R_h suggested that BA1 and BA2 micelles had a spherical shape ($R_g/R_h \sim 0.8$, theoretical value for a hard sphere: $R_g/R_h = 0.775$).¹²⁰ Values of $R_g/R_h > 1$, which on the other hand had been found for the samples BA4 and BA5, suggested that these micelles had a non-spherical or cylindrical morphology. Accordingly, the values of A_2 were positive for BA1 and BA2 (\rightarrow closed aggregation) and negative for BA4 and BA5 (\rightarrow open aggregation). However, the micelles of BA3 were too small in size ($R_h = 11$ nm, Table 3-3) to access the value of R_g with sufficiently high accuracy. Since $A_2 > 0$ and $Z = 93$, the BA3 micelles supposedly had a spherical shape like the ones of BA1 and BA2. For BA2 and BA5, light scattering results could be confirmed by the visualization of the micelles with ATOMIC FORCE MICROSCOPY (AFM; not shown).¹²¹

Table 3-3. Experimental light scattering results (DLS and SLS) obtained for the micellar aggregates of PBMA-*b*-PAEMA samples BA1-5 in dilute cyclohexane solution (BA1-4: 0.1-0.4 wt %, BA5: 0.005-0.00625 wt %) at 20 °C.

sample	R_h (nm) ^{&}	R_g (nm) [§]	R_g/R_h	Z [§]	$A_2 \cdot 10^8$ (mol cm ⁻³ g ⁻²) [#]
BA2	32	26	0.81	342	0.15
BA1	31	24	0.77	311	0.12
BA3	11	(38)	(3.45)	93	0.14
BA4	12	21	1.75	120	-1.50
BA5	49	54	1.10	1025	-81.4

[&] Hydrodynamic radius (DLS). [§] Radius of gyration (SLS). [§] Aggregation number, $Z = M_{w, \text{micelle}} / M_{w, \text{polymer}}$ (SLS/NMR, SEC). [#] Second virial coefficient (SLS).

Regarding the high value of $\chi \sim 0.8$ (see above), it appears appropriate to discuss the scaling behavior of aggregation numbers Z in the framework of the model introduced by Antonietti

and Förster.^{107,122} This model is based on the work of Zhulina and Birshtein¹²³ and describes spherical micelles in the strong segregation limit, where the strong enthalpic repulsion of two blocks A and B (here: PAEMA and PBMA, respectively) leads to the formation of a sharp core–corona interface. Because of the sharp boundaries, the size of the spherical core is determined by space filling arguments leading to a scaling relation $Z \propto N_A^2$ (N_A : number of repeating units of the insoluble block). Note that for cylindrical micelles it is $Z \propto N_A$. In addition, $Z \propto N_B^{-0.8}$ (N_B : number of repeating units of the soluble block) has experimentally been found for several block copolymer systems and low-molecular weight surfactants.¹⁰⁷

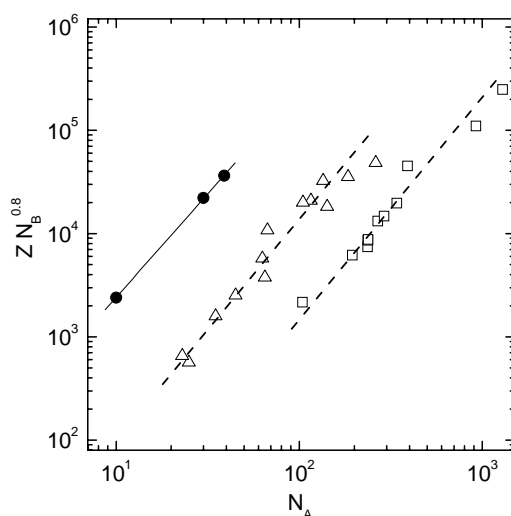


Figure 3-8. Plot of the aggregation number of block copolymer micelles (Z) as a function of the number of repeating units of the soluble block (N_B) and the insoluble block (N_A);¹⁰⁷ circles: PBMA-*b*-PAEMA/cyclohexane (this work; BA1-3), triangles: PS-*b*-P4VP/toluene (ref. ¹⁰⁷), squares: PS-*b*-PMAA/dioxane-water 80:20 (v/v) (ref. ¹²⁴). Linear fit, BA1-3: $Z_0 + \alpha N_A$, $Z_0 = 23.7 \pm 1.1$, $\alpha = 2.01 \pm 0.02$.

As can be seen from the plot in Figure 3-8, the aggregation numbers obtained for the micelles of BA1-3 in cyclohexane (see Table 3-3) are in very good agreement with the expected scaling law:

$$Z = Z_0 N_A^2 N_B^{-0.8} \quad (1)$$

with $Z_0 = 23.7 \pm 1.1$.¹⁰⁷ Note that the aggregation numbers of BA1-3 micelles are substantially larger than for example the ones reported in the literature for polystyrene-*block*-poly(4-vinylpyridine)/toluene¹⁰⁷ or polystyrene-*block*-poly(methacrylic acid)/dioxane-water 80:20 (v/v)¹²⁴ (triangles and squares in Figure 3-8).

The volume and the interface area of the spherical PAEMA core are given by

$$4\pi/3 R_c^3 = Z N_A v_0 \quad (2)$$

$$4\pi R_c^2 = Z b^2 \quad (3)$$

respectively. $v_0 = m_0 (\rho_0 N_L)^{-1} = 0.282 \text{ nm}^3$ (m_0 : molar mass ($214.22 \text{ g mol}^{-1}$), ρ_0 : bulk density (1.263 g cm^{-3} , Table 2-5), N_L : Avogadro's number) denotes the molar monomer volume, R_c the radius of the core, and b the interchain distance at the core–corona interface. The values of R_c and b , which were calculated for BA1-3, are summarized in Table 3-4.

From these two basic equations, the aggregation number is calculated by

$$Z = 36 \pi N_A^2 v_0^2 b^{-6} \quad (4)$$

According to experimental results,¹⁰⁷ the interchain distance b is determined by the number of repeating units of the soluble block (N_B) and does not depend on N_A :

$$b = b_0 N_B^\varepsilon \quad (5)$$

For BA1-3, linear regression of the data listed in Table 3-4 yielded $b_0 = (0.88 \pm 0.01) \text{ nm}$ and $\varepsilon = 0.127 \pm 0.001$ (bilogarithmic plot not shown, cf. Figure 3-9). It should be pointed out that b_0 , the interchain distance b extrapolated to $N_B \rightarrow 1$, is very similar to the ones obtained for ionic surfactants in water ($b_0 \sim 0.82 \text{ nm}$). For block copolymers, it is usually found $b_0 > 1 \text{ nm}$ and $\varepsilon \sim 0.14$.¹⁰⁷

The Z_0 parameter is then given as

$$Z_0 = 36 \pi v_0^2 b_0^{-6} = 36 \pi \Delta_0^3 \quad (6)$$

$\Delta_0 \equiv v_0^{2/3} b_0^{-2} = 0.59 \pm 0.01$ is a dimensionless intrinsic packing parameter, which is related to the geometric packing parameter Δ introduced by Israelachvili¹²⁵ via

$$\begin{aligned} \Delta &\equiv \nu(a l)^{-1} = (N_A v_0)(b^2 N_A v_0^{1/3})^{-1} = v_0^{2/3} b^{-2} \\ &= \Delta_0 N_B^{-2\varepsilon} \end{aligned} \quad (7)$$

For surfactants, $\nu/(a l)$ is calculated from the optimal head group area a , the volume ν , and the contour length l of the hydrocarbon chain. For block copolymers, it is considered $\nu = N_A v_0$, $a = b^2$, and $l = N_A v_0^{1/3}$.¹⁰⁷

Table 3-4. Geometric characteristics of the spherical micelles of PBMA-*b*-PAEMA samples BA1-3 in cyclohexane.

sample	N_A	N_B	Z	l_c (nm) ^{&}	R_c (nm) [§]	b (nm) [#]	Δ^*
BA2	39	342	342	10.1	9.6	1.8	0.13
BA1	30	206	311	7.8	8.6	1.7	0.14
BA3	10	58	93	2.6	4.0	1.5	0.20

[&] Contour length of the PAEMA chain, $l_c/\text{nm} = 0.26 \cdot N_A$. [§] Radius of the spherical PAEMA core, eq. 2. [#] Interchain distance at the core–corona interface, eq. 3. ^{*} Geometric packing parameter, eq. 7.

Knowing the value of Δ makes it possible to predict the shape and size of a surfactant or block copolymer micelle. Depending on Δ they will form spherical micelles ($\Delta < 1/3$), non-spherical or cylindrical micelles ($1/3 \leq \Delta \leq 1/2$), bilayers or vesicles ($1/2 \leq \Delta \leq 1$). For BA1-3, it is $\Delta = 0.13$ - 0.20 (see Table 3-4) and micelles should therefore have a spherical shape; this finding is consistent with the result from DLS/SLS measurements. As can be seen from the plot Δ vs. N_B in Figure 3-9, as calculated according to eq. 7, a decrease in N_B should cause a shape transition from spheres to cylinders to bilayers. Spheres should be formed if $N_B \geq 10$, cylinders if $N_B \sim 2$ - 10 , and bilayers or vesicles if $N_B = 1$ - 2 .

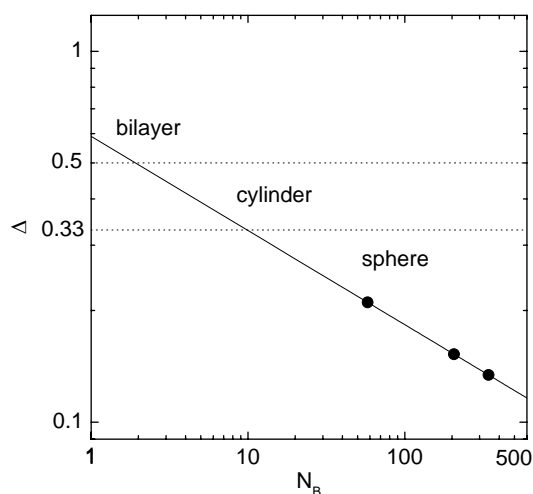


Figure 3-9. Plot of the geometric packing parameter, Δ , vs. the number of repeating units of the soluble block, N_B , for PBMA-*b*-PAEMA in cyclohexane (● BA1-3). The solid line was calculated according to eq. 7 using $\Delta_0 = 0.59$ and $\varepsilon = 0.127$ (see text).

Hence, any of the samples investigated (BA1-5, $N_B \geq 58$) should exhibit a spherical morphology. This prediction is in obvious disagreement with the experimental results from DLS/SLS and AFM measurements (see above), which clearly showed non-spherical or cylindrical micelles for BA4 ($N_B = 80$) and BA5 ($N_B = 74$).

It is important to note that, for the sake of simplicity, packing parameters Δ were calculated employing $l = N_A v_0^{1/3}$ as the length of the core-forming block segment (cf. eq. 7), i.e. monomer units were considered to have a cubical shape, which is certainly not true for AEMA. For local packing issues, however, it is indispensable to distinguish between long monomers with a small side group and short monomers with a large side group. The aspect ratio, i.e. the ratio of segment lengths parallel and perpendicular to the chain axis, appears to be a suitable parameter for describing the geometry of a given monomer unit. It can be expressed as

$$\sigma^{1/3} = L v_0^{-1/3} \quad (8)$$

with $L = l_c / N_A = 2.6 \text{ \AA}$ as the contour length of the AEMA unit. Eq. 7 then transforms into

$$\begin{aligned}\Delta &= (N_A v_0)(b^2 N_A L)^{-1} = (v_0^{2/3} b^{-2})(v_0^{1/3} L^{-1}) = (v_0^{2/3} b^{-2}) \sigma^{-1/3} \\ &= \sigma^{-1/3} \Delta_0 N_B^{-2\varepsilon}\end{aligned}\quad (9)$$

As can be seen from the plot in Figure 3-9, the aspect ratio of the insoluble monomer has considerable impact on the “phase diagram” of block copolymer micelles; the smaller the value of $\sigma^{1/3}$ the more the shape transition points are shifted to higher N_B . Hence, the Antonietti–Förster model extended by the aspect ratio $\sigma^{1/3}$, seems to describe the micellization behavior of PBMA-*b*-PAEMA correctly—at least on a semi-quantitative basis.

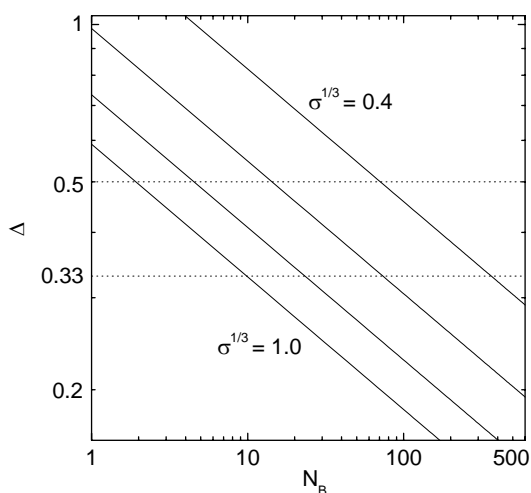


Figure 3-10. Plot of the geometric packing parameter, Δ , vs. the number of repeating units of the soluble block, N_B , for different aspect ratios of the insoluble monomer, $\sigma^{1/3} = 0.4, 0.6, 0.8,$ and 1.0 (top to bottom) (eq. 9; $\Delta_0 = 0.59$ and $\varepsilon = 0.127$).

For the special case $\sigma^{1/3} = 0.4$, the aspect ratio calculated for AEMA, the transition from spheres to cylinders should have occurred at $N_B \sim 370$ and that of cylinders to bilayers at $N_B \sim 70$. All PBMA-*b*-PAEMA samples (but BA3, see above) should then have formed cylindrical rather than spherical micelles, which obviously is not true. The apparent failure of the model, however, might be due to experimental errors in the determination of especially Δ_0 and ε (cf. eq. 9); these values had been obtained on the basis of eq. 5 considering just three data points (BA1-3). If the value of ε was just $\sim 10\%$ larger, shape transitions would have been expected to occur at $N_B \sim 200$ (sphere \rightarrow cylinder) and $N_B \sim 50$ (cylinder \rightarrow bilayer), which is in good agreement with experimental data. The micelles of BA3 ($N_B = 58$), however, should then be non-spherical in shape, contrary to what has earlier been proposed (see above).

Whether or not the proposed model can appropriately describe the micellization behavior of strongly segregated block copolymer systems remains an open question. An extension of the studies to a far larger number of block copolymer samples with different compositions and molecular weight will be necessary—this work is currently in progress.¹¹⁹

It is obvious, however, that the presence of a selective solvent (or metal ion salt, see chapter 4.1) should increase the molar volume of the core-forming monomer unit, thus affecting the value of the packing parameter ($\Delta \propto v_0$, eq. 9) and the morphology of the aggregates. A swelling of the micellar core would in Figure 3-9 be represented as a vertical line ($N_B = \text{const.}$).

Swelling experiments were performed with spherical micelles of BA1 in dilute cyclohexane solution using 2,2,2-trifluoroethanol (TFE) as a selective solvent for PAEMA (cf. Table 2-5). Since in addition TFE is not miscible with cyclohexane, TFE should quantitatively be taken up by the PAEMA core. Six samples of ~0.4 wt % solutions of BA1 in cyclohexane containing different amounts of TFE, molar ratio $f_T = [\text{TFE}]/[\text{AEMA}] = 0.33\text{--}10$ (12), were prepared and then analyzed by DLS and SLS—the results are summarized in Table 3-5.

Table 3-5. Characteristics of the micelles formed by PBMA-*b*-PAEMA sample BA1 in cyclohexane at 20 °C in the presence of different amounts of 2,2,2-trifluoroethanol (TFE), as obtained by dynamic and static light scattering (DLS and SLS).

sample	f_T^*	dn/dc ($\text{cm}^3 \text{g}^{-1}$) [∅]	R_h (nm) [#]	R_g (nm) [§]	R_g/R_h	$Z^{\&}$	$A_2 10^9$ ($\text{mol cm}^{-3} \text{g}^{-2}$) [§]	
BA1	0	0.0534	31	24	0.77	311	1.2	
BA1-0.33	0.33	0.0405	30	42	1.42	547	1.1	
BA1-1.0	1.0	0.0342	32	63	1.97	1075	-0.2	
BA1-2.0	2.0	0.0183	32	53	1.66	3193	0.7	
BA1-5.0	5.0	-0.0109	28	40	1.43	6505	0.8	
BA1-10.0	10.0	-0.0324	28	28	1.00	293	0.6	
BA1-12.0	20.0	————— precipitation / gelation —————						

* Molar ratio $[\text{TFE}]/[\text{AEMA}]$. [∅] Refractive index increment. [#] Hydrodynamic radius (DLS). [§] Radius of gyration. [&] Aggregation number, $Z = M_{w, \text{micelle}} / (M_{w, \text{BA1}} + 30 f_T M_{\text{TFE}})$. [§] Second virial coefficient (SLS).

As can be seen by the values of the ratio R_g/R_h , the addition of ~15 wt % TFE ($f_T = 0.33$) was already sufficient to transform the spherical BA1 micelles ($R_g/R_h = 0.77$) into cylindrical ones ($R_g/R_h > 1.4$). The existence of cylindrical micelles was observed up to $f_T = 5.0$. Aggregation numbers were found to increase tremendously with increasing amount of TFE, reaching a maximum value $Z \sim 6500$ at $f_T = 5.0$. At $f_T = 10$, light scattering data suggest the presence of vesicular aggregates ($R_g/R_h = 1$) with $Z \sim 290$. Further addition of TFE led to the precipitation of aggregates as a gel.

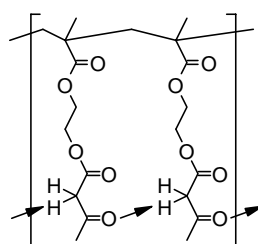
Evidently, the morphology of aggregates can be triggered by swelling of the PAEMA core with TFE. Although it is not yet possible (see above) to apply the extended Antonietti–Förster

model for a quantitative analysis of these swelling experiments, it is believed that this can be done in the near future.

3.2.2 Superstructures stabilized by hydrogen bridging

Hydrogen bonding interactions are well documented for β -dicarbonyl systems in literature.¹¹³ Acetylacetone, which is the most prominent example, shows both intra- and intermolecular hydrogen bonding motifs ($-\text{OH}\cdots\text{O}=\text{C}<$). However, as will be seen below, the homopolymers of 2-(acetoacetoxy)ethyl methacrylate (PAEMA) can produce large assemblies in solution and in the solid-state.¹¹⁵ Since homopolymers are not amphiphilic in nature, thus excluding the occurrence of micellization or segregation processes, the existence of these superstructures could only be explained by the presence of hydrogen bonding interactions between polymer chains (dipole moment observed for PAEMA: $\mu = 2.4$ Debye/monomer unit, Table 2-5).

As mentioned earlier in chapter 2.2.1, the acetoacetoxy groups in PAEMA preferentially exist in the form of a keto tautomer ($\sim 92\%$, ^1H NMR). However, considering the two possible tautomers, it is the β -ketoester which might at all give rise to intermolecular hydrogen bridging, as illustrated in Scheme 3-2. The circumstance that the AEMA units are connected *via* covalent bonds and thus are brought into close proximity should further promote the interacting between adjacent acetoacetoxy groups. This should not apply for low-molecular weight acetoacetates.



Scheme 3-2. Hydrogen bridging between adjacent acetoacetoxy groups in PAEMA.

FOURIER TRANSFORM-INFRARED SPECTROSCOPY (FT-IR) was first applied to show the existence of hydrogen bonds along PAEMA chains (sample A2, see Table 2-4); *tert*-butyl acetoacetate (*t*BAA) and poly(*tert*-butyl methacrylate) (*Pt*BMA) were used as reference materials. It was hoped that the spectrum of PAEMA would reveal additional signals in the region of carbonyl valence vibrations ($>\text{C}=\text{O}\cdots\text{H}-$; $\tilde{\nu} = 1600\text{-}1800\text{ cm}^{-1}$), which could not be observed for *t*BAA. However, this was not found to be the case. The spectra in Figure 3-11 suggest that the carbonyl signals of PAEMA are just a superposition of those of *t*BAA and *Pt*BMA. It should be pointed out that FT-IR measurements were performed with neat *t*BAA and PAEMA

specimens. Packing of acetoacetoxy groups in *t*BAA should therefore be nearly as close as in PAEMA, thus diminishing any differences in the tendency of forming hydrogen bridges.

In the ^1H NMR spectrum of PAEMA sample A1 (see Figure 3-12), which was measured at a concentration of ~ 5 wt % in CDCl_3 , the characteristic signals of the acetoacetoxy unit show at $\delta = 2.28$ ($-\text{CH}_3$) and 3.55 ppm ($-\text{CH}_2-$). The corresponding signals of *t*BAA arise at $\delta = 2.23$ and 3.33 ppm, respectively (acetylaceton, $\delta = 2.17$ and 3.62 ppm)¹²⁶. The downfield shift of the methylene proton signals by 0.22 ppm indicates a considerably stronger CH-acidity of the acetoacetoxy groups in PAEMA as compared to *t*BAA. This effect might be well explained by the presence of another electron-withdrawing group in the proximity of the methylene protons and hydrogen bonding interactions as illustrated in Scheme 3-2.

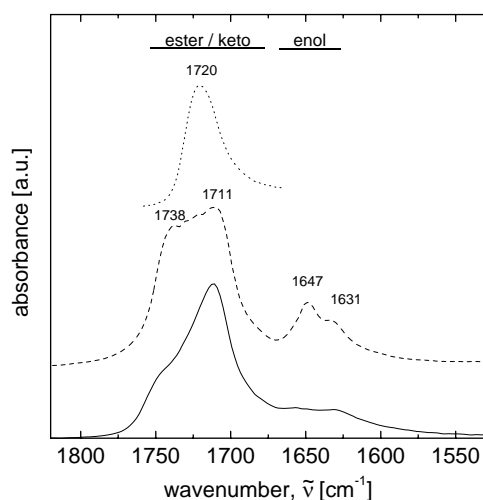


Figure 3-11. FT-IR spectra (region of carbonyl valence vibrations) of PAEMA sample A2 (solid line), *tert*-butyl acetoacetate (dashed line), and poly(*tert*-butyl methacrylate) (dotted line).

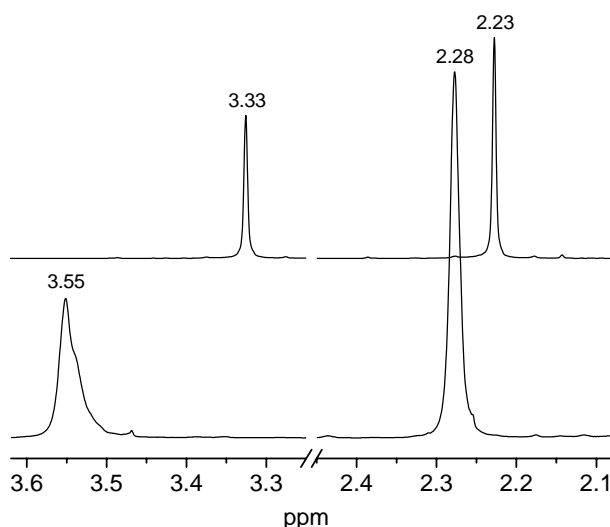


Figure 3-12. ^1H NMR spectra (400.1 MHz) of *t*BAA (top) and PAEMA sample A1 (bottom) in CDCl_3 at 25 °C; region of methylene ($\delta = 3.3$ -3.6 ppm) and methyl ($\delta = 2.2$ -2.3 ppm) proton signals of the acetoacetoxy group.

As mentioned above, hydrogen-bridging in the PAEMA homopolymers promoted the formation of very large assemblies in the solid state, for example when drying ~ 0.3 wt % solutions of PAEMA in tetrahydrofuran (THF) on a hydrophobic substrate. Figure 3-13 shows typical ATOMIC FORCE MICROSCOPY (AFM) images of rod-like superstructures formed by PAEMA sample A6 (number of AEMA repeating units, $n = 176$; Table 2-4) on graphite. The rods are ~ 12 nm in diameter and exhibit a persistence length (l_p) in the range of several hundreds of nanometers (compare: poly(γ -benzyl-L-glutamate) in *N,N*-dimethylformamide: $l_p \sim 150$ nm, DNA in 0.2 N aqueous NaCl: $l_p \sim 60$ nm)¹²⁷. AFM amplitude imaging with a sufficiently high resolution revealed a helical structure of these rods (see Figure 3-14), the pitch of the helix being ~ 25 nm. Rather as expected for a non-chiral system, both types of helices with opposite screw sense could be observed. Very similar structures were observed for PAEMA sample A2 with $n = 44$, i.e. the dimension of the helical superstructure seems not to depend on the length or molecular weight of the individual PAEMA chains. Nevertheless, both the thickness and the pitch are by far larger as expected for any kind of single-stranded helix.¹²⁷

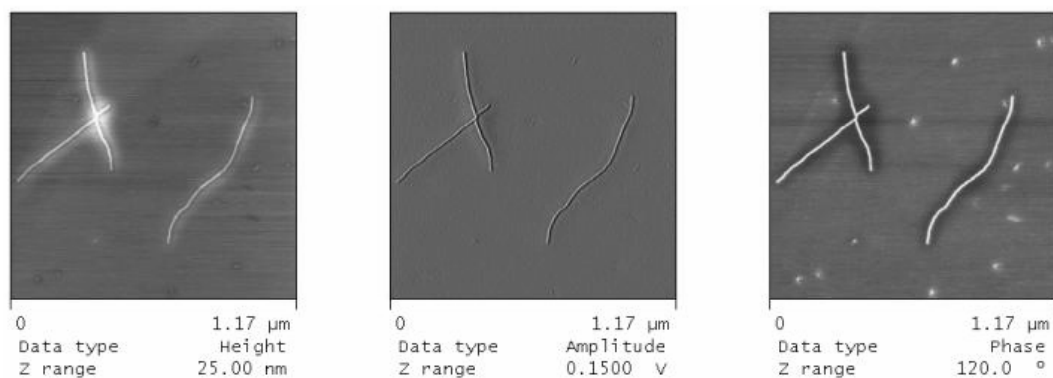


Figure 3-13. AFM tapping mode images ($1.17 \times 1.17 \mu\text{m}$) of the rod-like superstructures formed by PAEMA sample A6 at room temperature; the specimen was prepared by evaporating a drop of a ~ 0.3 wt % polymer solution in THF on graphite.

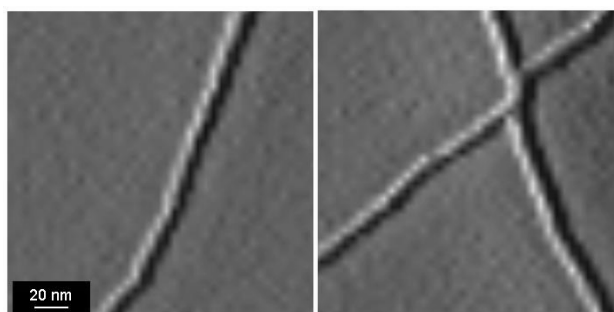


Figure 3-14. Magnification of the AFM amplitude image in Figure 3-13 ($0.18 \times 0.18 \mu\text{m}$) showing PAEMA helical strands with a left-handed (left) and a right-handed (right) sense.

However, the superhelices of hydrogen-bridged PAEMA chains were found to be not stable at room temperature. The AFM images in Figure 3-15, taken a few days after the first analysis

of the specimen (A2), showed a large number of small globules with a diameter of ~ 3 nm instead of a few large helices. Considering the bulk density of PAEMA (1.263 g cm^{-3} , see Table 2-5), a globule of that size should be made of just a single A2 chain. It is reasonable to assume that these globules result from the collapse (dissociation) of the superhelices, the driving force for the helix–globule transition being the considerable gain in entropy. Note that such a transformation in the solid-state could only take place because the glass transition of PAEMA is well below room temperature ($T_g \sim +3 \text{ }^\circ\text{C}$, see Table 2-5).

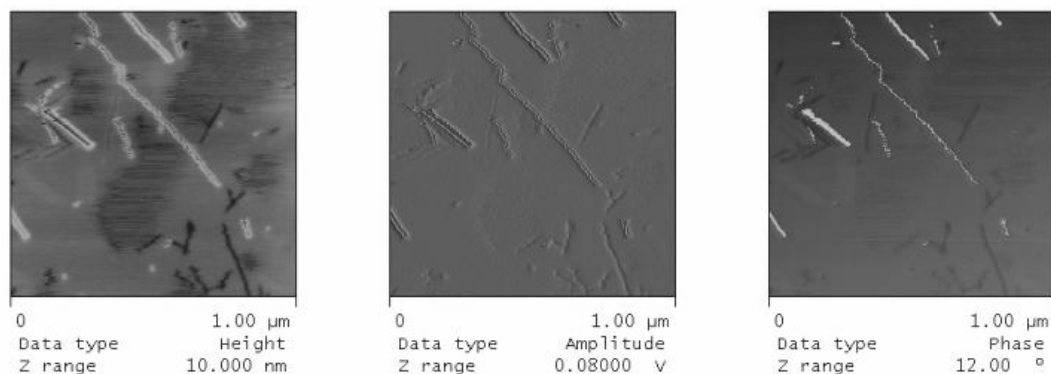


Figure 3-15. AFM tapping mode images ($1.0 \times 1.0 \mu\text{m}$) of PAEMA globules, which are produced upon aging of the helical superstructures (cf. Figure 3-13 and Figure 3-14) at room temperature; sample A2, substrate: graphite.

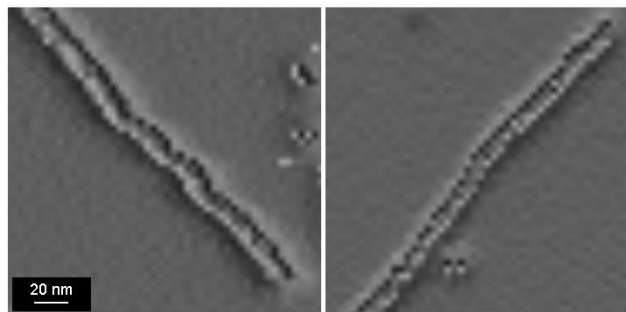


Figure 3-16. Magnification of the AFM amplitude image in Figure 3-15 ($0.18 \times 0.18 \mu\text{m}$) showing globules of single PAEMA chains.

It can be seen in Figure 3-16 that the PAEMA globules are aligned in two parallel rows. The occurrence of such a rather unusual arrangement might be a hint that the original superhelices were composed of two strands of PAEMA chains, like for example in DNA. However, even a DNA double-helix of the type A is no wider than 2.55 nm ,¹²⁸ which is one fourth the diameter of a PAEMA superhelix. A definite structure model of the superhelix cannot be given at the present stage of investigations; supposedly it should be a double helix with an inner hollow compartment. Detailed investigations of the structures with microscopic and scattering techniques are currently in progress. These studies might possibly be complicated by the fact that the PAEMA superhelices can arrange into larger bundles. First AFM results (not shown) in-

dicates that such bundles can have a diameter of ~ 25 nm and a persistence length of greater than 1 μm .

It is also noteworthy that these superstructures could not be observed in dilute THF solution (DYNAMIC LIGHT SCATTERING (DLS)). Supposedly, the THF molecules act as Lewis base and interfere with the hydrogen bridges in PAEMA, thus avoiding the growth of aggregates. This result, on the other hand, might be taken as evidence for the stabilization of superstructures *via* hydrogen bonding. However, first results suggest that very large assemblies are present in the dilute solutions of PAEMA in trifluoroethanol (TFE). TFE is well known, in contrast to THF, for its ability to stabilize hydrogen bonds. The structure of the PAEMA aggregates in TFE could not yet be determined—this is subject of ongoing work.

3.3 Polypeptide block copolymers

Gallot et al.^{48-50,129-131} introduced linear polyvinyl-polypeptide AB block copolymers and were the first to investigate their lyotropic phase behavior and solid-state morphologies. Due to the α -helical secondary structure of the polypeptide segment, these polymers are classified as rod-coil block copolymers. In the solid-state, a lamellar morphology of alternating polyvinyl and polypeptide sheets was found, regardless of the volume fraction of comonomers. The intersheet spacing or long period (d), as determined by SMALL-ANGLE X-RAY SCATTERING (SAXS), was 25-35 nm, just very weakly depending on the molecular weight of the copolymer. In addition to this lamellar superstructure, the α -helical polypeptide chains arranged in a hexagonal array with a characteristic lattice spacing $d_H \sim 1.5$ nm. The longer the polypeptide chains, the more often helices were back-folded (up to seven times). A schematic illustration of the *hexagonal-in-lamellar* morphology formed by polypeptide block copolymers is depicted in Chart 3-2.¹⁷

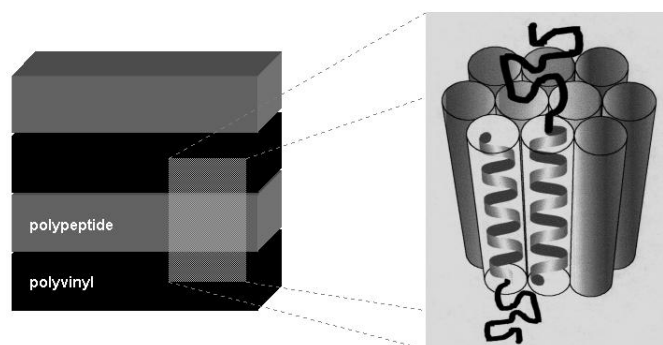


Chart 3-2. Schematic representation of the *hexagonal-in-lamellar* solid-state morphology of polyvinyl-polypeptide block copolymers.

As indicated by five to seven orders of SAXS reflections, the quality of lamellar order in the films was extraordinarily high.⁴⁹ In addition, X-RAY PHOTOELECTRON SPECTROSCOPY (XPS) showed that lamellae were aligned perpendicularly to the surface.¹³¹

Samyn et al.⁸⁶ and Hayashi et al.¹³²⁻¹³⁴ extended studies to ABA triblock copolymers, which consisted of a central polyvinyl/polydiene block and two outer polypeptide blocks, essentially supporting the results of Gallot et al. However, very peptide-rich copolymers did not form a *hexagonal-in-lamellar* morphology, instead it was observed spheres or cylinders of the minority phase dispersed in a matrix of hexagonally arranged polypeptide helices.¹³⁴ As reported by Klok et al.,^{89,135} polypeptide diblock oligomers formed a *hexagonal-in-hexagonal* structure.

Compared to solid-state structures, the aggregation behavior of polypeptide block copolymers has been examined to much lesser extent. Hayashi et al.^{132,136} investigated the micelles of

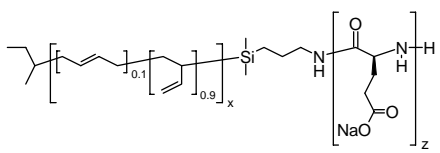
ABA triblock copolymers in various organic solvents, polypeptides (A) always forming the solvating corona of the aggregates. Depending on the volume fraction of the polybutadiene phase (B), either spheres (0.18-0.22), cylinders (0.28-0.51), or lamellae (0.56-0.72) could be observed by TRANSMISSION ELECTRON MICROSCOPY (TEM). Evidently, the helical secondary structure of the polypeptides had no effect on the phase behavior in dilute solution, in contrast to its dominant role for structure formation in concentrated solutions and in the solid-state.⁴³ Nolte et al.^{15,16} reported for polystyrene-*block*-poly(isocyanodipeptide)s an unexpectedly rich phase behavior including the formation of filaments and “helical superstructures” in aqueous media (see Figure 1-4). Very recently, Schlaad et al.¹¹¹ and Lecommandoux et al.^{137,138} independently described the pH-responsiveness of poly(L-glutamate)-based vesicles in aqueous solution.

In the following chapter 3.3.1 will be described the work on the aggregation behavior of polybutadiene-*block*-poly(L-glutamate) (PB-*b*-PLGluNa) copolymers.¹¹¹ Main focus of the project was to examine the effect of the helix-coil transition in the solvating peptide segments, triggered by the pH of the solution, on the properties of aggregates. Chapter 3.3.2 will summarize the structural investigations on thick films of linear and bottlebrush-shaped polystyrene-*block*-poly(Z-L-lysine)s (PS-*b*-PZLLys).^{139,140} The impact of the chain length distribution of polypeptide segments and the topology of copolymers on solid-state structures will be discussed.

3.3.1 Aggregates in dilute solution

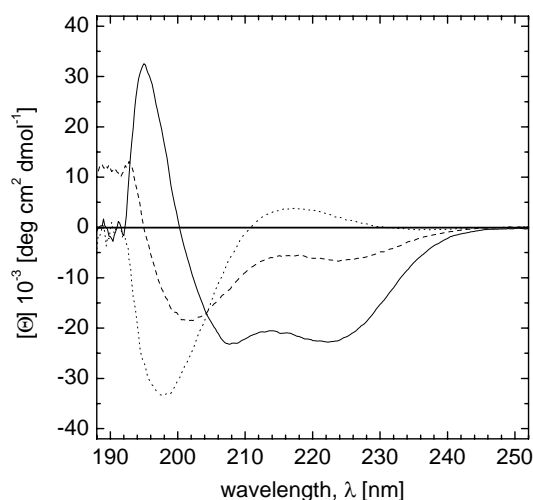
A series of four polybutadiene-*block*-poly(sodium L-glutamate) copolymers (PB-*b*-PLGluNa) (BN1-4, Table 3-6) was synthesized to study the aggregation behavior in dilute aqueous solution.¹¹¹ The γ -benzyl protecting groups of corresponding precursor polymers BG1-4 (Table 2-11) were removed by a palladium-catalyzed hydrogenation at room temperature using ammonium formate as the hydrogen source;¹⁴¹ carboxylic functional groups were subsequently neutralized with NaOH. FOURIER TRANSFORM-INFRARED SPECTROSCOPY (FT-IR) proved the successful deprotection of the samples by the lack of the characteristic ester vibrational bands ($\tilde{\nu} = 1731, 1165 \text{ cm}^{-1}$) and appearance of a carboxylate band ($\tilde{\nu} = 1395 \text{ cm}^{-1}$). Note that the hydrogenolysis, unlike hydrolysis in strongly alkaline or acidic environments, proceeds at very mild reaction conditions without risking considerable racemization or degradation of the polypeptide segment. It is also important to mention that the PB double bonds were not touched by the hydrogenolysis (FT-IR).

Table 3-6. Molecular characteristics of the linear PB-*b*-PLGluNa copolymers investigated with respect to the aggregation behavior in dilute aqueous solution.

chemical structure	sample	x	z	$f_z^\#$
	BN1	27	64	0.70
	BN2	85	75	0.47
	BN3	85	55	0.39
	BN4	119	24	0.17

[#] Mole fraction of L-glutamate units.

The samples BN1-4 dissolved readily in water or aqueous NaCl solution at room temperature. As suggested by Förster et al.,¹⁴² a soft poly(1,2-)butadiene block with a glass transition temperature of about $-14\text{ }^\circ\text{C}$, should promote the generation of equilibrium structures rather than frozen-in, metastable states. Poly(L-glutamate) was chosen as the water-soluble block because of its ability to perform a pH-induced coil-helix transition; the random coil conformation is adopted when glutamate units are neutralized and thus charged.¹⁴³ In the case of BN1-4, the transition from a random coil to an α -helix occurred at $\text{pH} \sim 5.2$, as indicated by CIRCULAR DICHROISM SPECTROSCOPY (CD) (cf. Figure 3-17). The appearance of a single isodichroistic point at $\lambda = 204\text{ nm}$ suggested that no other than these two conformations were present. From the absolute values of the molar ellipticity ($[\Theta]$), it was possible to estimate the percentage of coil at $\text{pH} > 6$ to be 100%, decreasing to $\sim 20\%$ at $\text{pH} = 4.3$.¹⁴⁴ Lowering the pH of the solution below the $\text{p}K_a$ value of glutamic acid (4.32) resulted in precipitation of the copolymers. Hence, 80% was the maximum percentage of α -helix which could be achieved for B1-4 under preservation of solubility.

**Figure 3-17.** CD spectra of the PB-*b*-PLGlu(Na) sample BN3 (0.05 wt %) in a 0.12 M aqueous NaCl solution at 25 °C: pH = 6.0 (dotted line, helix:coil 0:100), 5.2 (dashed line, helix:coil 20:80), 4.6 (solid line, helix:coil 70:30).¹⁴⁴

The solutions of BN1-4 (0.1-0.5 wt %) were analyzed by DYNAMIC LIGHT SCATTERING (DLS) at pH 4.6-6.0 to yield the size distribution and the average hydrodynamic radius (R_h) of the aggregates; the results are summarized in Table 3-7. The DLS measurements were performed in the presence of NaCl ($[\text{NaCl}]/[\text{LGlu}] > 6$) to suppress electrostatic interactions between the polyelectrolyte molecules. It is further important to mention that virtually identical results were obtained whether or not the solutions had been treated with ultrasound and/or heat, and the samples were re-analyzed after days or weeks of storage. The narrow size distributions obtained for BN1-4 aggregates (cf. Figure 3-18), however, suggested that the samples were in a well-equilibrated state.

Table 3-7. Hydrodynamic radii (R_h) of the aggregates formed by the PB-*b*-PLGlu(Na) samples BN1-4 in dilute aqueous NaCl solution in dependence of the pH and the conformation of the PLGu segment.

sample	$f_z^\#$	R_h (nm) ^{&}		
		pH 4.6 helix:coil 70:30 [§]	pH 5.2 helix:coil 20:80 [§]	pH 6.0 helix:coil 0:100 [§]
BN1	0.70	— [*]	16	17
BN2	0.47	32	—	35
BN3	0.39	81	70	90
BN4	0.17	84	86	90

[#] Mole fraction of the L-glutamate block. [&] Determined by DLS. [§] Estimated from CD molar ellipticities (cf. Figure 3-17) according to ref. ¹⁴⁴. ^{*} Precipitation of the copolymer.

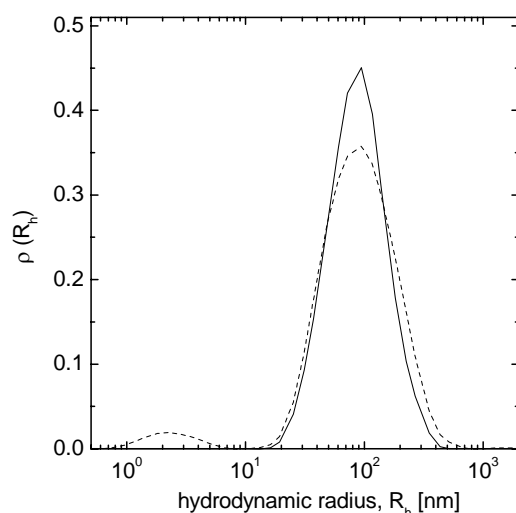


Figure 3-18. Intensity-weighted size distribution (CONTIN) of the aggregates formed by the PB-*b*-PLGluNa samples BN3 (dashed line) and BN4 (solid line) in a 0.5 wt % aqueous NaCl solution (pH ~ 6.0) at 20 °C.

Samples BN1 and BN2 (mole fraction of LGlu, $f_z > 0.4$) were found to form small aggregates with $R_h \sim 17$ and 35 nm, respectively, while the aggregates of BN3 and BN4 ($f_z < 0.4$) were

considerably larger, i.e. $R_h = 70-90$ nm (see Table 3-7). All aggregates had a spherical shape, as indicated by the absence of depolarized scattering of light, and consisted of a PB core and a PLGlu corona. The hydrodynamic size of the aggregates, however, was virtually not affected by the conformation of the PLGlu segment (see below). Note that, despite the fact that PB and PLGlu are highly incompatible and the critical micellization concentration (cmc) of copolymers should be considerably lower than 0.1 wt %, samples BN1-3 contained large amounts of supposedly non-aggregated chains ($R_h \sim 2$ nm; cf. Figure 3-18). SIZE EXCLUSION CHROMATOGRAPHY (SEC; eluent: 0.145 N aqueous NaCl at 25 °C, stationary phase: PL-aquagel, detectors: RI and MALLS) suggested that the weight fraction of aggregates was less than ~1%. Sample BN4 with the lowest content of LGlu ($f_z = 0.17$), on the other hand, showed only large aggregates (see Figure 3-18). It therefore appears that an intramolecular stabilization of the hydrophobic segment is not feasible when the radius of gyration (or volume) of the PB coil exceeds that of PLGlu, that is when $f_z < 0.32$.

The aggregates formed by BN1 and BN2 at pH 4.6-6.0 supposedly are spherical micelles. For BN1, estimation of the radius of the PB core and the thickness of the PLGlu corona yields 5 nm and 11 nm, respectively. The latter value is well between the limiting end-to-end distances of a randomly coiled (2.8 nm) and a fully stretched polypeptide chain (24.3 nm). It is interesting to note that an α -helix with 64 LGlu units would have a length of 9.6 nm,¹³⁰ which is very similar to that of a stretched corona chain. That is why a change in conformation of the PLGlu segment might not have been reflected in the size of the micelles. In the case of BN2 micelles, the thickness of the PLGlu corona at pH 6.0 is ~19 nm, and the length of the 70% α -helical PLGlu₇₅ chain at pH 4.6 should be in the order of 16 nm. A shrinkage of the hydrodynamic size of micelles by ~10% could indeed be observed ($\Delta R_h = -3$ nm, see Table 3-7), but this is within the range of experimental errors. Additional STATIC LIGHT SCATTERING (SLS) measurements are needed to characterize the micellar aggregates in greater detail. However, the determination of aggregation numbers by SLS is heavily complicated by the fact that PLGlu is a weak polyelectrolyte, for which the degree of ionization and conformation are dependant on concentration.

In the case of the copolymers BN3 and BN4, the hydrodynamic radius of the aggregates, although spherical, exceeded the contour length of the copolymer chains (~45 nm) by a factor of 1.5-2. The aggregates were therefore too large to be simple micelles¹⁰⁷ and should rather be polymer vesicles,¹⁴⁵⁻¹⁴⁷ also referred to as "polymersomes"¹⁴⁸ or "peptosomes"¹⁴⁹ (cf. Scheme 3-3). In order to prove the vesicular structure of the aggregates, the aqueous solutions of BN3

were investigated by SMALL-ANGLE NEUTRON SCATTERING (SANS) (see Figure 3-19). The form factors found at all examined concentrations (1-4 wt %) were in perfect agreement with the form factor of vesicles (see solid lines in Figure 3-19). Data analysis^{110,111} yielded an outer vesicle radius $R_h = 62$ nm and a bilayer thickness $\Delta R = 28$ nm with particle size distributions of 33% for any sample. The peptosomes of BN3 could be visualized in electron micrographs which were taken from freeze-fractured specimens of the aqueous polymer solution (see Figure 3-20). The micrographs showed spherical aggregates that are 110-190 nm in diameter, which is in accord with the results obtained from scattering experiments.

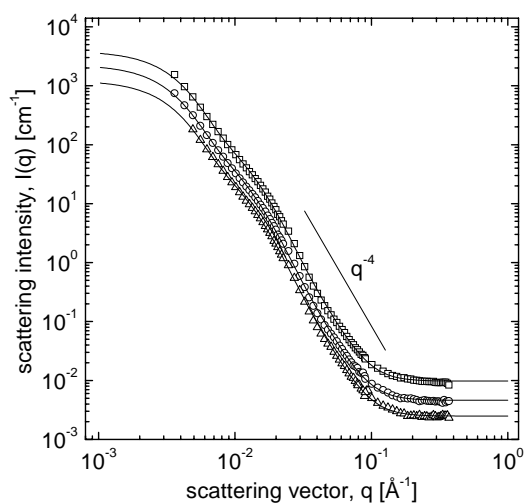


Figure 3-19. SANS curves of 1.0 (triangles), 2.0 (circles), and 4.0 (squares) wt % solutions of PB-*b*-PLGluNa sample BN3 in 0.12 M NaCl in D₂O at 25 °C (pH ~ 6). The solid lines are the result of fitting the data to the form factor of a polydisperse hollow sphere.^{110,111}

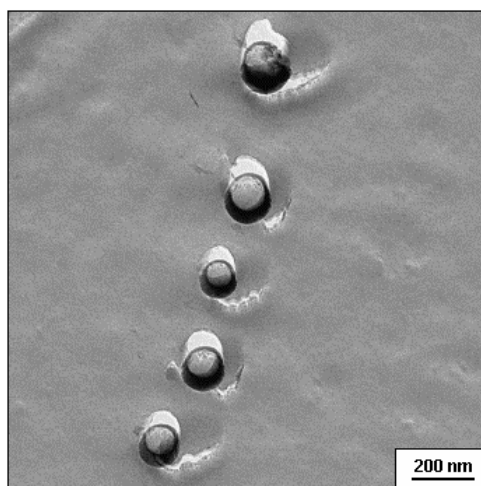
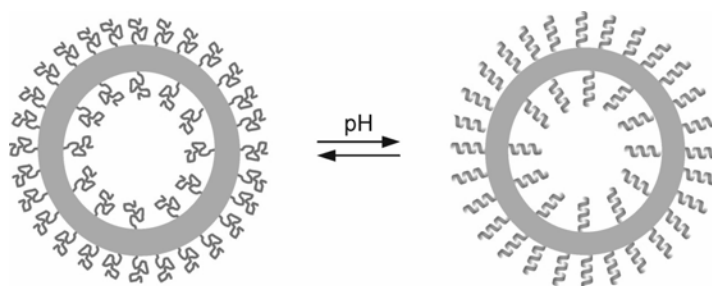


Figure 3-20. Freeze-fracture electron micrograph of a vesicular solution of PB-*b*-PLGluNa sample BN3 (5 wt %) in pure water (pH ~ 6).

It must be emphasized that those structures were generated by simple dissolution. Hence, there must be a driving minimum of free energy and an exchange of single block copolymer

units, which established the present equilibrium situation, independent of the history of the sample. The strong tendency of water-soluble amphiphilic block copolymers to form vesicular aggregates was already documented for other systems by a number of working groups.¹⁵⁰⁻¹⁵⁶ The novelty in the present case is that the solvating chains are polypeptides, which can perform a helix-coil transition in dependence on pH without serious change of the vesicle morphology (cf. Scheme 3-3).



Scheme 3-3. Schematic representation of the pH-induced coil-helix transition in PB-*b*-PLGlu(Na) vesicles in dilute aqueous solution.

It should be noted that Lecommandoux et al.^{137,138} reported for a PB₄₀-*b*-PLGlu₁₀₀ copolymer in aqueous NaCl solution the formation of polymer vesicles with $R_h = 100-150$ nm, the size depending strongly on pH and salt amount. However, this sample had the same composition as BN1, which formed spherical micelles with $R_h \sim 16$ nm. The reason for the discrepancy of results is not known yet.

3.3.2 Solid-state structures

In this section, the structural analysis of PS-PZLLys block copolymer films by CIRCULAR DICHROISM SPECTROSCOPY (CD), SMALL-ANGLE X-RAY SCATTERING (SAXS), and MICROSCOPY (AFM and TEM) will be described.^{139,140} The films of linear and bottlebrush-shaped polymer samples (Table 3-8 and Table 3-10) of about 1 mm thickness were prepared by solvent-casting from 5-10 wt % polymer solutions in *N,N*-dimethylformamide (DMF) as a non-selective solvent; liquid samples on teflon-coated aluminum foil (BYTAC[®]) were slowly dried within 12-24 hours at 40 °C. The solids were then scratched off the foil and analyzed as powders. It is important to note that virtually the same morphology was produced, irrespective of the solvent used for casting of the film (DMF, chloroform, or dioxane) and whether or not the film was annealed at 110 °C, above the glass transition temperature of the PS block. It is noteworthy that decomposition of the samples occurred at 250 °C before the melting of the PZLLys block (THERMOGRAVIMETRIC ANALYSIS (TGA) and DIFFERENTIAL SCANNING CALORIMETRY (DSC)).

3.3.2.1 Linear block copolymers

As mentioned above, PS-PZLLys block copolymers exhibit a *hexagonal-in-lamellar* structure in the solid state (see Chart 3-2), the formation of which being governed by the packing of the PZLLys helices. Gallot et al.^{48,49} reported three or more orders of sharp lamellar reflections in the X-ray diffraction patterns, indicating a very high quality of lamellar order (the films were prepared by “slow evaporation of dioxane”). The high ordering might be attributed to the fact that the stacks of polypeptide lamellae are very rigid and have an “infinite” persistence length. It is important to note that copolymer samples were carefully fractionated and thus had a nearly monodisperse molecular weight distribution.

For the films of non-fractionated PS-PZLLys samples, on the other hand, the SAXS patterns obtained at low angles were rather ill-defined, often showing just a single, broad peak (cf. Figure 3-21, left) (Schlaad et al.¹³⁹). Nevertheless, the long-range order in the films was very high, i.e. in the range of microns, as seen by ATOMIC FORCE MICROSCOPY (AFM) (see Figure 3-21, right).¹⁴⁰ The apparent discrepancy between SAXS and AFM results could be explained with the existence of an *undulated* or *zigzag lamellar* superstructure. Here, stacks of lamellae are extended “infinitely” but the thickness of individual polypeptide layers is statistically fluctuating as illustrated in Chart 3-3. As will be discussed below, the origin of the fluctuating PZLLys layer thickness lies in the chain length distribution of helices.¹⁴⁰

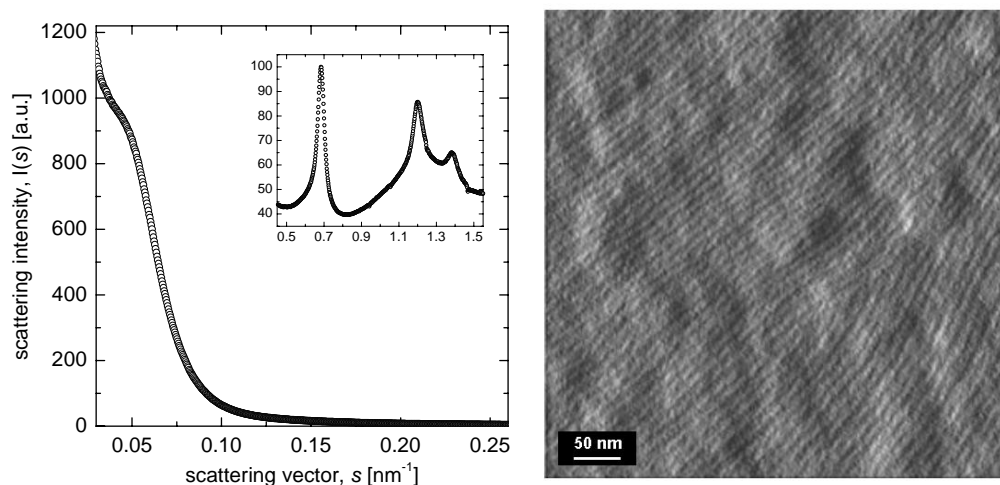


Figure 3-21. Left: Radial-averaged SAXS diffractogram of the DMF-cast film of PS-*b*-PZLLys sample SL1 (Table 3-8). The inset shows the first three reflections arising from a hexagonal array of PZLLys helices, see text. Right: AFM amplitude image ($0.5 \times 0.5 \mu\text{m}$, Z range: 25 mV) of a film prepared by spin-coating a ~2 wt % solution of SL1 in DMF on silicon. Note that the lamellae are oriented perpendicularly to the substrate.¹³¹

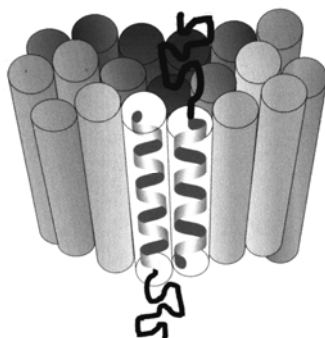


Chart 3-3. Schematic representation of the *hexagonal-in-undulated lamellar* or *zigzag* morphology of linear PS-*b*-PZLLys copolymers.

The molecular characteristics of the PS-*b*-PZLLys copolymers used for the fabrication of thick films are listed in Table 3-8. Note the different molecular weights and compositions of the samples and in particular the wide range of (absolute) polydispersity index values, PDI = ~1.01-1.64.

Table 3-8. Molecular characteristics of the linear PS-*b*-PZLLys copolymers used to study structure formation in the solid state.

chemical structure	sample	x	z	$f_z^{\#}$	ϕ_z^{\S}	PDI [§]
	SL1	52	69	0.57	0.74	1.64
	SL2	52	111	0.68	0.82	1.27
	SL3	217	93	0.30	0.48	1.32
	SL4	52	60	0.54	0.71	1.24
	SL7	52	50	0.49	0.68	(1.01)
	SL9	52	40	0.45	0.64	(1.01)

[#] Mole fraction of ZLLys. [§] Volume fraction of the ZLLys (densities used for calculation: $\rho/g\text{ cm}^{-3}$ = 1.090 (PS) and 1.265 (PZLLys), determined with DENSITY OSCILLATION TUBE in DMF at +40 °C). [§] Polydispersity index (SEC-UV/RI).

The radial-averaged SAXS curves (scattering vector, $s < 0.2\text{ nm}^{-1}$) of the films formed by these PS-*b*-PZLLys samples are shown in Figure 3-22. Evidently, only the highest-molecular weight sample SL3 showed at all a distinct second order Bragg peak, which allowed the clear assignment of the lamellar superstructure. Considering a lamellar structure for all specimens, the peak maximum is a measure of the long period (d) — results are summarized in Table 3-9. The presence of the PZLLys α -helix was confirmed by CD spectroscopy (spectra not shown), the estimated percentage of helix being usually greater than 80%.¹⁴⁰ The hexagonal packing of the helices was observed by SAXS at $s > 0.6\text{ nm}^{-1}$, i.e. three reflections with a Bragg spacing in the ratio 1:3^{0.5}:2 (cf. Figure 3-21), and the characteristic spacing between helix lattices was $d_H \sim 1.5\text{ nm}$ (distance between α -helices = $(4/3)^{0.5} d_H \sim 1.7\text{ nm}$). The correlation length

for SL3 was determined from the width of the SAXS peaks via the Scherrer equation to be ~ 20 nm, i.e. approximately 150 PZLLys helices were forming an ordered domains.¹³⁹

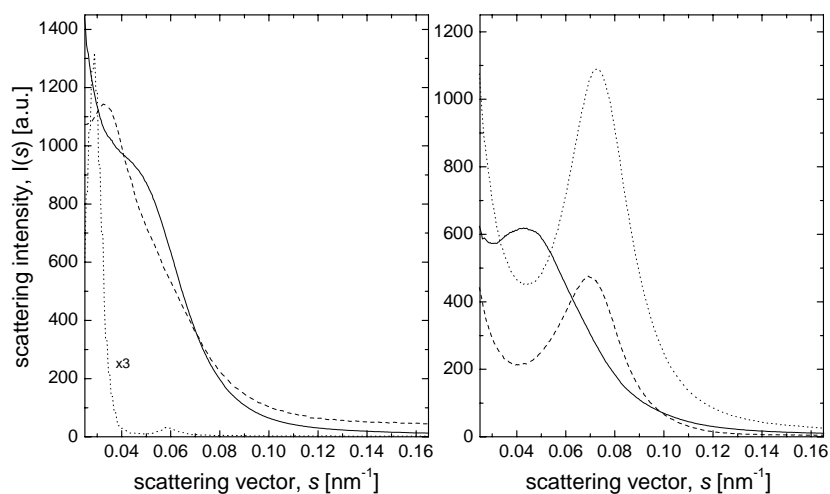


Figure 3-22. Radial-averaged SAXS diffractograms obtained for DMF-cast films of linear PS-*b*-PZLLys copolymers SL1 (left, solid line), SL2 (left, dashed line), SL3 (left, dotted line), SL4 (right, solid line), SL7 (right, dashed line), and SL9 (right, dotted line).

Table 3-9. Characteristics of the solid-state lamellar morphologies of the linear PS-*b*-PZLLys copolymers SL1-4,7,9 (Table 3-8) as obtained from SAXS analysis.

sample	d_H (nm) [#]	d (nm) [§]	d_S (nm) [§]	d_L (nm) [§]	κ ^{&}	i ^{&}
SL1	1.42	16.7	4.5	12.2	1.2 ± 0.1	2.0 ± 0.1
SL2	1.49	29.4	4.8	21.7	1.9 ± 0.2	2.2 ± 0.1
SL3	1.48	34.5	13.8	12.7	1.4	2.0
SL4	1.46	14.1	3.5	10.6	1.8 ± 0.2	2.0 ± 0.1
SL7	(1.49)	13.4	3.7	9.7	1.0 ± 0.1	2.0 ± 0.1
SL9	(1.46)	12.1	3.9	8.2	0.8 ± 0.1	2.0 ± 0.1

[#] Spacing between lattices of PZLLys α -helices. [§] Long period. [§] Thickness of PS (d_S) and PZLLys microdomains (d_L);¹⁵⁷ estimated experimental error: $\pm 10\%$. [&] Normalized scattering-average of curvature (κ) and averaged normalized interface area (i).¹⁵⁸

The concept of the “interface distribution function” (Ruland)¹⁵⁷ was applied to determine the thickness of the PS and PZLLys layers, d_S and d_L , respectively ($d = d_S + d_L$).¹⁵⁹ The results are shown in Table 3-9 and Figure 3-23. It can be seen that the thickness of the PZLLys layer (d_L) is linearly proportional to the number-average degree of polymerization of ZLLys (z). The slope of the line graph in Figure 3-23 indicates that the contribution of every ZLLys unit to the length of the helix is 1.9 Å, which is somewhat higher than the 1.5 Å calculated for a 100% crystalline polypeptide $\alpha(18_5)$ -helix.⁴⁹ Hence, the PZLLys lamellae are composed of monolayers of interdigitated α -helices,⁴⁹ as illustrated in Chart 3-3, and the main axis of the

helices is oriented perpendicularly to the PS-PZLLys interface. Backfolding of the helices, as described by Gallot et al.⁴⁹ for high-molecular weight samples, can be excluded for all samples but SL3, which had the largest PS block ($x = 217$). The thickness observed for the PZLLys layer of SL3, however, was very similar to that of SL1, which contained 24 ZLLys units less (cf. Table 3-8). Anyway, interdigitation or backfolding are ways to compensate the large dipole moments of α -helices ($\mu = 3.5$ Debye per unit)⁷⁵ and to minimize the energy of the PZLLys layers. Since the hexagonal packing of helices does not allow for a regular anti-parallel orientation of the dipole moments, it is expected that the thickness of PZLLys layers cannot exceed a certain limit. As seen from Figure 3-23, this limit should be well above ~ 20 nm.

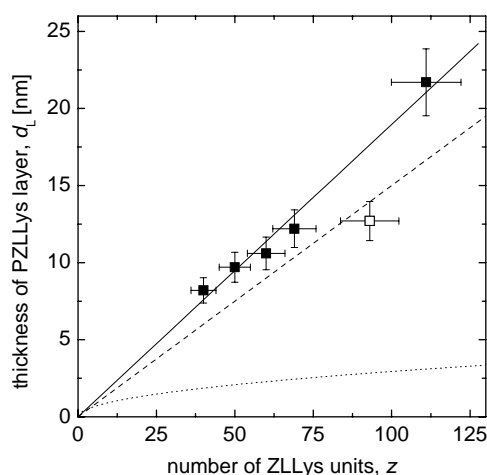


Figure 3-23. Dependence of the number-average thickness of PZLLys layers (d_L , SAXS) on the number-average number of ZLLys units (z , NMR). Solid line: linear fit through experimental data (except \square , SL3), slope: (0.19 ± 0.01) nm. Dashed line: $d_L/\text{nm} = 0.15 \cdot z$, calculated line assuming a fully extended α -helix with a projected length of a ZLLys segment of 1.5 \AA .⁴⁹ Dotted line: $d_L/\text{nm} \sim 2R_g = (2/3)^{0.5} l_L z^{0.5}$, calculated line assuming random coil conformation of PZLLys (R_g : radius of gyration, l_L : length of a ZLLys segment = 3.6 \AA).

SAXS data were further analyzed by the “*kappa-iota* (κ - ι) formalism” (Burger et al.¹⁵⁸); this approach is based on the extraction of characteristic geometric quantities, namely the dimensionless parameters describing the interface curvature (κ) and the specific interface (ι), from the asymptotic Porod regime. These parameters allow determination of structures on the basis of a general phase diagram comprising the most prominent block copolymer mesophases (cf. Figure 3-24). Most importantly, this method is applicable even when SAXS curves show only a single broad reflection. Also, local interface and curvature properties are assumed to equilibrate rapidly and should not depend on the pathway of film processing.¹³⁹

The results obtained from the κ - ι analysis of SAXS data are summarized in Table 3-9, and the experimental κ - ι values are inserted in the generalized phase diagram shown in Figure 3-24.

The value of the reduced specific interface was found to be $\iota = 2.0$ (SL2: $\iota = 2.2$), which is the expected value for a plane lamellar phase. Despite of that, all structures exhibit a noticeable curvature, as indicated by the values of the reduced mean curvature, $\kappa = 0.8$ -1.9. It is noteworthy that, taking into account the κ - ι phase diagram, lamellar structures exist at all with $\iota = 2.0$ and $\kappa > 1$. The most reasonable model of a structure exhibiting the given properties should be a disordered *zigzag lamellar* morphology as depicted in Figure 3-25. Note that a similar morphology on the 100-200 nm length scale has earlier been observed for a poly(hexyl isocyanate)-polystyrene rod-coil block copolymer system (see Figure 1-3).¹³ However, the generation of a plane PS-PZLLys interface ($\iota = 2.0$) between the “kinks” requires a fractionation of the copolymer chains according to length during the casting of the film. Otherwise a rough surface with a substantially larger interface area would have been formed, which for energy reasons is not favorable.

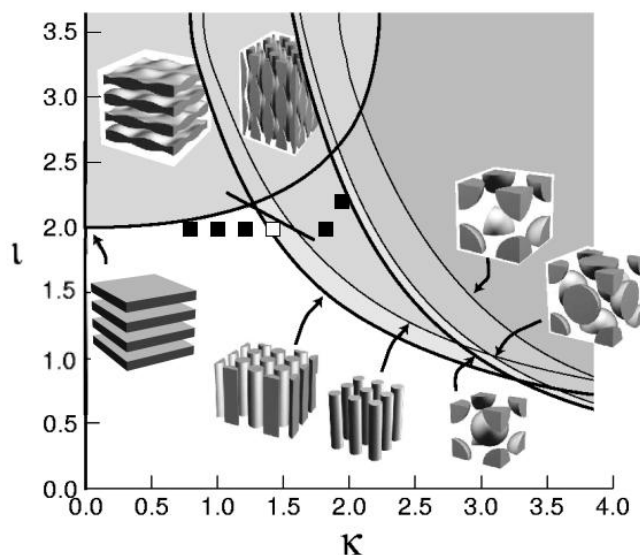


Figure 3-24. Experimental *kappa-iota* data obtained for films of linear PS-*b*-PZLLys copolymers, inserted in the generalized phase diagram.¹⁵⁸

It is evident that the structures with the smallest value of the curvature parameter κ were produced from the copolymers SL7 (1.0) and SL9 (0.8), which exhibit a nearly monodisperse Poisson distribution (PDI \sim 1.01). The highest values ($\kappa = 1.8$ -1.9), on the other hand, were observed for the samples SL2 and SL3 with a moderate PDI \sim 1.25. In fact, it is well expected that increasing the variance in the length of the helices produces larger fluctuations in the thickness of the PZLLys layers and more kinks, the latter contributing to the curvature of lamellae. The *zigzag* morphology can thus be rationalized as illustrated in Figure 3-25 (A and B). However, this seems to hold true as long as the entropic contributions to the free energy are greater than the interfacial tension between the PS and PZLLys layers. Note that the gen-

eration of a fluctuating thickness of layers is at the expense of a larger interface area. When the molecular weight distribution of the copolymer sample is too broad, as in the case of samples SL1 and SL3 ($PDI > 1.3$), plane lamellae with an intermediate $\kappa = 1.2$ -1.4 were formed. It is supposed that the dropping of the κ value is due to a decrease of the number of kinks per volume unit or, in other words, extension of the plane interfacial domains between two kinks, see Figure 3-25 (C). Fractionation of the copolymer chains occurs parallel to the interface, i.e. all PZLLys layers have the same average thickness. Thus, the existence of a plane lamellar structure consisting of uniform PZLLys layers, the thickness of which varying from layer to layer, can be excluded here. For such a structure, it should be $\iota = 2$ and $\kappa = 0$.

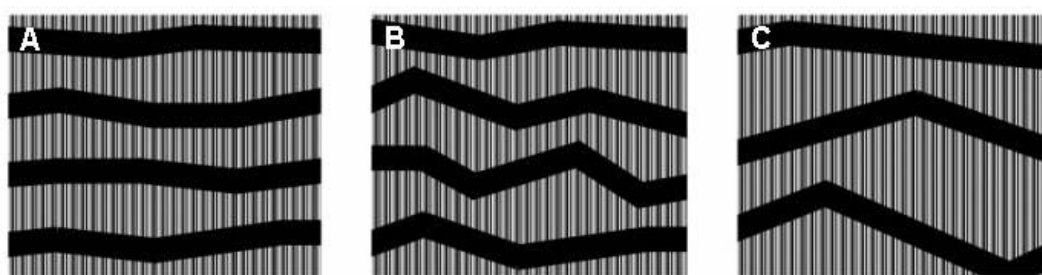


Figure 3-25. Schematic representation of the disordered zigzag lamellar morphology formed by linear PS-PZLLys block copolymers with low (A), moderate (B), and high polydispersity (C) with respect to the length of helices.

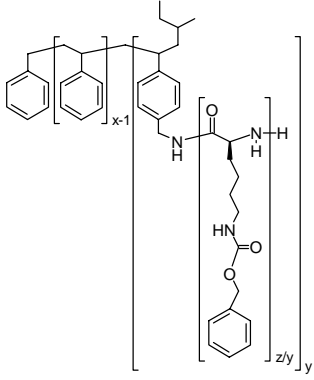
It is interesting to see that even for copolymers with a Poisson distribution, SAXS patterns are rather ill-defined and do not show higher orders of lamellar reflections. Based on the structure model described here, however, the situation should change when the PZLLys blocks are strictly monodisperse. Having monodisperse samples at hand would offer the possibility to learn more about the basic principles and energetics in the self-assembly processes of rod-coil block copolymers — this is subject of ongoing work.

However, it has so far not been paid much attention to polydispersity when dealing with structure formation of rod-coil block copolymers. In fact, many of the systems being investigated have been prepared by polycondensation reactions,¹² which usually produce polymers with a Schulz-Flory distribution ($PDI = 2$) or even broader molecular weight distribution. Polydispersity effects could play a considerable role in these systems and might explain deviations from the predicted phase behavior (cf. Gersappe et al.¹⁶⁰) as well as the appearance of unusual morphologies. In coil-coil systems, on the other hand, polydispersity might at all affect the dimension of a phase but not its structure.¹⁶¹

3.3.2.2 Bottlebrush-shaped block copolymers

Apart from the secondary structure effects arising from dipole-dipole interactions and chain length distribution of helices, it was also of interest to examine the impact of copolymer architecture on the phase structure in the solid state. It was a major question whether or not the entropic contributions introduced by branching (cf. Chart 3-4) would affect the packing of polypeptide helices, thus promoting the formation of other than lamellar morphologies. For this purpose, a series of heteroarm star- or bottlebrush-shaped PS-PZLLys block copolymers of the type AB_y was synthesized; the molecular characteristics of samples SL*1-6 are summarized in Table 3-10 (see also Table 2-11).

Table 3-10. Molecular characteristics of the star- or bottlebrush-shaped PS-*b*-PZLLys copolymers used to study structure formation in the solid state.

chemical structure	sample	x	z	y	$f_z^{\#}$	Φ_z^{\S}
	SL*1	182	243	4	0.57	0.74
	SL*2	193	65	8	0.25	0.41
	SL*3	193	255	8	0.57	0.73
	SL*4	188	54	12	0.22	0.37
	SL*5	188	123	12	0.40	0.57
	SL*6	188	227	12	0.55	0.71

[#] Mole fraction of the ZLLys. [§] Volume fraction of the ZLLys (densities used for calculation: $\rho / \text{g cm}^{-3} = 1.090$ (PS) and 1.265 (PZLLys), determined with DENSITY OSCILLATION TUBE in DMF at $+40$ °C).

Among the samples SL*1-6, only SL*1, SL*3, and SL*6 showed the characteristic CD signal arising from PZLLys segments adopting an α -helical conformation. For these samples, the number of PZLLys repeating units (z/y , Table 3-10) exceeded the minimum of 10-15 units, which is required for the formation of a stable helix.⁶² Accordingly, in SAXS/WAXS, only the films of SL*1, SL*3, and SL*6 might at all show the characteristic Bragg peaks of a hexagonal packing of α -helices. Indeed, such a structure with $d_H \sim 1.4$ nm could be observed for SL*1 ($z/y = 61$) and SL*3 ($z/y = 32$) but not for SL*6 ($z/y = 19$). Note that the diameter of a PZLLys α -helix exceeds the contour length of the styrene linking unit by a factor of about six, leading to some steric overcrowding of chains at the bottlebrush junction (cf. Chart 3-4). This is in particular true for sample SL*6 with the highest number of PZLLys branches ($y = 12$), not allowing the anti-parallel packing of helices in a hexagonal array. The correlation length

was determined to be 9-11 nm in the isotropically averaged state, which corresponds to six helices in a line.

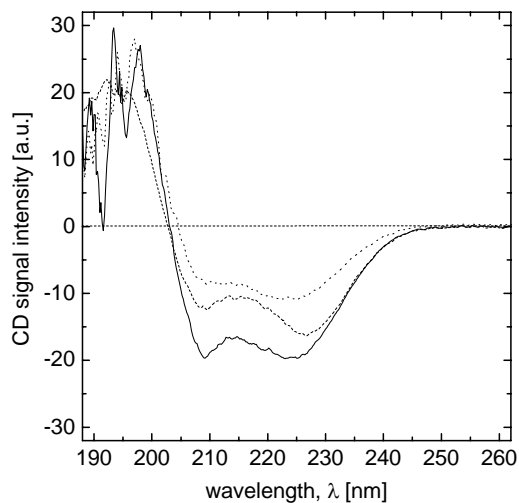


Figure 3-26. CD spectra of films (spin-coated from DMF solution onto a quartz plate) of bottlebrush-shaped PS-*b*-PZLLys copolymers SL*1 (solid line), SL*3 (dashed line), and SL*6 (dotted line). Note that the measured CD signal intensity is not a direct measure of the helix content as it also depends on the length of the polypeptide segment and the thickness of the film.¹⁴⁴

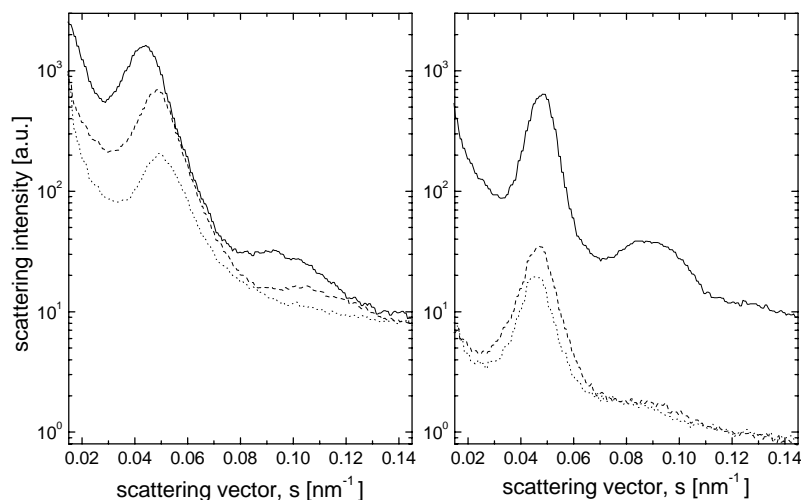


Figure 3-27. Radial-averaged SAXS diffractograms obtained for DMF-cast films of bottlebrush-shaped PS-*b*-PZLLys copolymers SL*1 (left, solid line), SL*3 (left, dashed line), SL*6 (left, dotted line), SL*4 (right, solid line), SL*2 (right, dashed line), and SL*5 (right, dotted line).

These specimens were thus in a less ordered state than the ones obtained from linear PS-*b*-PZLLys copolymers (see above). This was also reflected by the broad SAXS peaks in the low-angle region, and the fact that only SL*4 showed at all a second-order Bragg peak (see Figure 3-27), which allowed the clear identification of a lamellar phase. Analysis with the κ - ι formalism revealed a lamellar structure for all specimens SP*1-6 (see Table 3-11 and Figure 3-28). For most samples, strong dipole-dipole interactions could not be established, simply because the PZLLys chains were too short to form a helix (see above). Due to the high graft-

ing density of PZLLys segments, the PS bottlebrush backbone should be rather stiff, like for worm-like polymacromonomers,¹⁶²⁻¹⁶⁴ thus giving the preference for lamellar structures.

The long period was found to be $d \sim 21$ nm for SL*1-6, independent of molecular weight and relative volume fractions of the comonomers. It is evident that the dense branching of bottlebrushes led to significantly smaller repeat units as compared to linear chains, even though the overall molecular weights were much higher. Thus, PZLLys grafts should be arranged rather parallel to the PS–PZLLys interface, as illustrated in Chart 3-4, in contrast to the perpendicular orientation of helices in the films of linear block copolymers (Chart 3-3). Comparison of the thickness of phases (d_L , Table 3-11) with the contour length of the bottlebrush backbone ($l_c = 1-2$ nm) suggested that the brushes were stacked from both sides or formed a “cap” as depicted in Chart 3-4. However, the finer details of these structures remain to be analyzed. Also not known is the role of polydispersity or helix length distribution in the structure formation of bottlebrush-shaped block copolymers.

Table 3-11. Characteristics of the solid-state lamellar morphologies of the bottlebrush-shaped PS-*b*-PZLLys copolymers SL*1-6 (Table 3-10) as obtained from SAXS analysis.

sample	d_H [#] (nm) [#]	d [§] (nm) [§]	d_S [§] (nm) [§]	d_L [§] (nm) [§]	κ ^{&}	i ^{&}	morphology
SL*1	1.43	22.9	6.2	17.5	1.2	2.0	<i>undulated lamellar</i>
SL*2	–	21.3	8.8	12.7	1.3	2.1	<i>undulated lamellar</i>
SL*3	1.41	20.6	5.7	15.5	1.6	2.7	<i>undulated lamellar</i>
SL*4	–	17.0	–	–	1.6	2.1	<i>undulated lamellar</i>
SL*5	–	22.0	6.7	8.9	1.3	3.0	<i>undulated lamellar</i>
SL*6	–	20.4	6.5	16.0	0.3	2.0	<i>plane lamellar</i>

[#] Spacing between lattices of PZLLys α -helices. [§] Long period. [§] Thickness of PS (d_S) and PZLLys microdomains (d_L).¹⁵⁷ & Normalized scattering-average of curvature (κ) and averaged normalized interface area (i).¹⁵⁸

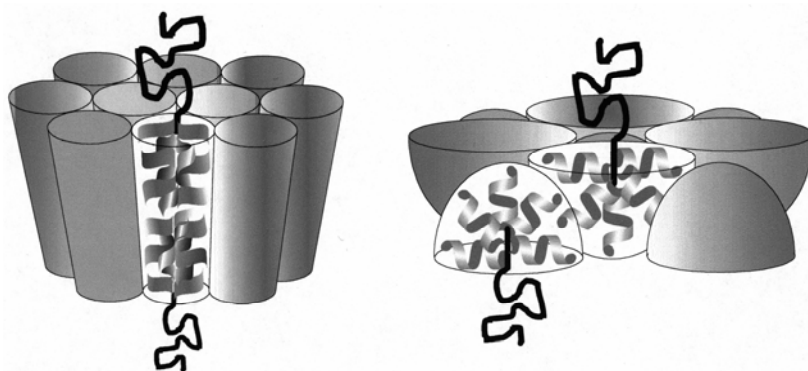


Chart 3-4. Schematic representations of lamellar superstructures formed by bottlebrush-shaped PS-*b*-PZLLys copolymers.

It is obvious that PZLLys bottlebrushes can stabilize a larger interface area than linear chains (see also chapter 4.1), which might promote the generation of undulations. In fact, analysis of SAXS data with the κ - l formalism revealed only for SL*6 a plane lamellar morphology, whereas SL*1-5 produced undulated and curved structures (see Figure 3-28). In the case of SL*3 and SL*5 (Figure 3-28: circles at the furthest top), quantitative evaluation of the scattering peaks^{165,166} revealed an excess area of 35 and 50%, respectively, which indicated the presence of “superundulated” lamellar phases. Similar structures have previously been reported for polystyrene-poly(hexyl isocyanate) rod-coil block copolymers^{13,14} (disordered *zigzag* phase, Figure 1-3) and for polyelectrolyte-lipid complexes (*egg carton* phase).^{165,166} However, evaluation of the experimental interface distribution curves $g_1(r)$ (r = cord length)¹⁶⁷⁻¹⁶⁹ for SL*1-6 suggested the existence of lamellar structures with a perfect lateral order and a statistically fluctuating thickness of individual layers. As can be seen from the TEM micrograph in Figure 3-29, the film of SL*4 indeed showed an extremely long persistence length with practically no tilt of domain orientation in the observed area of $2 \times 2 \mu\text{m}$. Unfortunately, due to problems with the thickness of the specimen and projection averaging, undulations could not be observed directly.

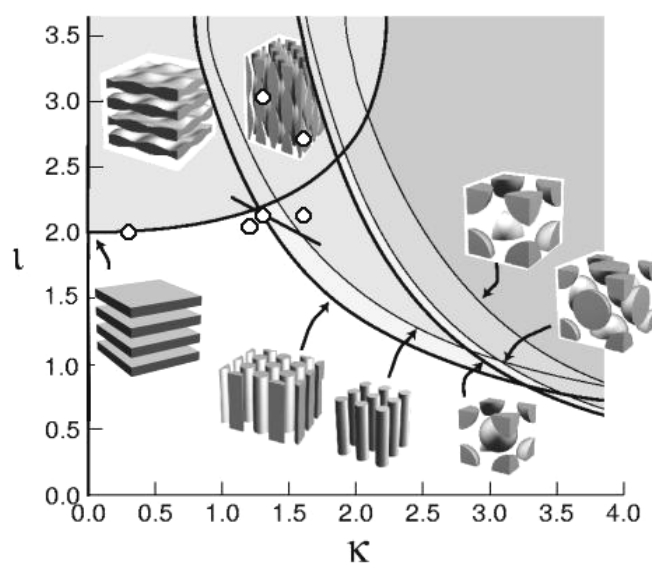


Figure 3-28. Experimental κ - l data obtained for films of bottlebrush-shaped PS-*b*-PZLLys copolymers, inserted in the generalized phase diagram.¹⁵⁸

Note that undulations were always considered as statistical fluctuations of the layer thickness. However, 2D-SAXS analysis of the SL*4 film revealed a highly ordered undulated lamellar phase. Film alignment perpendicular to the X-ray beam led to the observation of centrosymmetric rings, whereas a distorted hexagonal pattern was found for the parallel alignment (not shown).¹³⁹ These two patterns as well as the κ - l data were in agreement with the structure

of *corrugated lamellae*, where the one-dimensional undulations were localized in a distorted hexagonal lattice as depicted in Chart 3-5. Such localized undulations led to a stiffening of the lamellae and a coupled increase of the long-range order, as visualized by TEM (Figure 3-29).

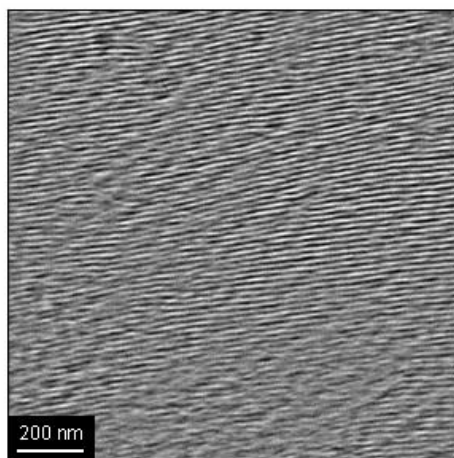


Figure 3-29. TEM micrograph of the *undulated lamellar* structure of the polymer film SL*4, microtomed perpendicular to the film surface and stained with RuO_4 (dark: PZLLys, bright: PS).

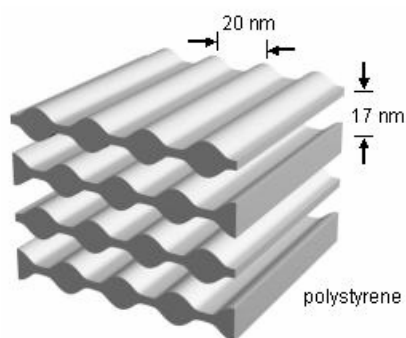


Chart 3-5. Schematic representation of the *corrugated lamellar* morphology of the polymer film SL*4, revealed from 2D-SAXS analysis with orthogonal and parallel alignment of the specimen to the X-ray beam.¹³⁹

4 FUNCTIONAL COLLOIDS

In the following section will be described some potential applications of chelating block copolymers (chapter 4.1) and polypeptide block copolymers (chapters 4.2 and 4.3).

The strong affinity of chelating block copolymers based on 2-acetoacetoxy-ethyl methacrylate (AEMA) towards metals and metal ion salts can be used for the production of polymer-metal hybrid materials. However, for reasons of availability, most of the work in this field has been done with poly(acrylic acid)- or polyvinylpyridine-based block copolymers,^{7,30} see for example work of Antonietti et al.,¹⁷⁰⁻¹⁷⁹ Möller et al.,¹⁸⁰⁻¹⁸⁸ and Eisenberg et al.¹⁸⁹⁻¹⁹¹ First results on the loading of PAEMA reverse micelles with metal ions (Fe^{3+} , Pd^{2+} , and Co^{2+}) will be presented in chapter 4.1, demonstrating the great potential of PAEMA block copolymers in the generation of monodisperse hybrid nanoparticles and thin, ordered films.

Chapter 4.2 deals with the use of polypeptide block copolymers as stabilizers in the heterophase polymerization of styrene.¹⁹² The aim of this project was to study the impact of the polymer architecture on the properties of the resulting latexes. It was expected that, due to the increased bulkiness of the head group, multi-arm polyelectrolyte star block polymers exhibit a higher stabilization efficiency and should therefore produce smaller particles than their linear analogs. Also, whether polypeptide chains were linear or branched should be reflected in the thickness of the stabilizing corona and thus the stability of particles against electrolytes. Note that polypeptide-decorated latexes are interesting materials for biomedical applications, for example as carriers in drug delivery systems.¹⁹³

In chapter 4.3, the use of poly(ethylene oxide)-*block*-polypeptide copolymers as carriers for *cis*-dichlorodiammineplatinum(II) (cisplatin) in anti-cancer therapy will be presented; this work has been done in collaboration with Prof. Dr. J. A. Werner and Dr. A. Dünne, Klinikum der Philipps-Universität Marburg, Germany. This special drug-carrier system, described for the first time by Kataoka et al.,¹⁹⁴⁻¹⁹⁷ was chosen for the therapy of squamous cell carcinomas of the head and neck regions (HNSCC), which spread *via* the lymph node system.¹⁹⁸ Current therapies of the HNSCC are not very efficient and seized by severe side-effects (reduction of the survival rate in more than 50 % of the patients).¹⁹⁹ In pre-clinical studies on the model VX2 carcinoma of the New Zealand white rabbit, the new therapy was successful in 90 % of the cases. Building on these very promising results, it is planned to continue the project and to enter the clinical stage of HNSCC chemotherapy.

4.1 Polymer-metal hybrid materials

The ability of PBMA-*b*-PAEMA copolymers to complex and solvate different metal ion salts in organic media is attributed to the presence of the bidentate acetoacetoxy (β -dicarbonyl) group in AEMA. As already mentioned in chapter 2.2, there are two (three) tautomeric forms of the acetoacetoxy unit in equilibrium, the major one being the keto tautomer ($\sim 92\%$). Both the keto and the enol tautomer can form complexes with transition metal ions.^{112,200} The keto tautomer is a “soft” ligand, only capable of replacing neutral molecules like water or ethers, whereas the enolate can well exchange acetate or halide anions (see below).

Initial complexation studies were performed with iron(III) chlorides, namely $\text{FeCl}_3 \cdot 6\text{H}_2\text{O}$ and anhydrous FeCl_3 , the structures of which are depicted in Chart 4-1. The solids were added to a ~ 0.1 wt % micellar solution of PBMA₃₄₂-*b*-PAEMA₃₉ (sample BA2, Table 2-7) in cyclohexane at room temperature. Note that these micelles were spherical in shape ($R_h = 32$ nm, DLS), consisting of a PAEMA core and a PBMA corona (cf. chapter 3.2.1). Due to their very poor solubility in the hydrophobic continuous phase, the ferric salts should preferentially be located inside the micellar core. It is obtained a sterically stabilized colloidal dispersion.

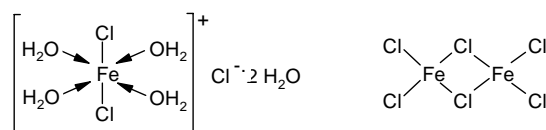


Chart 4-1. Structures of $\text{FeCl}_3 \cdot 6\text{H}_2\text{O}$ (left) and FeCl_3 (right).²⁰¹

The $\text{FeCl}_3 \cdot 6\text{H}_2\text{O}$ was found to dissolve readily within a few minutes, and the color of the micellar solution changed from colorless to wine red. The presence of the polymer–metal complex was confirmed by UV/VISIBLE SPECTROSCOPY (see Figure 4-1),¹²¹ but its structure had not been investigated in detail. Supposedly, it exhibited the same octahedral structure as $\text{FeCl}_3 \cdot 6\text{H}_2\text{O}$, see Chart 4-1, with the four water molecules adjacent to the iron atom being replaced by two keto tautomeric acetoacetoxy ligands ($f_{\text{Fe}} = [\text{Fe}]/[\text{AEMA}] = 0.33$). The two chloride substituents, on the other hand, should not have been touched by the acetoacetoxy groups. Accordingly, the solubilization of anhydrous FeCl_3 failed when applying the same experimental protocol. Right after small amounts of a water/methanol mixture had been added to the dispersion, transforming the iron(III) chloride into a hydrate, the red-purple complex was formed immediately.

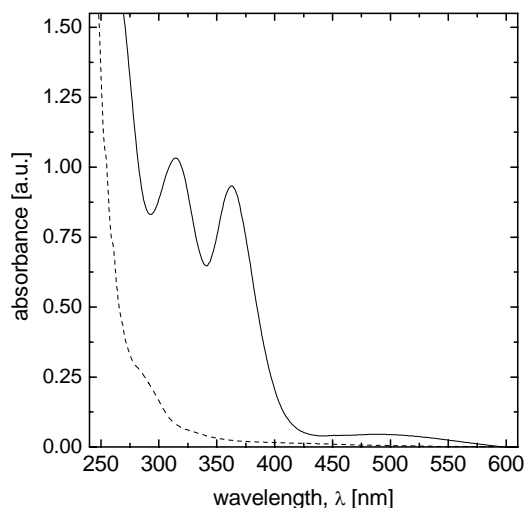


Figure 4-1. UV-visible spectra of the ~ 0.1 wt % micellar solutions of PBMA-*b*-PAEMA sample BA2 (dashed line) and BA2/FeCl₃·6H₂O ($f_{\text{Fe}} = 0.33$; solid line) in cyclohexane.

Due to the different densities of organic and inorganic components (FeCl₃·6H₂O: $\rho = 1.82$ g cm⁻³), ANALYTICAL ULTRACENTRIFUGATION (AUC) could be used to examine the chemical composition of BA2–FeCl₃·6H₂O colloids. As can be seen from the sedimentation-velocity experiments (see Figure 4-2), the sedimentation coefficient distribution ($g(S)$) of the BA2 micelles in cyclohexane were shifted to higher S values after the loading with FeCl₃·6H₂O ($f_{\text{Fe}} = 0.5$). Both distributions exhibited the same shape, which suggested that the ferric salt was evenly distributed among the aggregates. Since complexation was a heterogeneous process (see above), there must have been a dynamic intermolecular exchange of salt molecules between the aggregates, for example *via* a fusion-fission mechanism.²⁰² The polymer–metal colloids might therefore be considered as equilibrium structures.

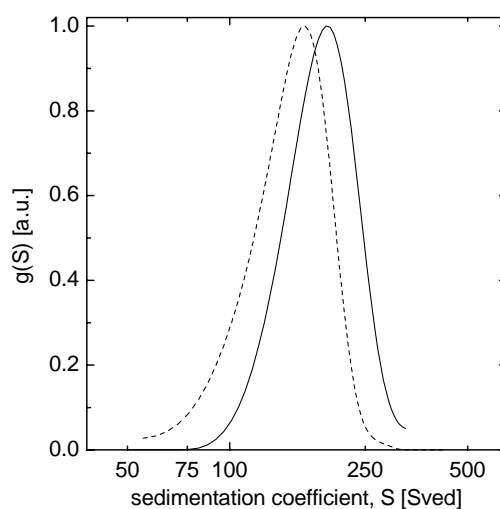


Figure 4-2. Sedimentation coefficient distributions $g(S)$ of ~ 0.4 wt % micellar solutions of PBMA-*b*-PAEMA sample BA2 (dashed line) and BA2/FeCl₃·6H₂O ($f_{\text{Fe}} = 0.5$; solid line) in cyclohexane at 25 °C.

The LIGHT SCATTERING results obtained for the ~0.4 wt % micellar solutions of BA2 in cyclohexane in the presence of different amounts of $\text{FeCl}_3 \cdot 6\text{H}_2\text{O}$, $f_{\text{Fe}} = 0-1.0$, are summarized in Table 2-1. Evidently, neither the shape nor the size of micelles was affected by the loading of the ferric salt into the PAEMA core. All solutions contained spherical micelles, as indicated by the ratio $R_g/R_h \sim 0.8$, with a hydrodynamic radius $R_h \sim 30$ nm. The aggregation number (Z) of the micelles, on the other hand, was found to decrease with increasing amount of $\text{FeCl}_3 \cdot 6\text{H}_2\text{O}$; at $f_{\text{Fe}} = 0.85$, the aggregation number had dropped to ~60% of the initial Z value observed for the pure BA2 micelles. Having in mind the results described in chapter 3.2.1, it was expected that the loading of the PAEMA core with the ferric salt would lead to a growing of the aggregates and eventually to a shape transition from spheres to cylinders. Evidently, the system seemed to follow opposite rules, thus suggesting that the PAEMA core was rather shrinking but swelling upon loading with $\text{FeCl}_3 \cdot 6\text{H}_2\text{O}$. Whether or not it is the case is not known yet for sure. Additional ANALYTICAL ULTRACENTRIFUGATION (AUC) and SMALL-ANGLE X-RAY SCATTERING (SAXS) studies shall be performed to obtain the missing information about the true density and dimension of the polymer–metal micellar core.

Table 4-1. Characteristics of the micelles formed by PBMA-*b*-PAEMA sample BA2 in cyclohexane at 20 °C in the presence of different amounts of $\text{FeCl}_3 \cdot 6\text{H}_2\text{O}$ (f_{Fe}), as obtained by dynamic and static light scattering (DLS and SLS).

sample	f_{Fe}^*	R_h (nm) [#]	R_g (nm) [§]	R_g/R_h	$A_2 \cdot 10^9$ (mol cm ⁻³ g ⁻²) [§]	$Z^{\&}$
BA2	0	32	26	0.81	1.50	342
BA2-0.25	0.25	33	29	0.88	0.92	274
BA2-0.33	0.33	33	28	0.85	0.94	269
BA2-0.45	0.45	31	27	0.87	1.30	297
BA2-0.60	0.60	30	27	0.90	1.10	266
BA2-0.85	0.85	28	24	0.86	-0.61	207
BA2-1.00	1.00	coagulation				

* Molar ratio $[\text{Fe}]/[\text{AEMA}]$. [#] Hydrodynamic radius (DLS). [§] Radius of gyration (SLS). [§] Second virial coefficient (SLS). [&] Aggregation number (SLS) = $M_{w, \text{micelle}} / (M_{w, \text{BA2}} + 39 \cdot f_{\text{Fe}} \cdot M_{\text{FeCl}_3 \cdot 6\text{H}_2\text{O}})$, refractive index increments used for evaluation of Zimm plots: $dn/dc = (0.0619 + 0.0151 \cdot f_{\text{Fe}})$ cm³ g⁻¹ 121.

It is worth mentioning that DLS provided identical values for the hydrodynamic radius of micelles, regardless of the concentration of the solution and the measuring angle, which indicated the existence of a narrow, monodisperse size distribution of particles. The narrow size distribution of the polymer–metal hybrid micelles could also be visualized by ATOMIC FORCE MICROSCOPY (AFM), see the typical micrographs of the BA2-0.33 micelles ($f_{\text{Fe}} = 0.33$) spin-

coated from dilute cyclohexane solution on mica. Also, dispersions were only stable when $f_{\text{Fe}} < 0.9$, and coagulation of the aggregates occurred at $f_{\text{Fe}} \geq 1$. Note the first negative value of the second virial coefficient (A_2) of sample BA2-0.85 (see Table 4-1). The steric stabilization by the PBMA layer then might not have been sufficient to shield the attractive forces between the PAEMA–metal centers and to avoid coalescence.²⁰²

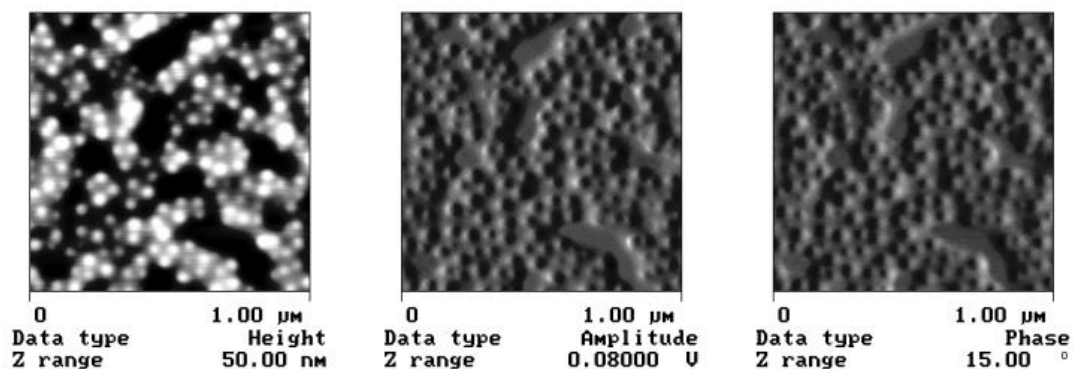
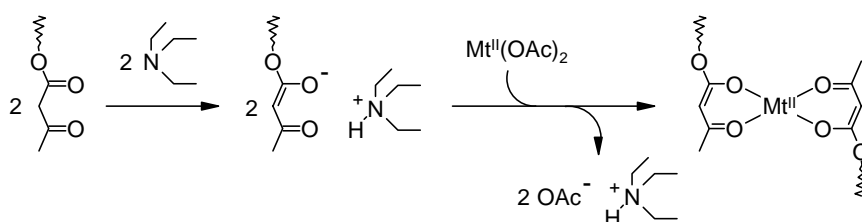


Figure 4-3. AFM tapping mode images ($1.0 \times 1.0 \mu\text{m}$) of PBMA-*b*-PAEMA micelles loaded with $\text{FeCl}_3 \cdot 6\text{H}_2\text{O}$ (sample BA2-0.33, Table 4-1), spin-coated from cyclohexane solution on mica.

As mentioned earlier, AEMA in the keto tautomeric form is only capable of replacing neutral ligands in metal ion salts. The exchange of acetate (OAc) substituents requires the presence of β -ketoesterenolates, which can be produced by deprotonation of the AEMA units with for example triethylamine (TEA) (see Scheme 4-1).²⁰³ Assisted by the addition of TEA, it was indeed possible to transfer cobalt(II) ($\rightarrow \text{Co}(\text{OAc})_2 \cdot x\text{H}_2\text{O}$), copper(II) ($\rightarrow \text{Cu}(\text{OAc})_2 \cdot x\text{H}_2\text{O}$), and palladium(II) ($\rightarrow \text{Pd}(\text{OAc})_2$) metal ions into the PAEMA core of BA2 micelles in cyclohexane ($f_{\text{metal}} \sim 0.5$). Complexation of the metal ions was accompanied by a precipitation of triethylammonium acetate and a change of color of the solution from colorless to either pink (Co), green (Cu), or yellow (Pd) (UV/visible spectra not shown).¹²¹ Similar observations concerning the color of metal acetoacetates have been reported in literature.^{112,204-206} Again, as indicated by DLS and AFM studies, the micelles maintained their spherical shape and size ($R_h \sim 33 \text{ nm}$). As a matter of a very narrow particle size distribution, micelles tend to form ordered domains upon evaporation of the solvent (cf. Figure 4-4).



Scheme 4-1. Formation of a β -ketoesterenolate by deprotonation of acetoacetoxy units in AEMA with triethylamine (TEA) and complexation of metal(II) acetates ($\text{Mt}^{\text{II}}(\text{OAc})_2$).

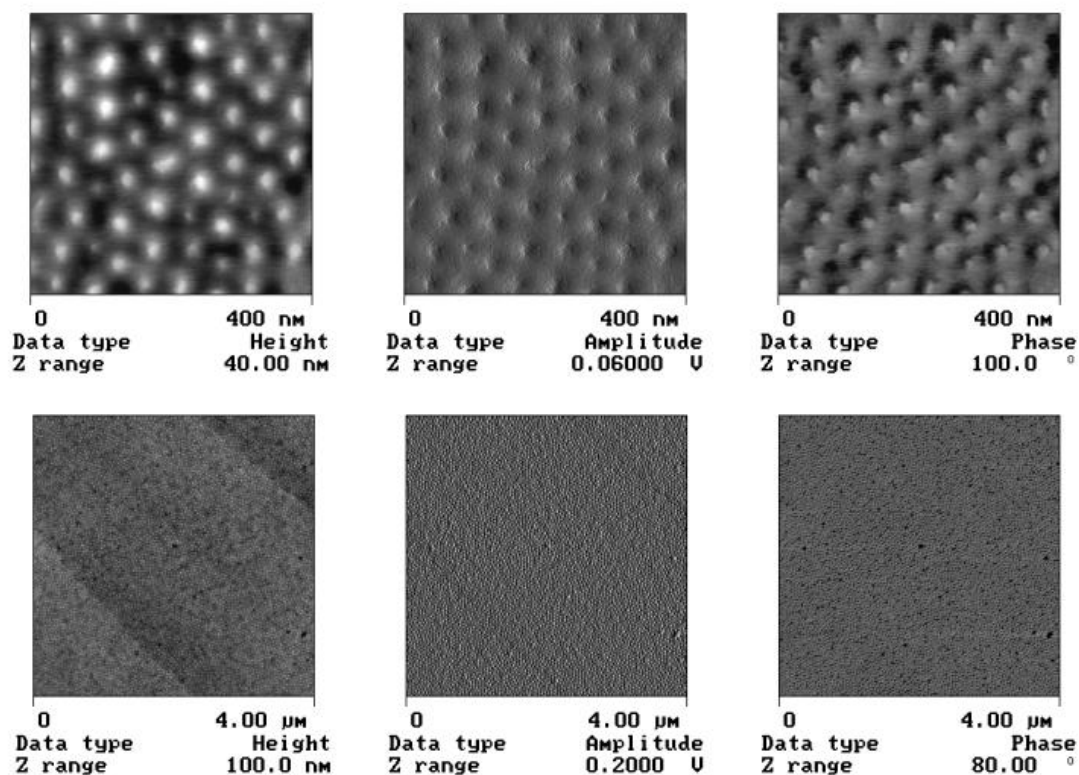


Figure 4-4. AFM tapping mode images (top: $0.4 \times 0.4 \mu\text{m}$, bottom: $4.0 \times 4.0 \mu\text{m}$) of PBMA-*b*-PAEMA micelles loaded with palladium(II) ions ($f_{Pd} = 0.55$). The specimen was prepared by drying a drop of the micellar solution on graphite.

These first results demonstrate that PAEMA-based block copolymers are interesting materials to produce well-defined polymer–metal hybrid materials. However, many questions remain to be addressed, for example the scaling laws for hybrid micelles ($R \propto f_{\text{metal}}^{\alpha}$, $Z \propto f_{\text{metal}}^{\beta}$) and the structure of the polymer-metal adducts formed in the confinement of a micellar core. It is further planned to enter the fields of catalysis and biomineralization processes. Water-soluble PAEMA block copolymers in particular shall be used as additives for controlling the mineralization of biominerals (e.g. CaCO_3) or semiconducting materials (e.g. CdS).

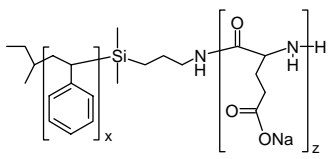
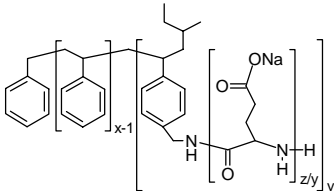
4.2 Polypeptide-decorated latexes

Heterophase polymerization, one of the oldest polymerization techniques, enables the facile preparation of aqueous dispersions, so called latexes, with a high polymer content but low viscosity. For this and other reasons, it plays a very important role in industrial-scale syntheses of e.g. dispersion colors, adhesives, or clues.^{202,207} However, the ease of operation opposes the complexity of the mechanism of heterophase polymerizations, which is still subject of current investigations.^{208,209}

In a typical procedure, hydrophobic monomers like styrenes or acrylates are polymerized in a free-radical process in aqueous media in the presence of an emulsifier, usually a low-molecular weight surfactant (tenside) or amphiphilic block copolymer. Commonly used tensides such as sodium dodecylsulfate (SDS) or cetyltrimethylammonium bromide (CTAB) will prevent the latex from coagulation via electrostatic repulsion between polymer particles; non-ionic surfactants and block copolymers with e.g. hydrophilic PEG segments instead will stabilize particles by steric repulsion. Block copolymers with a polyelectrolyte stabilizing moiety combine the best properties of both stabilization modes, namely the long-range electrostatic repulsion between polymer colloids and the good stability against ionic additives. Even though block copolymers are available in a large variety,^{7,210} only a very few studies have been reported yet about the stabilization abilities of linear polymeric surfactants with polyelectrolyte sequences.²¹¹⁻²¹⁶ However, studies referring to the effects of branching on the stabilization ability of copolymers are not known in literature.

In the present work, the emulsifying properties of linear polystyrene-*block*-poly(sodium D,L-glutamate)s (PS-*b*-PGluNa) are compared with those of heteroarm star-shaped analogues with the same chemical composition.¹⁹² Samples were prepared by hydrolysis of PS-*b*-PBLGlu copolymers SG1-2 and SG*1-2 (Table 2-11) with aqueous NaOH; the molecular characteristics of these samples are listed in Table 4-2. Heterophase polymerization reactions were carried out in sealed test tubes under an argon atmosphere in a rotational thermostat at 80 °C using the following recipe: 1.0 g styrene, 2.0 g de-ionized water, 10-50 mg block copolymer in 2 g 0.1 N NaOH, and 32 mg 2,2'-azobis[2-methyl-*N*-(2-hydroxyethyl)propionamide]. Table 4-3 summarizes the main characteristics of the obtained polystyrene latexes, namely the average particle sizes and polydispersity indexes (PDI) of the particle size distributions. All polymerization runs yielded stable latexes with a polymer content of ~20% (as targeted) and particles of 70–220 nm in diameter (d_h ; DYNAMIC LIGHT SCATTERING, DLS).

Table 4-2. Structures and molecular characteristics of linear and star-shaped PS-*b*-PGluNa copolymers used as emulsifiers in the heterophase polymerization of styrene.

chemical structure	entry	$x^{\#}$	z^{\S}	y^{\S}	$w_z^{\&}$
	SN1	52	104	1	0.74
	SN2	57	274	1	0.87
	SN3	63	176	8	0.78
	SN4	63	293	8	0.85

[#] Number-average degree of polymerization of PS. [§] Average number of GluNa repeating units. [§] Average number of PGluNa arms. [&] Weight fraction of GluNa in the copolymer.

Table 4-3. Characteristics of latexes obtained from aqueous heterophase polymerization of styrene at 80 °C in the presence of different amounts of linear and star-shaped PS-*b*-PGluNa emulsifiers (Table 4-2).

run	$c_{\text{stabilizer}}$ (wt %)	$d_h^{\#}$ (nm)	d_{core}^{\S} (nm)	l_{corona}^{\S} (nm)	PDI ^{&}	$E_{\text{stabilizer}}^*$ ($10^7 \text{ cm}^2 \text{ g}^{-1}$)
SN1/1	1.1	153	144	5	1.01	3.061
/2	3.1	116	79	19	1.03	2.377
/3	4.7	99	76	12	1.03	1.784
SN2/1	1.0	214	194	10	1.01	2.047
/2	3.1	141	121	10	1.02	1.649
/3	4.9	132	107	13	1.02	1.070

SN*1/1	1.0	131	125	3	1.16	4.178
/2	3.9	76	62	4	1.22	2.697
/3	4.9	74	68	3	1.23	1.901
SN*2/1	1.0	130	123	4	1.14	4.444
/2	3.0	91	61	(15)	1.18	2.779
/3	5.0	88	92	(-4)	1.15	1.128

[#] Hydrodynamic diameter of dispersed latex particles; DLS. [§] Weight-average diameter of dried particles with collapsed corona; TEM. [§] Thickness of PGluNa corona, $(d_h - d_{\text{core}})/2$. [&] Polydispersity index; TEM. ^{*} Stabilizer efficiency.

As expected,²⁰² the hydrodynamic diameter of particles decreases with increasing amount of stabilizer; this is true for both linear and star-shaped stabilizers. However, a clear difference between both types of stabilizers exists with respect to the average particle size, the width of the particle size distribution, and the thickness of the corona. In general, the linear block copolymers lead to significantly larger particles ($d_h = 100\text{-}220 \text{ nm}$) than the star-shaped ones

(70-130 nm), which is observed for both the hydrodynamic and the hard core diameter (d_{core} ; TRANSMISSION ELECTRON MICROSCOPY, TEM). The thickness of the PGluNa corona (l_{corona}) of linear and branched polypeptide chains is clearly different with 10-20 nm and 3-4 nm, respectively. Apparently, linear hydrophilic blocks are stretched out into the aqueous phase whereas branched polypeptide blocks form a much thinner but more compact corona.

As indicated by experimental data on the stabilizer efficiency (see Table 4-3), the star-shaped block copolymers are able to stabilize a considerably larger particle surface than their linear analogues. It is noteworthy that, on a weight base, the efficiencies obtained with PS-*b*-PGluNa copolymers are only by a factor of two lower compared to SDS ($\sim 6 \cdot 10^7 \text{ cm}^2 \text{ g}^{-1}$ at 1 wt % stabilizer based on monomer). The differences in stabilizing capacity and the possible occurrence of a second nucleation step in the course of polymerization, however, might be the reason for the different particle size distributions of the latexes (see Table 4-3). Apparently, the branched stabilizers are efficient enough to stabilize both newly formed particles and those of the older generation, especially at lower degrees of surface coverage, thus producing broadened or even bimodal particle size distributions ($\text{PDI} > 1.1$; see Figure 4-5) — this process is illustrated in Chart 4-2. In the case of the linear stabilizers, where such a stabilization is possible, both generations will coalesce and form a "mixed" generation with a monomodal or even narrow, almost monodisperse size distribution ($\text{PDI} < 1.04$).

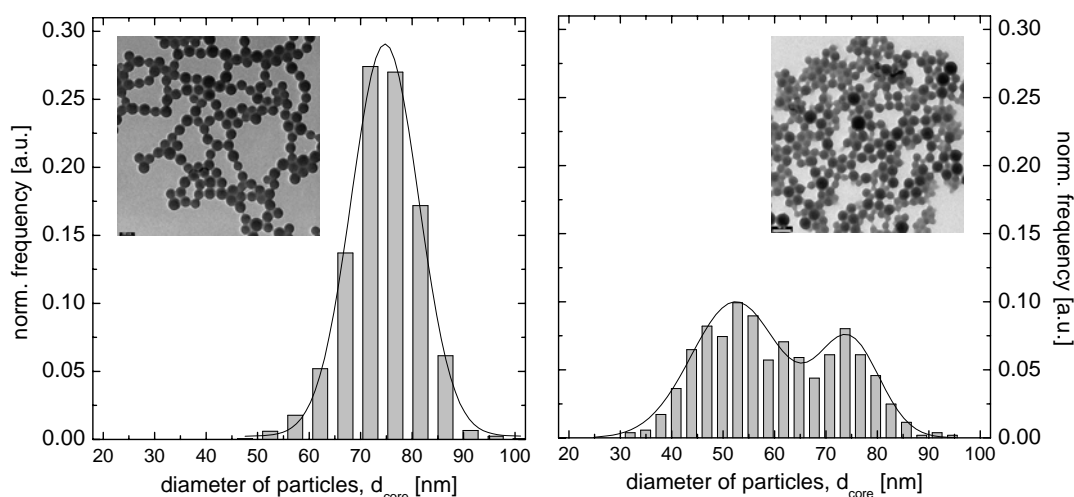


Figure 4-5. Particle size distributions of the latexes obtained in the presence of the linear PS-*b*-PGluNa stabilizer SN1 (run 3; left) and the branched analogue SN*1 (run 3; right). Insets show the corresponding TEM micrographs (scale bar = 100 nm) of the dried latex samples.

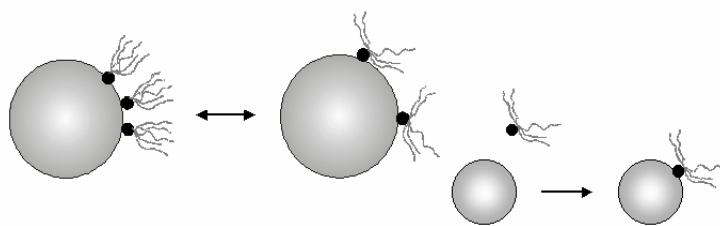


Chart 4-2. Schematic drawing of the adsorption of branched stabilizers onto a particle surface at high/low surface coverage and stabilization of secondary nucleated particles.

Another behavior of latexes which is strongly influenced by the kind of stabilizer and its arrangement is the stability against electrolytes. It was both theoretically predicted²¹⁷ and experimentally verified²¹³ that the critical coagulation concentration depends strongly on the thickness of the corona. For example, polystyrene latexes stabilized with SDS or PEE₄₄-*b*-PSS₄₄₈ (EE = ethyl ethylene, SS = styrene sulfonate) coagulate at 0.03 M and 6.0 M NaCl. The latex particles prepared with the PS-*b*-PGluNa stabilizers exhibit an intermediate ccc, which is about 1.0 M and 0.2 M for linear and star-shaped samples (normal saline: ~0.15 M NaCl). These data indicate that the linear block copolymers act as electrosteric stabilizers. However, even though the corona thickness is almost the same, the star-shaped stabilizers lead to a critical coagulation concentration, which is about one order of magnitude higher than that of SDS — this confirms expectations that branched polypeptide chains form a more dense and compact stabilizing layer than sulfonate headgroups.

The nature of the stabilizer not only determines the stability of colloidal particles but also its electrophoretic mobility. The mobility of charged colloidal particles in an electric field mainly depends on the charge density (ρ_{\pm}), effective particle size (d_{eff}), and electrolyte concentration in the continuous phase. Particles being electrosterically stabilized with for example PEE₄₄-*b*-PSS₄₄₈ ($d_h = 294$ nm, $\rho_{\pm} = 159$ $\mu\text{C cm}^{-2}$), exhibit a constant electrophoretic mobility of ~ 3.5 $\mu\text{m s}^{-1} \text{ cm V}^{-1}$ up to 0.1 M KCl. The mobility of particles is decreasing at higher KCl concentrations due to the shielding of charges.²¹⁸ The electrolyte concentration-dependent mobility of purely electrostatically stabilized particles, on the other hand, shows a maximum, and the maximum mobility (~ 6.5 $\mu\text{m s}^{-1} \text{ cm V}^{-1}$ for particles with $d_h = 31$ nm and $\rho_{\pm} = 6.1$ $\mu\text{C cm}^{-2}$) is considerably higher compared to electrosterically stabilized systems.²¹⁹ However, as can be seen in Figure 4-6 (left), particles with a branched PGluNa stabilizing layer exhibit the characteristics of electrosterically stabilized particles. The electrophoretic mobility is only slightly decreasing up to 1 mM KCl, whereas the decrease is much steeper at higher electrolyte concentrations.

As a matter of the pH-dependent degree of ionization of the PGlu segment ($pK_a \sim 4.3$), the electrophoretic mobility of particles is also affected by changes of pH (cf. Figure 4-6). In the pH range from 3.5 to 10.0, mobility is strongly increasing from pH 3.5 to ~ 6 and is almost constant at $pH > 6$. Since the size of particles (d_h) was found to remain constant within experimental errors, the strong increase in the mobility should be caused by an increasing charge density of the particles with increasing pH.

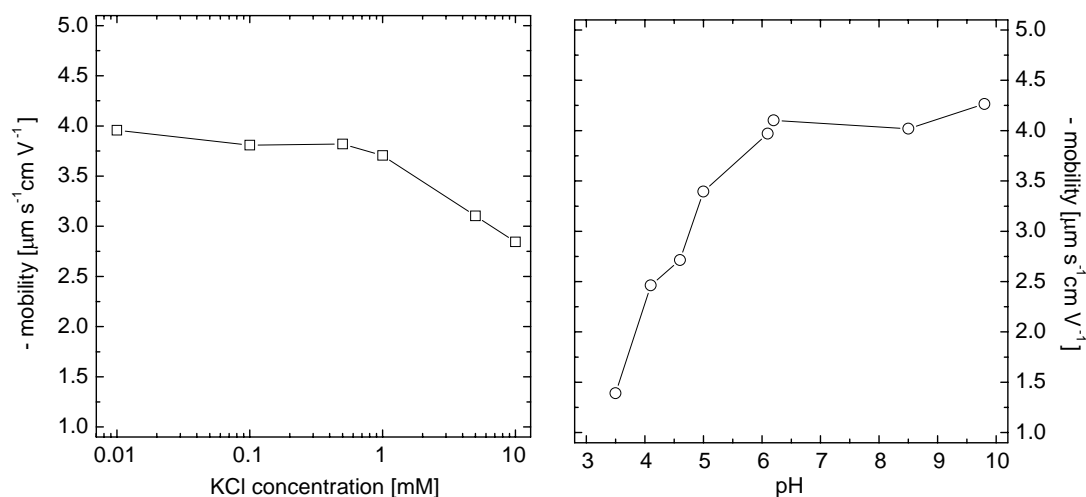


Figure 4-6. Dependence of the electrophoretic mobility of PS particles stabilized with the star-shaped PS-*b*-PGluNa (SN3, 1.0 wt %) on KCl concentration (left) and on pH (right).

4.3 Polypeptide-based drug carriers

Polymeric micelles with a typical size of 20-50 nm in diameter have been receiving much attention as colloidal carriers for the targeting of poorly water-soluble and amphiphilic drugs or genes.^{197,220-222} Polymeric micelles are one example of polymer-based pharmaceuticals or “polymer therapeutics”, i.e. rationally designed macromolecular drugs, polymer–drug and polymer–protein conjugates, polymeric micelles containing covalently bond drugs, and polyplexes for DNA delivery²²² (see the pioneering work of Ringsdorf et al.²²³). Most polymeric micelles in aqueous media are composed of amphiphilic block copolymers with a solvating poly(ethylene oxide) (PEO) shell, due to the good solubility of PEO in water and good biocompatibility.^{54,224-226} In addition, these micelles exhibit a unique disposition characteristics in the body.¹⁹⁷

Kataoka et al.^{194,195,227} examined very intensively PEO-PAsp (Asp = α,β -aspartic acid) block copolymer micelles as carriers for the anti-tumor agent *cis*-dichlorodiammineplatinum(II) (cisplatin, CDDP)^{228,229} (see the chemical structure in Chart 4-3). Note that the clinical use of CDDP has a limitation due to significant toxic side effects and short circulation periods in the blood.^{230,231} When solubilized within the polypeptide core of PEO-PAsp micelles, the chloride ligands of CDDP are substituted with the carboxylate residues of Asp, which are good leaving groups. Hence, this system promotes a sustained release of CDDP through ligand exchange reaction. In contrast, when the chloride ligands are substituted with amino acids containing S- or N-groups in the side chain, e.g. cysteine or lysine, the resultant complexes are too stable and eventually show no anti-tumor activity.²²⁷

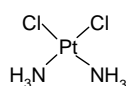
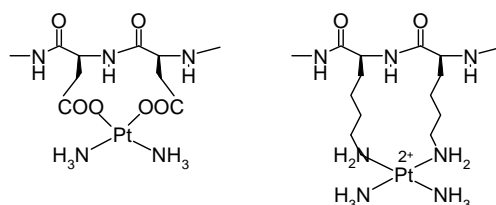


Chart 4-3. Structure of the square planar CDDP complex.

However, just the opposite was observed in the CDDP therapy of VX2 carcinomas, which is a model of the squamous cell carcinomas of the head and neck regions (HNSCC), spreading *via* the lymph node system.²³²

The drug–carrier systems used were CDDP-loaded micelles of PEO₁₁₄-*b*-PLGlu₃₀ (→ sample EG1, Table 2-11) and PEO₁₁₄-*b*-PLLys₄₀ (→ sample EL1, Table 2-11), which were prepared following a procedure described by Kataoka et al.²²⁷ Briefly, the solutions containing 100 mg polymer in 10 mL H₂O and 93.6 mg CDDP in 10 mL H₂O were combined and stirred for 2 days at 35 °C. Mixtures were then either ultrafiltrated (molecular weight cut-off: 1 kDa) or fil-

tered through a 0.2 μm Millipore filter to remove non-solubilized CDDP. As indicated by ATOMABSORPTION SPECTROSCOPY (Labor Rolf Sachse, Berlin, Germany), the samples contained 0.86-1.11 wt % Pt (EG1/CDDP) and 0.004-0.015 wt % Pt (EL1/CDDP). Evidently, despite of the fact that PLGlu should form less stable complexes with CDDP than PLLys (cf. Scheme 4-2), the loading capacity of EG1 micelles was two orders of magnitude higher than that of EL1 micelles.



Scheme 4-2. Tentative structure of the complexes of CDDP with LGlu (left) and LLys (right) amino acid residues.

Pre-clinical studies were carried out by Dr. A. Dünne and Prof. J. A. Werner (Klinikum der Universität Marburg, Germany) on the VX2 carcinoma of the New Zealand white rabbit. Note that carcinomas of rats spread *via* the blood vessel system, and are thus not suited as models for the lymphogenic metastasizing HNSCC. The protocol was as follows: Samples of cancer cells of the VX2 carcinoma were extracted from the thigh and injected into the ears of the rabbits;²³³ the first appearance of microtumors was observed after eight days. CDDP therapy was applied for 14-21 days, injecting 3×0.3 mL (series I) or 0.15 mL per day (series II) of the ~ 1 wt % aqueous solutions of EG1/CDDP (I) and EL1/CDDP (I+II) into the rabbits' ears.

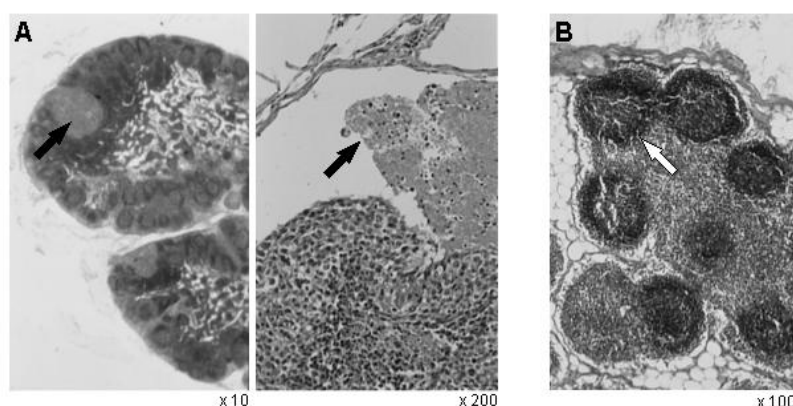


Figure 4-7. Histological cuts of the lymphatic tissue of New Zealand white rabbits before (A) and after (B) chemotherapy with CDDP (series I, see text). Lymph node: A/left and B; lymphatic vessel: A/right).

In the control experiment of series I, where no CDDP therapy had been applied, macroscopic metastasizing in the lymph nodes of the rabbit's ear could be observed. The histological cuts (see Figure 4-7/A) showed not only tumors in the first draining lymph nodes but also in the

afferent lymphatic vessels, which proofed the lymphogenic metastasizing of the VX2 carcinoma. On the other hand, those rabbits (12) that received chemotherapy with EG1/CDDP or EL1/CDDP were free of metastases. The histological cuts (cf. Figure 4-7/B) also revealed the presence of secondary follicles in the lymph nodes, which are the immuno response of B-lymphocytes to an antigene contact. In series II, applying a lower dose of the drug, nine out of ten rabbits had successfully been treated with EL1/CDDP.²³²

It is important to note that both CDDP–carrier systems gave the same positive results in the therapy of the VX2 carcinoma. However, the amount of platinum was substantially lower in EL1/CDDP than in the EG1/CDDP micelles (see above), which suggested a higher anti-tumor activity of the first system. This is a surprising result, at a first glance, as the drug was covalently trapped inside the EL1/CDDP micelles, thus avoiding a sustained release (see above). It is a working hypothesis that the targeting of drug-loaded micelles occurred by the “enhanced permeability and retention” (EPR) effect,^{234,235} i.e. the passive accumulation of high molecular-weight macromolecules (> 50 kDa) or micelles in tumor rather than normal tissue, as illustrated in Figure 4-8. The drug–carrier should be entering the tumor cells by endocytosis and be transferred to the lysosomes. Liberation of the drug should finally be accomplished by an enzymatic or acidic degradation of the polymer carrier within the lysosomes (“lysomotropic delivery”).²²²

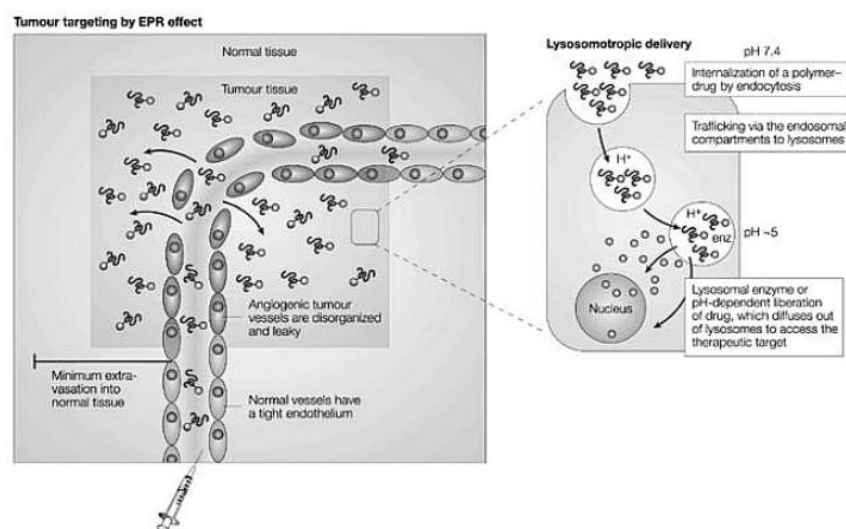


Figure 4-8. Passive targeting of long-circulating polymer therapeutics by the “enhanced permeability and retention” (EPR) effect and lysomotropic delivery of small molecule drugs (picture taken from ref. ²²²).

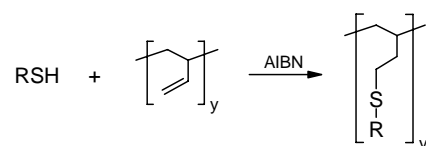
However, the true mechanism of drug targeting and delivery remains to be clarified. It is further planned to optimize the preparation of the PEO-*b*-PLLys/CDDP micelles and to enter the clinical stage of chemotherapy of the lymphogenic metastasizing HNSCC.

5 SUMMARY AND OUTLOOK

The main goal of this work was to examine the basic principles of self-organization of diblock copolymers having the inherent property of selective or specific non-covalent binding. By the introduction of electrostatic, dipole–dipole, or hydrogen bonding interactions, it was hoped to add complexity to the self-assembled mesostructures and to extend the level of ordering from the nanometer to a larger length scale. In some sense, this work may be seen in the framework of biomimetics, as it combines features of synthetic polymer and colloid chemistry with basic concepts of structure formation in supramolecular and biological systems.

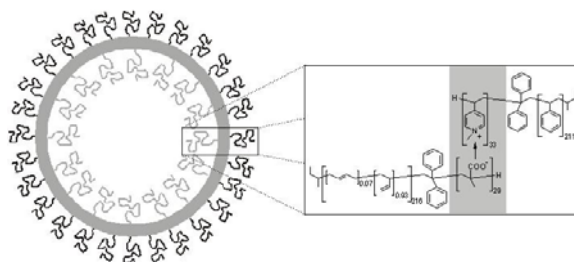
Focus in this work was put on linear diblock copolymers, which are the polymer amphiphiles with the most simple primary structure. Diblock copolymers can usually be produced in high quality with a reasonable expenditure of synthetic work and, very important for later systematic studies on phase behavior and structure formation as well as for applicational issues, appropriately characterized on a molecular level. The copolymer systems under study were (i) block ionomers, (ii) block copolymers with acetoacetoxy chelating units, and (iii) polypeptide block copolymers. Block ionomer samples could readily be prepared using standard recipes reported in the literature. For the synthesis of well-defined chelating and polypeptide block copolymers, on the other hand, development of new strategies and/or considerable improvements of established procedures were necessary. The same applied for the characterization of especially polypeptide-based copolymers, which in the past had not appropriately been addressed.

(i) Block ionomers were prepared by sequential anionic polymerization and subsequent modification of functional block segments. As an alternate route, the radical addition of ω -functional mercaptanes onto polybutadiene-based block copolymer has been described (chapter 2.1).

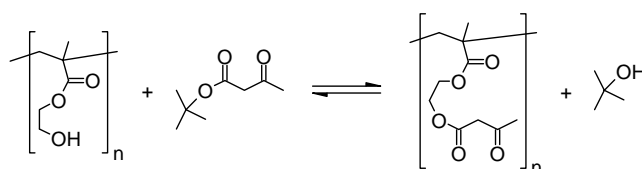


Mixing dilute THF solutions of oppositely charged block ionomers, polystyrene-*block*-poly(1-methyl-4-vinyl-pyridinium iodide) and poly(1,2-butadiene)-*block*-poly(cesium methacrylate), led to the spontaneous formation of a polyion complex, which self-assembled into vesicular aggregates. Due to a very high incompatibility of the solvating block segments, i.e. $\chi N \gg 10$, vesicles had a microphase-separated, asymmetric membrane and were thus amphiphilic in na-

ture. The structure of the membrane was subject to inversion upon application of an external stimulus like changing the selectivity of the solvent (chapter 3.1).

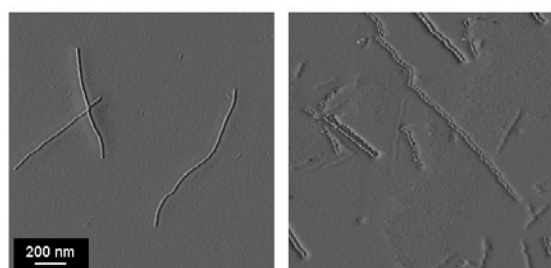


(ii) Well-defined block copolymers based on 2-(acetoacetoxy)ethyl methacrylate (AEMA) were prepared for the first time making use of RAFT radical polymerization or Group Transfer Polymerization (GTP) / azeotropic acetoacetylation (chapter 2.2).



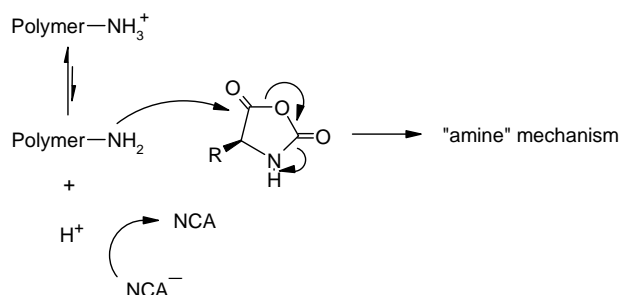
PBMA-*b*-PAEMA copolymers were found to exhibit the phase behavior of a (super) strongly segregated system ($\chi \sim 0.8$, $\chi N \sim 100$ at $N \sim 125$). The micellization behavior and appearance of spherical and cylindrical morphologies could appropriately be described on the basis of simple geometric considerations. Packing parameters for the reverse micelles in cyclohexane were calculated according to Antonietti–Förster model, taking additionally the aspect ratio of the insoluble monomer unit (AEMA) into consideration. Covered by this model, swelling of the PAEMA core was accompanied by a change of the shape of aggregates from spheres to cylinders to vesicles (chapter 3.2.1).

Promoted by hydrogen bridging interactions between adjacent acetoacetoxy units, PAEMA homopolymers produced large double-stranded superhelices in the solid state. Diameter and pitch of the helices were ~ 12 nm and 25 nm, respectively, and the persistence length was >300 nm. The helical superstructure was found to collapse within a few days at room temperature, dissociating into small globules of single polymer chains (chapter 3.2.2).

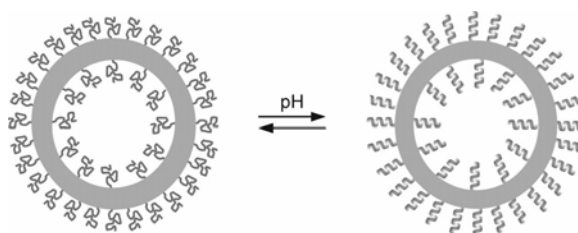


PAEMA-based block copolymers were further used for the fabrication of colloidal organic–inorganic hybrid materials and thin ordered films (chapter 4.1).

(iii) Polypeptide-based block copolymers were prepared by ring-opening polymerization of α -aminoacid-*N*-carboxyanhydrides (NCA) using ω -primary amino-functional macroinitiators. Advanced characterization with especially SIZE EXCLUSION CHROMATOGRAPHY (SEC-UV/RI method) showed that the samples produced by standard recipes had a broad molecular weight distribution with a polydispersity index PDI \sim 1.5. Screening of the free amine initiating/propagating species as hydrochlorides was found to promote a well-controlled polymerization of NCA, producing block copolymer samples with a nearly monodisperse distribution (PDI \sim 1.01) (chapter 2.3).

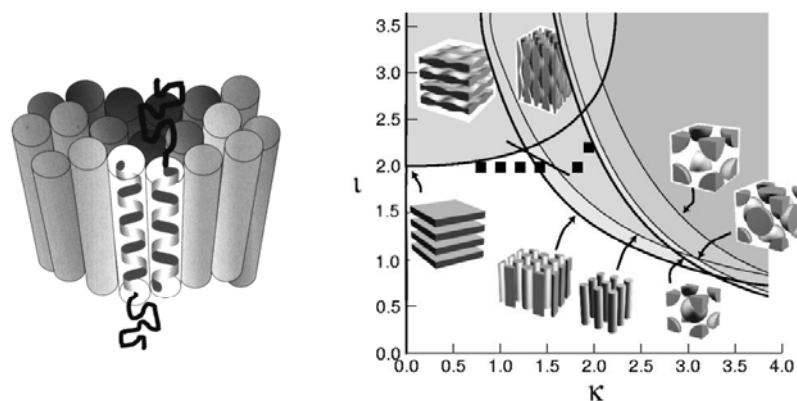


Depending on chemical composition, poly(1,2-butadiene)-*block*-(L-glutamate) copolymers self-assembled into spherical micelles (hydrodynamic radius, $R_h < 40$ nm) or vesicles ($R_h = 70$ –90 nm) in dilute aqueous NaCl solution. The conformation or secondary structure of the solvating polypeptide segments could be triggered *via* the pH of the solution, the coil–helix transition occurring at pH \sim 5. The dimension and morphology of the aggregates was, however, not affected by the change of conformation (chapter 3.3.1).

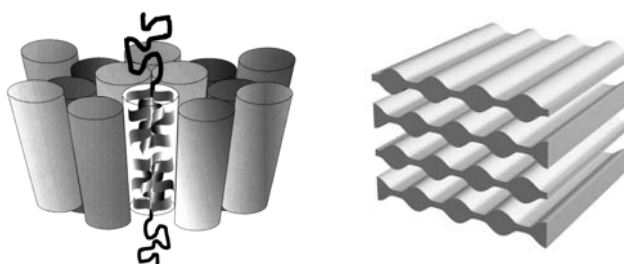


The solid films of linear polystyrene-*block*-poly(Z-L-lysine) (PS-*b*-PZLLys) coil-rod copolymers exhibited a *hexagonal-in-lamellar* morphology (intersheet spacing, $d = 12$ –35 nm) with high long-range order (persistence length: >1 μm). The preferential formation of this kind of morphology was attributed to the existence of strong dipole–dipole interactions and a hexagonal packing of the PZLLys α -helices within polypeptide layers. The average thickness of polypeptide layers was found to be linearly proportional to the number of PZLLys repeating

units, thus suggesting an orientation of helices perpendicular to the PS–PZLLys interface. The evaluation of SMALL-ANGLE X-RAY SCATTERING (SAXS) data with the *kappa-iota* formalism showed that the interface between the PS and PZLLys layers was not planar but considerably curved or undulated. Such undulations, i.e. statistical fluctuations in the thickness of the polypeptide layers, were produced in response to the chain length distribution of PZLLys helices. A detailed analysis of interface–curvature properties of structures obtained in dependence of the molecular weight distribution of copolymers supported the existence of a *hexagonal-in-zigzag lamellar* morphology (chapter 3.3.2.1).



Films of bottlebrush-shaped PS-*b*-PZLLys copolymers (AB_y) exhibited an *undulated lamellar* morphology ($d \sim 21$ nm, independent of composition). PZLLys chains were oriented parallel to the PS–PZLLys interface, thus stabilizing a larger surface area and producing disordered (super-)undulated lamellar structures. In one special case, the formation of a regular corrugated lamellar phase could be observed (chapter 3.3.2.2).



Linear and star-shaped polypeptide-based block copolymers were further used as stabilizers in the heterophase polymerization of styrene to produce electrosterically stabilized latexes with a polypeptide decoration. The colloidal properties of the latexes were found to depend vastly on the architecture of the block copolymer stabilizer. Branched copolymers yielded smaller latex particles with broader (bimodal) size distribution and a lower critical coagulation concentration (chapter 4.2).

Finally, poly(ethylene oxide)-*block*-poly(L-lysine) was successfully used as a carrier for *cis*-dichlorodiammineplatinum(II) (cisplatin) in the anti-cancer therapy of the lymphogenic metastasizing HNSCC (chapter 4.3).

The obvious next steps in the particular projects have already been mentioned in the previous chapters. These include establishment of the radical addition of mercaptanes onto unsaturated polymers as a general modular methodology for the production of well-defined functional block copolymers and systematic studies on the mechanism of NCA polymerization initiated by primary ammonium salts. The comprehensive characterization of polypeptide block copolymers will be further pursued. Also, work in the field of stimulus-responsive materials shall be intensified. It appears especially interesting, keeping in mind the results described in chapter 3.2.1, to make the insoluble core of aggregates responding to the external stimulus rather than the solvating corona; poly(1,2-butadiene)-*block*-(L-glutamate)s, for example, shall therefore be investigated in dilute organic solution. The studies on the aggregation behavior of polypeptide block copolymers shall also be extended to samples with bottlebrush architecture (“macro-tenside”).

Most emphasis will be on the exploitation of the modular concept of mixing strongly segregating diblock copolymers with complementary recognition sites. This concept has so far only been applied to oppositely charged block ionomers making use of electrostatic interactions. It is planned to employ diblock copolymer systems comprising hydrogen bonding or donor–acceptor interactions or stereocomplex formation motifs, to mention just a few. The attractiveness of this approach is seen in the possibility to access a library of complex superstructures and the simplicity of producing stimulus-responsive materials with tunable properties.

6 EXPERIMENTAL PROCEDURES AND METHODS

SYNTHESIS

A detailed description of synthetic procedures, if not included in the text, can be found in the PhD theses of Hildegard Kukula (University of Potsdam, 2001), Stefan Schrage (University of Potsdam, 2002), and Theodora Krasia (University of Potsdam, 2003).

ANALYTICS

ANALYTICAL ULTRACENTRIFUGATION. Measurements were performed on an Optima XL-I ultracentrifuge (Beckman-Coulter, Palo Alto, CA) with Rayleigh interference and UV/visible absorption optics. Sedimentation velocity experiments were done with 0.1-1.0 wt % polymer solutions at 25-40 °C and 60000 rpm. Time-dependent concentration profiles were evaluated with correction for diffusion broadening using the SEDFIT 5 software (Peter Schuck, Division of Bioengineering and Physical Science, National Institutes of Health, Bethesda, USA; <http://www.analyticalultracentrifugation.com/>).

ATOMIC FORCE MICROSCOPY. Measurements were performed with a Nanoscope Multimode IIIa (Digital instruments, Santa Barbara, CA) employing silicon cantilevers ($k = 42$ N/m; Olympus Optical Co. Ltd., Japan). Specimens were prepared by spin-coating of 0.1 wt % polymer solutions on a mica, silicon, or graphite substrate. Surfaces were scanned in the tapping mode at a resonance frequency of 250-300 kHz.

CIRCULAR DICHROISM SPECTROSCOPY. Spectra were recorded with a JASCO J 715 at 25 °C. Measurements were performed on ~0.1 wt % polymer solutions (solvent: THF, dioxane, or DMF) or on thin films, which were obtained by spin-coating of concentrated solutions on a quartz plate.

DENSITY OSCILLATION TUBE. Density measurements were performed on a density meter DMA 5000 (Anton Paar) at 25 °C. The specific density of the bulk polymer was extrapolated from the density data measured for ~1-5 wt % solutions of the polymer in an organic solvent.

DIELECTRIC RELAXATION SPECTROSCOPY. Measurements were performed in dry nitrogen between -140 and +60 °C and from 0.1 Hz to 10 MHz. The Novocontrol ALPHA frequency-response analyzer was used together with the QUATRO cryosystem. Data were recorded

as a function of frequency under nearly isothermal conditions ($\Delta T_{\max} = 0.25$ K) in steps of 10 K and 5 K below and above -10 °C, respectively.

DIFFERENTIAL SCANNING CALORIMETRY. Measurements were performed on a Netzsch DSC 200 at a heating/cooling rate of 10 K min^{-1} . Glass transition temperatures were determined from the inclination point of the second heating curve.

FOURIER-TRANSFORM INFRARED SPECTROSCOPY. Spectra of neat samples were recorded on a BioRad 6000 FT-IR being equipped with a Single Reflection Diamond ATR. For the analysis of chromatographic fractions, samples were sprayed onto a germanium disc using an LC 500 interface (Lab Connections, Inc., USA) and measured off-line on a commercial FT-IR instrument.

LIGHT SCATTERING. Static light scattering experiments (SLS) were carried out at 20 °C with a frequency-doubled Neodym-YAG laser light source (Coherent DPSS532, intensity: 300 mW, $\lambda = 532$ nm), an ALV goniometer, and an ALV-5000 multiple-tau digital correlator (ALV GmbH, Langen, Germany). Measurements were performed on 0.005-0.4 wt % polymer solutions at scattering angles from 15° - 150° at 3° intervals. Data were evaluated by a standard Zimm analysis. Refractive index increments (dn/dc) were measured on an NFT-Scanref differential refractometer operating at $\lambda = 633$ nm. Dynamic light scattering (DLS) experiments were carried out on a spectrometer consisting of an argon ion laser ($\lambda = 488 / 633$ nm, intensity: 30-600 mW; Coherent Innova 300), a self-constructed goniometer, a single-photon detector (ALV SO-SIPD), and a multiple-tau digital correlator (ALV-5000/FAST). DLS autocorrelation functions were measured at different polymer concentrations (0.005-0.4 wt %) and scattering angles (30° , 50° , 70° , and 90°). Autocorrelation functions were evaluated with the program FASTORT.EXE (Schnablegger, H.; Glatter, O. *Appl. Opt.* **1991**, *30*, 4889) to obtain diffusion coefficients, which then were transformed into hydrodynamic radii *via* the Stokes–Einstein equation.

LIQUID ADSORPTION CHROMATOGRAPHY AT CRITICAL CONDITIONS OF ADSORPTION. Measurements were done on a Hewlett Packard HPLC system (HP1090) using an Evaporative Light Scattering Detector (SEDEX 45, ERC) at 45 °C. The flow rate was 0.5 mL min^{-1} and 10 μL of about 1.5 wt % polymer solutions were injected. The eluent with the critical solvent composition for polystyrene at 45 °C was THF/*n*-hexane 60/40 (w/w), and the column used was a 250×4 mm SGX NH_2 (silica gel modified with aminopropyltriethoxysilane, Separon) with a 120 Å pore size and 7 μm average particle size.

MATRIX-ASSISTED LASER DESORPTION/IONIZATION TIME-OF-FLIGHT SPECTROMETRY. Mass spectra were recorded on a Bruker Reflex III or a Kratos MALDI 3 employing a nitrogen laser source ($\lambda = 337$ nm) in the reflectron or linear mode, respectively. Either 1,8-dihydroxy-9[10H]-anthracenone or 2,5-dihydroxy benzoic acid was used as the matrix and silver trifluoroacetate as the cation source. Bovine insulin was used to calibrate the equipment.

MEMBRANE OSMOMETRY. Measurements were done on a membrane osmometer Osmomat 90 (Gonotec GmbH, Berlin, Germany) using a membrane of regenerated cellulose (RC; molecular weight cut-off: 20 KDa). Series of measurements were performed on four 0.1-1.0 wt % polymer solutions in DMF at 20 °C.

NMR SPECTROSCOPY. ^1H and ^{13}C NMR spectra were recorded at 25 °C on a Bruker DPX-400 spectrometer operating at 400.1 MHz and 100.6 MHz, respectively. Signals were referenced to the characteristic signal arising from traces of protonated solvent.

SIZE EXCLUSION CHROMATOGRAPHY. Standard SEC analysis was performed on Thermo Separation Products set-ups being equipped with TSP UV1000 and Shodex RI-71 detectors. The eluents used were THF or CHCl_3 at 25 °C and a flow rate of 1.0 mL min^{-1} . 100 μL of about 0.15 wt % polymer solutions were injected. The column sets consisted of three 300 x 8 mm MZ-SD*plus* (spherical polystyrene gel with 5 μm average particle size) with a pore size of 10^3 , 10^5 , and 10^6 Å, respectively. Polystyrene, poly(1,2-butadiene), poly(*n*-butyl methacrylate), and poly(ethylene oxide) (Polymer Standards Service GmbH, Mainz, Germany) were used for calibration.

A third SEC set-up was equipped with TSP UV2000, Viscotek H502B on-line differential viscometer, and Shodex RI-71. DMA containing 0.5 wt % LiBr was used as the eluent at 70 °C and a flow rate of 0.7-1.0 mL min^{-1} . The column set consisted of four 300 x 8 mm PSS-GRAM (spherical polyester gel with 10 μm average particle size) with a pore size of 30, 30, 100, and 3000 Å, respectively. The standard and the universal calibration curve ($\log [\eta] \cdot M$ vs. elution volume) was recorded with polystyrene standards. Chromatograms were evaluated using the NTeqGPC V5.1.5 software package (hs GmbH, Ober-Hilbersheim, Germany).

SMALL-ANGLE NEUTRON SCATTERING. Measurements were performed at the facilities of the Hahn-Meitner-Institut (HMI, Berlin, Germany) and the Forschungszentrum Jülich (FRJ-2, Jülich, Germany). Exemplary, at the HMI, neutrons were derived from a liquid hydrogen

source cold source and monochromated by a mechanical velocity selector; the mean de Broglie wavelength was set to $\lambda = 0.60$ nm with a wavelength distribution of $\Delta\lambda/\lambda_0 = 0.1$. The 2D ^3He detector with 64×64 elements of 10×10 mm² was positioned at sample-to-detector distances of 1, 4, and 16 m. Quartz cells with a path length of 1 mm were used as sample containers which were inserted into aluminum sample holders. All measurements were carried out at 25 °C, and the scattered intensity was put on absolute scale by a calibration with the solvent.

SMALL-ANGLE X-RAY SCATTERING. SAXS curves were recorded on Kratky camera and rotating anode instruments with slit and pinhole collimation, respectively, at room temperature. Any of the set-ups was equipped with a Cu K $_{\alpha}$ X-ray radiation source ($\lambda = 0.15418$ nm). For the Kratky camera, which enabled the recording of data in the scattering vector range of $s = 2/\lambda \cdot \sin\theta = 0.03\text{-}0.95$ nm⁻¹ (2θ : scattering angle), a proportional counter (Anton Paar, Graz, Austria) was employed. With respect to the pinhole system, a Nonius rotating anode (4 kW, Cu K $_{\alpha}$) and an image-plate detector system were used. Placing the sample at a distance of 40-140 cm to the image plates made $s = 0.02\text{-}0.95$ nm⁻¹ available. Also, a Rigaku rotating anode (18 kW, Cu K $_{\alpha}$) with a two-dimensional detector (1024 \times 1024 pixels, Bruker) was employed (MPI-P, Mainz, Germany). The beam diameter was 0.5 mm and the sample to detector distance was 1.3 m. 2D diffraction patterns were transformed into an 1D radial average of the scattering intensity.

THERMOGRAVIMETRIC ANALYSIS. TGA was performed on a Netzsch TG 209 at a scanning rate of 20 K min⁻¹.

TRANSMISSION ELECTRON MICROSCOPY. Studies were performed with a Zeiss EM 912 Omega operating at 120 kV. Specimens were prepared by placing a drop of 0.01 wt % solutions onto a 400 mesh carbon-coated copper grid, the solvent was left to evaporate at room temperature. Polymer films were obtained by solvent-casting and were ultramicrotomed with a Leica Ultracut UCT. Specimens with a thickness of 30-50 nm were transferred onto carbon-coated copper grids and stained with OsO₄ (\rightarrow polybutadiene) or RuO₄ (\rightarrow polystyrene or polypeptides).

UV/VISIBLE SPECTROSCOPY. Spectra were recorded at room temperature on an UVIKON 940/941 dual-beam grating spectrophotometer (Kontron Instruments) using a quartz cell with 1 cm optical path length. Measurements were performed with 0.1-0.2 wt % polymer solutions in cyclohexane.

7 ACKNOWLEDGMENTS

This work would not have been possible without the help and contributions of many people. I would like to thank all of them...

The first places in a long list of names deserve my mentor Prof. Dr. Dr. Markus Antonietti, for providing a utmost stimulating atmosphere and environment during the last five years, and all former and current members of my working group: Dr. Hildegard Kukula, Dr. Stefan Schrage, Dr. Theodora Krasia, Dr. Ivaylo Dimitrov, Dr. Rémi Soula, Magdalena Łosik, Justyna Justynska, Marlies Gräwert, and Ines Below.

I am very grateful to Dr. habil. Helmut Cölfen for all the support he gave me in scientific as well as private life. I would like to thank Dr. Reinhard Sigel, Dr. Bernd Smarsly, Dr. sc. Klaus Tauer, and Dr. Hans G. Börner for the very fruitful collaborations and discussions.



Also many many thanks to Antje Völkel, Olaf Niemeyer, Dr. Charl F. Faul, Ingrid Zenke, Rona Pitschke, Birgit Schonert, Margit Barth, Carmen Remde, Dr. Jürgen Hartmann, Dr. Jan Rudloff, Dr. Marc Schneider, Anne Heilig, Dr. Hans-Peter Hentze, Dr. Katharina Landfester, Dr. Gudrun Rother, Dr. Inga Stapff, Heidemarie Zastrow, Cliff Janiszewski, and Annette Pape (MPI-KGF),...

... Dr. Jana Falkenhagen and Dr. Ralph-Peter Krüger (BAM, Berlin), Prof. Dr. Stephan Förster (Universität Hamburg), Dr. Astrid Brandt (HMI, Berlin), Anette Nordskog and Dr. Thomas Hellweg (TU Berlin), Prof. Dr. Tadeuz Pakula (MPI-P, Mainz), Dr. Christian Burger (City University of New York, USA), Dr. Dietmar Schwahn (FZ Jülich), Dr. Brigitte Tiersch and Dr. Peter Frübung (Universität Potsdam), Peter Kilz (PSS, Mainz), Dr. Anja Dünne and Prof. J. A. Werner (Klinikum der Universität Marburg), New Zealand white rabbits, ...

... Prof. Dr. Adi Eisenberg (McGill University, Montreal, Canada) and Prof. Dr. Krzysztof Matyjaszewski (Carnegie Mellon University, Pittsburgh, USA) for agreeing to referee this work, ...

... Prof. Dr. Axel H. E. Müller (Universität Bayreuth) for his continuing support, ...

... *Max-Planck-Gesellschaft* and *Deutsche Forschungsgemeinschaft* for funding, ...

... *Erich C.*  , and the coffee-producing industry, ...

... and finally, in love, Simone and Paula



8 REFERENCES

- (1) Lehn, J.-M. *Supramolecular Chemistry - Concepts and Perspectives*; VCH: Weinheim, 1995.
- (2) Elemans, J. A. A. W.; Rowan, A. E.; Nolte, R. J. M. *J. Mater. Chem.* **2003**, *13*, 2661.
- (3) Bates, F. S.; Fredrickson, G. H. *Physics Today* **1999**, *52*, 32.
- (4) Förster, S.; Plantenberg, T. *Angew. Chem. Int. Ed.* **2002**, *41*, 688.
- (5) Park, C.; Yoon, J.; Thomas, E. L. *Polymer* **2003**, *44*, 6725.
- (6) Bates, F. S.; Fredrickson, G. H. *Annu. Rev. Phys. Chem.* **1990**, *41*, 525.
- (7) Förster, S.; Antonietti, M. *Adv. Mater.* **1998**, *10*, 195.
- (8) Matsen, M. W.; Bates, F. S. *Macromolecules* **1996**, *29*, 1091.
- (9) Auschra, C.; Stadler, R. *Macromolecules* **1993**, *26*, 2171.
- (10) Goldacker, T.; Abetz, V.; Stadler, R.; Erukhimovich, I.; Leibler, L. *Nature* **1999**, *398*, 137.
- (11) Breiner, U.; Krappe, U.; Stadler, R. *Macromol. Rapid Commun.* **1996**, *17*, 567.
- (12) Lee, M.; Cho, B.-K.; Zin, W.-C. *Chem. Rev.* **2001**, *101*, 3869.
- (13) Chen, J. T.; Thomas, E. L.; Ober, C. K.; Hwang, S. S. *Macromolecules* **1995**, *28*, 1688.
- (14) Chen, J. T.; Thomas, E. L.; Ober, C. K.; Mao, G.-P. *Science* **1996**, *273*, 343.
- (15) Cornelissen, J. J. L. M.; Fischer, M.; Sommerdijk, N. A. J. M.; Nolte, R. J. M. *Science* **1998**, *280*, 1427.
- (16) Cornelissen, J. J. L. M.; Donners, J. J. J. M.; de Gelder, R.; Graswinckel, W. S.; Metselaar, G. A.; Rowan, A. E.; Sommerdijk, N. A. J. M.; Nolte, R. J. M. *Science* **2001**, *293*, 676.
- (17) Schlaad, H.; Antonietti, M. *Eur. Phys. J. E* **2003**, *10*, 17.
- (18) Eisenberg, A.; Kim, J.-S. *Introduction to Ionomers*; John Wiley & Sons: New York, 1998.
- (19) Nugay, N.; Hosotte, C.; Nugay, T.; Riess, G. *Eur. Polym. J.* **1994**, *30*, 1187.
- (20) Varshney, S. K.; Hautekeer, J. P.; Fayt, R.; Jérôme, R.; Teyssié, P. *Macromolecules* **1990**, *23*, 2618.
- (21) Feldthusen, J.; Ivan, B.; Müller, A. H. E. *Macromolecules* **1998**, *31*, 578.
- (22) Hsieh, H. L.; Quirk, R. P. *Anionic Polymerization: Principles and Practical Applications*; Marcel Dekker: New York, 1996.
- (23) Justynska, J.; Schlaad, H. *in preparation*.
- (24) Griesbaum, K. *Angew. Chem.-Int. Edit. Engl.* **1970**, *9*, 273.

- (25) Boutevin, G.; Ameduri, B.; Boutevin, B.; Joubert, J.-P. *J. Appl. Polym. Sci.* **2000**, *75*, 1655.
- (26) Romani, F.; Passaglia, E.; Aglietto, M.; Ruggeri, G. *Macromol. Chem. Phys.* **1999**, *200*, 524.
- (27) Förster, S.; Krämer, E. *Macromolecules* **1999**, *32*, 2783.
- (28) Quirk, R. P.; Ma, J.-J. *J. Polym. Sci., Part A: Polym. Chem.* **1988**, *26*, 2031.
- (29) Schlaad, H.; Kukula, H.; Rudloff, J.; Below, I. *Macromolecules* **2001**, *34*, 4302.
- (30) Kaliyappan, T.; Kannan, P. *Prog. Polym. Sci.* **2000**, *25*, 343.
- (31) Matyjaszewski, K.; Davis, T. P., Eds. *Handbook of Radical Polymerization*; Wiley-Interscience: Hoboken, 2002.
- (32) Krasia, T.; Soula, R.; Börner, H. G.; Schlaad, H. *Chem. Commun.* **2003**, 538.
- (33) Webster, O. W. *J. Polym. Sci., Part A: Polym. Chem.* **2000**, *38*, 2855.
- (34) Schlaad, H.; Krasia, T.; Patrickios, C. S. *Macromolecules* **2001**, *34*, 7585.
- (35) Matyjaszewski, K.; Xia, J. *Chem. Rev.* **2001**, *101*, 2921.
- (36) Xia, J.; Zhang, X.; Matyjaszewski, K. *Macromolecules* **1999**, *32*, 3531.
- (37) Chong, Y. K. B.; Le, T. P. T.; Moad, G.; Rizzardo, E.; Thang, S. H. *Macromolecules* **1999**, *32*, 2071.
- (38) Chiefari, J.; Chong, Y. K. B.; Ercole, F.; Krstina, J.; Jeffery, J.; Le, T. P. T.; Mayadunne, R. T. A.; Meijs, G. F.; Moad, C. L.; Moad, G.; Rizzardo, E.; Thang, S. H. *Macromolecules* **1998**, *31*, 5559.
- (39) Bovey, F. A. *High resolution NMR of macromolecules*; Academic Press: New York, 1972.
- (40) Costa, C. N.; Patrickios, C. S. *J. Polym. Sci., Part A: Polym. Chem.* **1999**, *37*, 1597.
- (41) Witzeman, J. S.; Nottingham, W. D. *J. Org. Chem.* **1991**, *56*, 1713.
- (42) Deming, T. J. *Adv. Mater.* **1997**, *9*, 299.
- (43) Gallot, B. *Prog. Polym. Sci.* **1996**, *21*, 1035.
- (44) Deming, T. J. *Nature* **1997**, *390*, 386.
- (45) Brzezinska, K. R.; Deming, T. J. *Macromolecules* **2001**, *34*, 4348.
- (46) Cosani, A.; Peggion, E.; Scoffone, E.; Verdini, A. S. *Makromol. Chem.* **1966**, *97*, 113.
- (47) Kukula, H.; Schlaad, H.; Falkenhagen, J.; Krüger, R.-P. *Macromolecules* **2002**, *35*, 7157.
- (48) Billot, J.-P.; Douy, A.; Gallot, B. *Makromol. Chem.* **1977**, *178*, 1641.
- (49) Douy, A.; Gallot, B. *Polymer* **1982**, *23*, 1039.
- (50) Billot, J.-P.; Douy, A.; Gallot, B. *Makromol. Chem.* **1976**, *177*, 1889.

- (51) Dimitrov, I.; Kukula, H.; Cölfen, H.; Schlaad, H. *Macromol. Symp.* **2004** (to be published).
- (52) Dimitrov, I.; Schlaad, H. *Chem. Commun.* **2003**, 2944.
- (53) Soula, R.; Dimitrov, I.; Schlaad, H. *in preparation*.
- (54) Zalipski, S. *Bioconjugate Chem.* **1995**, *6*, 150.
- (55) Sugimoto, H.; Saika, M.; Hosokawa, Y.; Aida, T.; Inoue, S. *Macromolecules* **1996**, *29*, 3359.
- (56) Eßwein, B.; Möller, M. *Angew. Chem.* **1996**, *108*, 703.
- (57) Eßwein, B.; Steidl, N. M.; Möller, M. *Macromol. Rapid Commun.* **1996**, *17*, 143.
- (58) Leito, I.; Rodima, T.; Koppel, I. A.; Schwesinger, R.; Vlasov, V. M. *J. Org. Chem.* **1997**, *62*, 8479.
- (59) Nagasaki, Y.; Iijima, M.; Kato, M.; Kataoka, K. *Bioconjugate Chem.* **1995**, *6*, 702.
- (60) Cammas, S.; Nagasaki, Y.; Kataoka, K. *Bioconjugate Chem.* **1995**, *6*, 226.
- (61) Bahr, U.; Deppe, A.; Karas, M.; Hillenkamp, F.; Giessmann, U. *Anal. Chem.* **1992**, *64*, 2866.
- (62) Kricheldorf, H. R. *Alpha-Aminoacid-N-Carboxyanhydrides and Related Heterocycles*; Springer: Berlin, 1987.
- (63) Abhimanyu, O. P.; Schulz, D. N.; Novac, B. M., Eds. *Functional Polymers: Modern Synthetic Methods and Novel Structures*; ACS: Washington DC, USA, 1998.
- (64) Hirao, A.; Hayashi, M. *Acta Polym.* **1999**, *50*, 219.
- (65) Hong, K.; Uhrig, D.; Mays, J. M. *Curr. Opin. in Solid State and Materials Science* **1999**, *4*, 531.
- (66) Quirk, R. P.; Yoo, T.; Lee, Y.; Kim, J.; Lee, B. *Adv. Polym. Sci.* **2000**, *153*, 67.
- (67) Jagur-Grodzinski, J. *Reactive & Functional Polymers* **2001**, *49*, 1.
- (68) Quirk, R. P.; Lynch, T. *Macromolecules* **1993**, *26*, 1206.
- (69) Ueda, K.; Hirao, A.; Nakahama, S. *Macromolecules* **1990**, *23*, 939.
- (70) Peters, M. A.; Belu, A. M.; Linton, R. W.; Dupray, L.; Meyer, T. J.; DeSimone, J. M. *J. Am. Chem. Soc.* **1995**, *117*, 3380.
- (71) Bestmann, H. J.; Wölfel, G. *Chem. Ber.* **1984**, *117*, 1250.
- (72) Pasch, H.; Trathnigg, B. *HPLC of Polymers*; Springer: Heidelberg, 1997.
- (73) Suzuki, K.; Hirao, A.; Nakahama, S. *Makromol. Chem.* **1989**, *199*, 2893.
- (74) Daly, W. H.; Poché, D. S. *Tetrahedron Lett.* **1988**, *29*, 5859.
- (75) Hol, W. G. J.; Vanduijnen, P. T.; Berendsen, H. J. C. *Nature* **1978**, *273*, 443.

- (76) Somsen, G. W.; Visser, T. In *Encyclopedia of Analytical Chemistry*; Meyers, R. A., Ed.; John Wiley & Sons: Chichester, 2001.
- (77) Elliot, A. *Proc. Royal Soc. London A* **1954**, *221*, 104.
- (78) Blout, E. R.; Asadourian, A. *J. Am. Chem. Soc.* **1956**, *78*, 955.
- (79) Kilz, P.; Pasch, H. In *Encyclopedia of Analytical Chemistry*; Meyers, R. A., Ed.; John Wiley & Sons: Chichester, 2000; p 7495.
- (80) Kilz, P. In *Encyclopedia of Chromatography*; Cazes, J., Ed.; Marcel Dekker: New York, 2001; pp 195.
- (81) Grubisic, Z.; Rempp, P.; Benoit, H. *J. Polym. Sci.* **1967**, *B5*.
- (82) Mori, S.; Barth, H. G. *Size exclusion chromatography*; Springer: Berlin Heidelberg, 1999.
- (83) Yau, W. W. *Chemtracts, Macromol. Chem.* **1990**, *1*, 1.
- (84) Schlaad, H.; Kilz, P. *Anal. Chem.* **2003**, *75*, 1548.
- (85) Ovsianikova, L. A.; Rudkovskaya, G. D.; Vlasov, G. P. *Makromol. Chem.* **1986**, *187*, 2351.
- (86) Janssen, K.; van Beylen, M.; Samyn, C.; Scherrenberg, R.; Reynaers, H. *Makromol. Chem.* **1990**, *191*, 2777.
- (87) Yoda, R.; Hiorkawa, Y.; Hayashi, T. *Eur. Polym. J.* **1994**, *30*, 1397.
- (88) Harada, A.; Kataoka, K. *Macromolecules* **1995**, *28*, 5294.
- (89) Klok, H.-A.; Langenwalter, J. F.; Lecommandoux, S. *Macromolecules* **2000**, *33*, 7819.
- (90) Klok, H.-A.; Hernández, J. R.; Becker, S.; Müllen, K. *J. Polym. Sci, Part A: Polym. Chem.* **2001**, *39*, 1572.
- (91) Poché, D. S.; Moore, M. J.; Bowles, J. L. *Synth. Commun.* **1999**, *29*, 843.
- (92) Deming, T. J.; Curtin, S. A. *J. Am. Chem. Soc.* **2000**, *122*, 5710.
- (93) Knobler, Y.; Bittner, S.; Frankel, M. *J. Chem. Soc.* **1964**, 3941.
- (94) Knobler, Y.; Bittner, S.; Virov, D.; Frankel, M. *J. Chem. Soc.* **1969**, 1821.
- (95) Harada, A.; Kataoka, K. *J. Macromol. Sci.-Pure Appl. Chem.* **1997**, *A34*, 2119.
- (96) Harada, A.; Kataoka, K. *Science* **1999**, *283*, 65.
- (97) Erhardt, R.; Böker, A.; Zettl, H.; Kaya, H.; Pyckhout-Hintzen, W.; Krausch, G.; Abetz, V.; Müller, A. H. E. *Macromolecules* **2001**, *34*, 1069.
- (98) Xu, H.; Erhardt, R.; Abetz, V.; Müller, A. H. E.; Goedel, W. A. *Langmuir* **2001**, *17*, 6787.
- (99) Erhardt, R.; Zhang, M. F.; Böker, A.; Zettl, H.; Abetz, C.; Frederik, P.; Krausch, G.; Abetz, V.; Müller, A. H. E. *J. Am. Chem. Soc.* **2003**, *125*, 3260.

- (100) Luo, L.; Eisenberg, A. *Angew. Chem.* **2002**, *114*, 1043.
- (101) Stoenescu, R.; Meier, W. *Chem. Commun.* **2002**, 3016.
- (102) Orwoll, R. A. In *Polymer Handbook*, 3 ed.; Brandrup, J.; Immergut, E. H., Eds.; Wiley-Interscience: New York, 1989; p VII/517.
- (103) Schrage, S.; University of Potsdam: Potsdam, 2002.
- (104) Schrage, S.; Sigel, R.; Schlaad, H. *Macromolecules* **2003**, *36*, 1417.
- (105) Desjardins, A.; Eisenberg, A. *Macromolecules* **1991**, *24*, 5779.
- (106) Desjardins, A.; van de Ven, T. G. M.; Eisenberg, A. *Macromolecules* **1992**, *25*, 2412.
- (107) Förster, S.; Zisenis, M.; Wenz, E.; Antonietti, M. *J. Chem. Phys.* **1996**, *104*, 9956.
- (108) Provencher, S. W. *Computer Phys. Commun.* **1982**, *27*, 229.
- (109) Cölfen, H.; Pauck, T. *Colloid Polym. Sci.* **1997**, *275*, 175.
- (110) Förster, S.; Burger, C. *Macromolecules* **1998**, *31*, 879.
- (111) Kukula, H.; Schlaad, H.; Antonietti, M.; Förster, S. *J. Am. Chem. Soc.* **2002**, *124*, 1658.
- (112) Mehrotra, R. C.; Bohra, B.; Gaur, D. P. *Metal β -Diketonates and Allied Derivatives*; Academic Press: New York, 1978.
- (113) Jeffrey, G. A. *An Introduction to Hydrogen Bonding*; Oxford University Press: New York, 1997.
- (114) Jeffrey, G. A.; Saenger, W. *Hydrogen Bonding in Biological Structures*; Springer: Berlin, 1994.
- (115) Schlaad, H.; Krasia, T.; Antonietti, M. *in preparation*.
- (116) van Ekenstein, G. O. R. A.; Meyboom, R.; ten Brinke, G.; Ikkala, O. *Macromolecules* **2000**, *33*, 3752.
- (117) Xu, R.; Winnik, M. A.; Riess, G.; Chu, B.; Croucher, M. D. *Macromolecules* **1992**, *25*, 644.
- (118) Nyrkova, I. A.; Khokhlov, A. R.; Doi, M. *Macromolecules* **1993**, *26*, 26.
- (119) Krasia, T.; Sigel, R.; Schlaad, H.; Antonietti, M. *in preparation*.
- (120) Burchard, W. In *Advances in Polymer Science*; Gordon, M., Ed.; Springer: Berlin, 1983; Vol. 48, pp 1.
- (121) Krasia, T.; University of Potsdam: Potsdam, 2003.
- (122) Antonietti, M.; Heinz, S.; Schmidt, M.; Rosenauer, C. *Macromolecules* **1994**, *27*.
- (123) Zhulina, E. B.; Birshtein, T. M. *Vysokomol. Soedin.* **1985**, *27*, 511.
- (124) Qin, A.; Tian, M.; Ramireddy, C.; Webber, S. E.; Munk, P. *Macromolecules* **1994**, *27*, 120.
- (125) Israelachvili, J. N. *Intermolecular and Surface Forces*; Academic Press: London, 1985.

- (126) Hesse, M.; Meier, H.; Zeeh, B. *Spektroskopische Methoden in der organischen Chemie*; Thieme: Stuttgart, 1987.
- (127) Elias, H.-G. *Makromoleküle - Physikalische Strukturen und Eigenschaften*; VCH: Weinheim, 2001.
- (128) Stryer, L. *Biochemie*; Spektrum-der-Wissenschaft-Verlagsgesellschaft: Heidelberg, 1990.
- (129) Perly, B.; Douy, A.; Gallot, B. *C. R. Acad. Sci (Paris), Ser. C* **1974**, 279, 1109.
- (130) Perly, B.; Douy, A.; Gallot, B. *Makromol. Chem.* **1976**, 177, 2569.
- (131) Gervais, M.; Douy, A.; Gallot, B.; Erre, R. *Polymer* **1988**, 29, 1779.
- (132) Nakajima, A.; Hayashi, T.; Kugo, K.; Shinoda, K. *Macromolecules* **1979**, 12, 840.
- (133) Kugo, K.; Hayashi, T.; Nakajima, A. *Polym. J.* **1982**, 14, 391.
- (134) Hayashi, T.; Chen, G. W.; Nakajima, A. *Polym. J.* **1984**, 16, 739.
- (135) Lecommandoux, S.; Achard, M.-F.; Langenwalter, J. F.; Klok, H.-A. *Macromolecules* **2001**, 34, 9100.
- (136) Hayashi, T. In *Developments in block copolymers*; Goodman, I., Ed.; Elsevier Applied Science Publishers: London, 1985; pp 109.
- (137) Chécot, F.; Lecommandoux, S.; Gnanou, Y.; Klok, H.-A. *Angew. Chem. Int. Ed. Engl.* **2002**, 41, 1340.
- (138) Chécot, F.; Lecommandoux, S.; Klok, H.-A.; Gnanou, Y. *Eur. Phys. J. E* **2003**, 10, 25.
- (139) Schlaad, H.; Kukula, H.; Smarsly, B.; Antonietti, M.; Pakula, T. *Polymer* **2002**, 43, 5321.
- (140) Schlaad, H.; Smarsly, B.; Losik, M. *Macromolecules* **2004** (to be published).
- (141) Anwer, M. K.; Spatola, A. F. *Synthesis* **1980**, 929.
- (142) Förster, S.; Hermsdorf, N.; Leube, W.; Schnablegger, H.; Regenbrecht, M.; Akari, S.; Lindner, P.; Böttcher, C. *J. Phys. Chem. B* **1999**, 103, 6657.
- (143) Chou, P. Y.; Fasman, G. D. *Biochemistry* **1974**, 13, 222.
- (144) Greenfield, N.; Fasman, G. D. *Biochemistry* **1969**, 8, 4108.
- (145) Döbereiner, H.-G. *Curr. Opin. in Colloid and Interface Science* **2000**, 5, 256.
- (146) Discher, B. M.; Hammer, D. A.; Bates, F. S.; Discher, D. E. *Curr. Opin. in Colloid and Interface Science* **2000**, 5, 125.
- (147) Discher, D. E.; Eisenberg, A. *Science* **2002**, 297, 967.
- (148) Discher, B. M.; Won, Y.-Y.; Ege, D. S.; Lee, J. C.-M.; Bates, F. S.; Discher, D. E.; Hammer, D. A. *Science* **1999**, 284, 1143.
- (149) Kimura, S.; Kim, D.-H.; Sugiyama, J.; Imanishi, Y. *Langmuir* **1999**, 15, 4461.

- (150) Zhang, L. F.; Eisenberg, A. *Science* **1995**, *268*, 1728.
- (151) Yu, K.; Eisenberg, A. *Macromolecules* **1998**, *31*, 3509.
- (152) Regenbrecht, M.; Akari, S.; Förster, S.; Möhwald, H. *J. Phys. Chem. B* **1999**, *103*, 6669.
- (153) Shen, H. W.; Eisenberg, A. *J. Phys. Chem. B* **1999**, *103*, 9473.
- (154) Nardin, C.; Hirt, T.; Leukel, J.; Meier, W. *Langmuir* **2000**, *16*, 1035.
- (155) Maskos, M.; Harris, J. R. *Macromol. Rapid. Commun.* **2001**, *22*, 271.
- (156) Terreau, O.; Luo, L.; Eisenberg, A. *Langmuir* **2003**, *19*, 5601.
- (157) Ruland, W. *Colloid Polym. Sci.* **1977**, *255*, 417.
- (158) Micha, M. A.; Burger, C.; Antonietti, M. *Macromolecules* **1998**, *31*, 5930.
- (159) Smarsly, B.; Antonietti, M.; Wolff, T. *J. Chem. Phys.* **2002**, *116*, 2618.
- (160) Li, W.; Gersappe, D. *Macromolecules* **2001**, *34*, 6783.
- (161) Matsushita, Y.; Noro, A.; Iinuma, M.; Suzuki, J.; Ohtani, H.; Takano, A. *Macromolecules* **2003**, *36*, 8074.
- (162) Wintermantel, M.; Gerle, M.; Fischer, K.; Schmidt, M.; Wataoka, I.; Urakawa, H.; Kajiwara, K.; Tsukahara, Y. *Macromolecules* **1996**, *29*, 978.
- (163) Sheiko, S. S.; Gerle, M.; Fischer, K.; Schmidt, M.; Möller, M. *Langmuir* **1997**, *13*, 5368.
- (164) Terao, K.; Nakamura, Y.; Norisuye, T. *Macromolecules* **1999**, *32*, 711.
- (165) Antonietti, M.; Kaul, A.; Thünemann, A. *Langmuir* **1995**, *11*, 2633.
- (166) Antonietti, M.; Wenzel, A.; Thünemann, A. *Langmuir* **1996**, *12*, 2111.
- (167) Méring, J.; Techoubar, D. *J. Appl. Crystallogr.* **1968**, *1*, 153.
- (168) Perret, R.; Ruland, W. *J. Appl. Crystallogr.* **1970**, *3*, 525.
- (169) Torquato, S.; Lu, B. *Phys. Rev. E* **1993**, *47*.
- (170) Antonietti, M.; Wenz, E.; Bronstein, L.; Seregina, M. *Adv. Mater.* **1995**, *7*, 1000.
- (171) Antonietti, M.; Förster, S.; Hartmann, J.; Oestreich, S. *Macromolecules* **1996**, *29*, 3800.
- (172) Antonietti, M.; Förster, S.; Hartmann, J.; Oestreich, S.; Wenz, E. *Nachr. Chem. Tech. Lab.* **1996**, *44*, 579.
- (173) Antonietti, M.; Thünemann, A.; Wenz, E. *Coll. Polym. Sci.* **1996**, *274*, 795.
- (174) Seregina, M. V.; Bronstein, L. M.; Platonova, O. A.; Chernyshov, D. M.; Valetsky, P. M.; Hartmann, J.; Wenz, E.; Antonietti, M. *Chem. Mater.* **1997**, *9*, 923.
- (175) Platonova, O. A.; Bronstein, L. M.; Solodovnikov, S. P.; Yanovskaya, I. M.; Obolonkova, E. S.; Valetsky, P. M.; Wenz, E.; Antonietti, M. *Coll. Polym. Sci.* **1997**, *275*, 426.

- (176) Antonietti, M.; Förster, S.; Oestreich, S. *Macromol. Symp.* **1997**, *121*, 75.
- (177) Klingelhöfer, S.; Heitz, W.; Greiner, A.; Oestreich, S.; Förster, S.; Antonietti, M. *J. Am. Chem. Soc.* **1997**, *119*, 10116.
- (178) Breulmann, M.; Förster, S.; Antonietti, M. *Macromol. Chem. Phys.* **2000**, *201*, 204.
- (179) Steunou, N.; Förster, S.; Florian, P.; Sanchez, C.; Antonietti, M. *J. Mater. Chem.* **2002**, *12*, 3426.
- (180) Spatz, J. P.; Sheiko, S.; Möller, M. *Adv. Mater.* **1996**, *8*, 513.
- (181) Spatz, J. P.; Mossmer, S.; Möller, M. *Chem. Eur. J.* **1996**, *2*, 1552.
- (182) Selvan, S. T.; Spatz, J. P.; Klok, H. A.; Möller, M. *Adv. Mater.* **1998**, *10*, 132.
- (183) Spatz, J. P.; Herzog, T.; Mossmer, S.; Ziemann, P.; Möller, M. *Adv. Mater.* **1999**, *11*, 149.
- (184) Spatz, J. P.; Mossmer, S.; Hartmann, C.; Möller, M.; Herzog, T.; Krieger, M.; Boyen, H. G.; Ziemann, P.; Kabius, B. *Langmuir* **2000**, *16*, 407.
- (185) Mossmer, S.; Spatz, J. P.; Möller, M.; Aberle, T.; Schmidt, J.; Burchard, W. *Macromolecules* **2000**, *33*, 4791.
- (186) Kastle, G.; Boyen, H. G.; Weigl, F.; Ziemann, P.; Riethmuller, S.; Hartmann, C. H.; Spatz, J. P.; Möller, M.; Garnier, M. G.; Oelhafen, P. *Phase Transitions* **2003**, *76*, 307.
- (187) Boyen, H. G.; Kastle, G.; Zurn, K.; Herzog, T.; Weigl, F.; Ziemann, P.; Mayer, O.; Jerome, C.; Möller, M.; Spatz, J. P.; Garnier, M. G.; Oelhafen, P. *Adv. Func. Mater.* **2003**, *13*, 359.
- (188) Haupt, M.; Miller, S.; Glass, R.; Arnold, M.; Sauer, R.; Thonke, K.; Möller, M.; Spatz, J. P. *Adv. Mater.* **2003**, *15*, 829.
- (189) Moffitt, M.; McMahon, L.; Pessel, V.; Eisenberg, A. *Chem. Mater.* **1995**, *7*, 1185.
- (190) Moffitt, M.; Eisenberg, A. *Macromolecules* **1997**, *30*, 4363.
- (191) Moffitt, M.; Vali, H.; Eisenberg, A. *Chem. Mater.* **1998**, *10*, 1021.
- (192) Kukula, H.; Schlaad, H.; Tauer, K. *Macromolecules* **2002**, *35*, 2538.
- (193) Yang, L.; Alexandridis, P. *Curr. Opin. in Colloid and Interface Science* **2000**, *5*, 132.
- (194) Yokoyama, M.; Okano, T.; Sakurai, Y.; Suwa, S.; Kataoka, K. *J. Control. Release* **1996**, *39*, 351.
- (195) Nishiyama, N.; Kataoka, K. *J. Control. Release* **2001**, *74*, 83.
- (196) Nishiyama, N.; Kato, Y.; Sugiyama, Y.; Kataoka, K. *Pharmaceutical Research* **2001**, *18*, 1035.
- (197) Kataoka, K.; Harada, A.; Nagasaki, Y. *Adv. Drug Deliv. Rev.* **2001**, *47*, 113.
- (198) Lindberg, R. *Cancer* **1972**, *29*, 1446.

- (199) Werner, J. A. *Laryngorhinootol* **2001**, 80, 400.
- (200) Veeraraj, A.; Sami, P.; Raman, N. *Proc. Indian Acad. Sci. (Chem. Sci.)* **2000**, 112, 515.
- (201) Holleman, A. F.; Wiberg, E. *Lehrbuch der anorganischen Chemie*; de Gruyter: Berlin - New York, 1985.
- (202) Evans, D. F.; Wennerström, H. *The Colloidal Domain - Where Physics, Chemistry, Biology, and Technology Meet*; VCH: New York, 1994.
- (203) Mastroilli, P.; Nobile, C. F.; Suranna, G. P.; Taurino, M. R.; Latronico, M. *Inorg. Chim. Acta* **2002**, 335, 107.
- (204) Teyssié, P.; Smets, G. *Makromol. Chem.* **1958**, 26, 245.
- (205) De Wilde-Delvaux, M. C.; Teyssié, P. *Spectrochimica Acta* **1958**, 12, 280.
- (206) Corain, B.; Zecca, M.; Mastroilli, P.; Lora, S.; Palma, G. *Makromol. Chem., Rapid Commun.* **1993**, 14, 799.
- (207) Fitch, R. *Polymer Colloids - A Comprehensive Introduction*; Academic Press: London, 1997.
- (208) Tauer, K.; Kühn, I. In *Polymeric Dispersions: Principles and Applications*; Kluwer: Dordrecht, 1997; p 49.
- (209) Gilbert, R. G. *Emulsion Polymerization: A Mechanistic Approach*; Academic Press: London, 1995.
- (210) Piirma, I. In *Surfactant Science Series*; Dekker: New York, 1992; Vol. 42, p 17.
- (211) Leemans, L.; Fayt, R.; Teyssié, P.; de Jaeger, N. C. *Macromolecules* **1991**, 24, 5922.
- (212) Müller, H.; Leube, W.; Tauer, K.; Förster, S.; Antonietti, M. *Macromolecules* **1997**, 30, 2288.
- (213) Tauer, K.; Müller, H.; Rosengarten, L.; Riedelsberger, K. *Colloids Surf A: Physicochem. Eng. Aspects* **1999**, 153, 75.
- (214) Bouix, M.; Gouzi, J.; Charleux, B.; Vairon, J.-P.; Guinot, P. *Macromol. Rapid Commun.* **1998**, 19, 209.
- (215) Burguière, C.; Pascual, S.; Coutin, B.; Polton, A.; Tardi, M.; Charleux, B.; Matyjaszewski, K.; Vairon, J.-P. *Macromol. Symp.* **2000**, 150, 39.
- (216) Jaeger, W.; Wendler, U.; Lieske, A.; Bohrisch, J.; Wandrey, C. *Macromol. Symp.* **2000**, 161, 87.
- (217) Pincus, P. *Macromolecules* **1991**, 24, 2912.
- (218) Vorwerg, L.; Antonietti, M.; Tauer, K. *Coll. Surf. A: Physicochem. Eng. Aspects* **1999**, 150, 129.
- (219) Antonietti, M.; Vorwerg, L. *Coll. Polym. Sci.* **1997**, 275, 883.

- (220) Jones, M.-C.; Leroux, J.-C. *European Journal of Pharmaceutics and Biopharmaceutics* **1999**, *48*, 101.
- (221) Brigger, I.; Dubernet, C.; Couvreur, P. *Adv. Drug Deliv. Rev.* **2002**, *54*, 631.
- (222) Duncan, R. *Nature Reviews, Drug Discovery* **2003**, *2*, 347.
- (223) Gros, L.; Ringsdorf, H.; Schupp, H. *Angew. Chem.-Int. Ed. Engl.* **1981**, *20*, 305.
- (224) Allen, C.; Maysinger, D.; Eisenberg, A. *Colloids Surf. B: Biointerf.* **1999**, *16*, 3.
- (225) La, S. B.; Nagasaki, Y.; Kataoka, K. *ACS Symp. Ser.* **1997**, *680*, 99.
- (226) Greenwald, R. B.; Conover, C. D.; Choe, Y. H. *Therapeutic Drug Carrier Systems* **2000**, *17*, 101.
- (227) Nishiyama, N.; Yokoyama, M.; Aoyagi, T.; Okano, T.; Sakurai, Y.; Kataoka, K. *Langmuir* **1999**, *15*, 377.
- (228) Rosenberg, B.; VanCamp, L.; Trosko, J. E.; Mansour, V. H. *Nature* **1969**, *222*, 385.
- (229) Takahara, P. M.; Rosenzweig, A. C.; Frederick, C. A.; Lippard, S. J. *Nature* **1995**, *377*, 649.
- (230) Pinzani, V.; Bressolle, F.; Hang, I. J.; Galtier, M.; Blayac, J. P.; Balmes, P. *Cancer Chemother. Pharmacol.* **1994**, *35*, 1.
- (231) Leroy, A. F.; Lutz, R. J.; Dedrick, R. L.; Litterst, C. L.; Guarino, A. M. *Cancer Treatment Reports* **1979**, *63*, 59.
- (232) Kukula, H.; Schlaad, H.; Antonietti, M.; Dünne, A.; Werner, J. A. *unpublished results*.
- (233) Tanigawa, N.; Satomura, K.; Hikasa, Y.; Hashida, M.; Muranishi, S.; Sezaki, H. *Surgery* **1980**, *87*, 147.
- (234) Seymour, L. W.; Miyamoto, Y.; Maeda, H.; Brereton, M.; Strohalm, J.; Ulbrich, K.; Duncan, R. *Eur. J. Cancer* **1995**, *31A*, 766.
- (235) Noguchi, Y.; Wu, J.; Duncan, R.; Strohalm, J.; Ulbrich, K.; Akaike, T.; Maeda, H. *Jpn. J. Cancer Res.* **1998**, *89*, 307.

9 LIST OF PUBLICATIONS

In the following is given a list of publications in reverse chronological order, categorized in different subjects: polymer synthesis and characterization, block copolymer mesophases, heterophase polymerization, polymerization kinetics and mechanisms, reviews, and miscellaneous.

Polymer synthesis

- J. Justynska, H. Schlaad, in preparation.
MODULAR SYNTHESIS OF FUNCTIONAL BLOCK COPOLYMERS.
- R. Soula, I. Dimitrov, H. Schlaad, in preparation.
SYNTHESIS OF PRIMARY AMINO-ENDFUNCTIONALIZED POLYACRYLATES BY MEANS OF ANIONIC AND RAFT RADICAL POLYMERIZATION.
- I. Dimitrov, H. Schlaad, *Chem. Commun.* **2003** (23), 2944-2945.
SYNTHESIS OF NEARLY MONODISPERSE POLYSTYRENE-POLYPEPTIDE BLOCK COPOLYMERS VIA POLYMERISATION OF *N*-CARBOXYANHYDRIDES.
- T. Krasia, R. Soula, H. G. Börner, H. Schlaad, *Chem. Commun.* **2003** (4), 538-539.
CONTROLLED SYNTHESIS OF HOMOPOLYMERS AND BLOCK COPOLYMERS BASED ON 2-(ACETOACETOXY)ETHYL METHACRYLATE VIA RAFT RADICAL POLYMERIZATION.
- H. Kukula, H. Schlaad, J. Falkenhagen, R.-P. Krüger, *Macromolecules* **2002**, 35 (18), 7157-7160.
IMPROVED SYNTHESIS AND CHARACTERIZATION OF ω -PRIMARY AMINO-FUNCTIONAL POLYSTYRENES AND POLYDIENES.
- H. Schlaad, T. Krasia, C. S. Patrickios, *Macromolecules* **2001**, 34 (22), 7585-7588.
CONTROLLED SYNTHESIS OF COORDINATION BLOCK COPOLYMERS WITH β -DICARBONYL LIGATING SEGMENTS.
- H. Schlaad, H. Kukula, J. Rudloff, I. Below, *Macromolecules* **2001**, 34 (13), 4302-4304.
SYNTHESIS OF α,ω -HETEROBIFUNCTIONAL POLY(ETHYLENE GLYCOL)S BY METAL-FREE ANIONIC RING-OPENING POLYMERIZATION.
- H. Schlaad, B. Schmitt, A. H. E. Müller, *Angew. Chem.* **1998**, 110 (10), 1497-1499; *Angew. Chem. Int. Ed. Engl.* **1998**, 37 (10), 1389-1391.
LIVING AND CONTROLLED ANIONIC POLYMERIZATION OF METHACRYLATES AND ACRYLATES IN THE PRESENCE OF TETRAALKYLAMMONIUM HALIDE-ALKYLALUMINIUM COMPLEXES IN TOLUENE.
- H. Schlaad, B. Schmitt, A. H. E. Müller, S. Jüngling, H. Weiss, *Macromol. Symp.* **1998**, 132, 293-302.
NOVEL INITIATOR SYSTEMS FOR THE ANIONIC POLYMERIZATION OF ACRYLATES AND METHACRYLATES.

Polymer characterization

- H. Cölfen, A. Völkel, H. Schlaad, in preparation.
DETERMINATION OF ABSOLUTE MOLECULAR WEIGHT DISTRIBUTIONS OF SYNTHETIC POLYPEPTIDE-BASED DIBLOCK COPOLYMERS WITH ANALYTICAL ULTRACENTRIFUGATION.
- H. Schlaad, P. Kilz, *Anal. Chem.* **2003**, 75 (6), 1548-1551.
DETERMINATION OF MOLECULAR WEIGHT DISTRIBUTIONS OF DIBLOCK COPOLYMERS WITH CONVENTIONAL SIZE EXCLUSION CHROMATOGRAPHY.
- J. Spickermann, K. Martin, H. J. Räder, K. Müllen, H. Schlaad, A. H. E. Müller, R.-P. Krüger, *Eur. Mass Spectrom.* **1996**, 2 (2-3), 161-165.
QUANTITATIVE ANALYSIS OF BROAD MOLECULAR WEIGHT DISTRIBUTIONS OBTAINED BY MATRIX-ASSISTED LASER DESORPTION IONISATION-TIME-OF-FLIGHT MASS SPECTROMETRY.

Block copolymer mesophases

- T. Krasia, H. Schlaad, in preparation.
POLY[2-(ACETOACETOXY) ETHYL METHACRYLATE]-BASED HYBRID MICELLES.
- T. Krasia, H. Schlaad, M. Antonietti, in preparation.
SUPERHELICES OF POLY[2-(ACETOACETOXY)ETHYL METHACRYLATE].
- T. Krasia, R. Sigel, H. Schlaad, M. Antonietti, in preparation.
MICELLIZATION BEHAVIOR OF DIBLOCK COPOLYMERS BASED ON 2-(ACETOACETOXY)-ETHYL METHACRYLATE.
- H. Schlaad, B. Smarsly, M. Łosik, *Macromolecules* **2004** (to be published).
THE ROLE OF CHAIN LENGTH DISTRIBUTION IN THE FORMATION OF SOLID-STATE STRUCTURES OF POLYPEPTIDE-BASED ROD-COIL BLOCK COPOLYMERS.
- A. Nordskog, T. Fütterer, H. von Berlepsch, C. Böttcher, A. Heinemann, H. Schlaad, T. Hellweg, *Phys. Chem. Chem. Phys.* **2004** (to be published).
FORMATION OF MIXED MICELLES OF PB₄₀PEO₆₂ AND THE ANIONIC SURFACTANT SDS IN AQUEOUS SOLUTIONS.
- A. Nordskog, H. Egger, G. H. Findenegg, T. Hellweg, H. Schlaad, H. von Berlepsch, C. Böttcher, *Phys. Rev. E* **2003**, 68, 11406/1-14.
STRUCTURAL CHANGES OF POLY(BUTADIENE)-POLY(ETHYLENE OXIDE) DIBLOCK-COPOLYMER MICELLES INDUCED BY A CATIONIC SURFACTANT: SCATTERING AND CRYOGENIC TRANSMISSION ELECTRON MICROSCOPY STUDIES.
- A. Thomas, H. Schlaad, B. Smarsly, M. Antonietti, *Langmuir* **2003**, 19 (10), 4455-4459.
REPLICATION OF LYOTROPIC BLOCK COPOLYMER MESOPHASES INTO POROUS SILICA BY NANOCASTING: LEARNING ABOUT FINER DETAILS OF POLYMER SELF-ASSEMBLY.
- S. Schrage, R. Sigel, H. Schlaad, *Macromolecules* **2003**, 36 (5), 1417-1420.
FORMATION OF AMPHIPHILIC POLYION COMPLEX VESICLES FROM MIXTURES OF OPPOSITELY CHARGED BLOCK IONOMERS.

- H. Schlaad, H. Kukula, B. Smarsly, M. Antonietti, T. Pakula, *Polymer* **2002**, *43* (19), 5321-5328.
SOLID-STATE MORPHOLOGIES OF LINEAR AND BOTTLEBRUSH-SHAPED POLYSTYRENE-POLY(Z-L-LYSINE) BLOCK COPOLYMERS.
- H. Kukula, H. Schlaad, M. Antonietti, S. Förster, *J. Am. Chem. Soc.* **2002**, *124* (8), 1658-1663.
THE FORMATION OF POLYMER VESICLES OR 'PEPTOSOMES' BY POLYBUTADIENE-BLOCK-POLY(L-GLUTAMATE)S IN DILUTE AQUEOUS SOLUTION.

Heterophase Polymerization

- H. Kukula, H. Schlaad, K. Tauer, *Macromolecules* **2002**, *35* (7), 2538-2544.
LINEAR AND STAR-SHAPED POLYSTYRENE-BLOCK-POLY(SODIUM GLUTAMATE)S AS EMULSIFIERS IN THE HETEROPHASE POLYMERIZATION OF STYRENE.
- K. Tauer, A. Zimmermann, H. Schlaad, *Macromol. Chem. Phys.* **2002**, *203* (2), 319-327.
NEW REACTIVE BLOCK COPOLYMERS AS STABILIZERS IN EMULSION POLYMERIZATION.

Polymerization kinetics and mechanisms

- I. Dimitrov, H. Kukula, H. Cölfen, H. Schlaad, *Macromol. Symp.* **2004** (to be published)
ADVANCES IN THE SYNTHESIS AND CHARACTERIZATION OF POLYPEPTIDE-BASED HYBRID BLOCK COPOLYMERS.
- H. Schlaad, Y. Kwon, L. Sipos, R. Faust, B. Charleux, *Macromolecules* **2000**, *33* (22), 8225-8232.
DETERMINATION OF PROPAGATION RATE CONSTANTS IN CARBOCATIONIC POLYMERIZATION OF OLEFINS. 1. ISOBUTYLENE.
- H. Schlaad, Y. Kwon, R. Faust, H. Mayr, *Macromolecules* **2000**, *33* (3), 743-747.
KINETIC STUDY ON THE CAPPING REACTION OF LIVING POLYISOBUTYLENE WITH 1,1-DIARYLETHYLENES, 2. EFFECT OF CHAIN LENGTH.
- H. Schlaad, K. Erentova, R. Faust, B. Charleux, M. Moreau, J.-P. Vairon, H. Mayr, *Macromolecules* **1998**, *31* (25), 8058-8062.
KINETIC STUDY ON THE CAPPING REACTION OF LIVING POLYISOBUTYLENE WITH 1,1-DIPHENYLETHYLENE, 1. EFFECT OF TEMPERATURE AND COMPARISON TO THE MODEL COMPOUND 2-CHLORO-2,4,4-TRIMETHYLPENTANE.
- B. Schmitt, H. Schlaad, A. H. E. Müller, B. Mathiasch, S. Steiger, H. Weiss, *Macromolecules* **2000**, *33* (8), 2887-2893.
ANIONIC POLYMERIZATION OF (METH)ACRYLATES IN THE PRESENCE OF TETRAALKYL-AMMONIUM HALIDE-ALUMINUM ALKYL COMPLEXES IN TOLUENE, 2. NMR AND QUANTUM-CHEMICAL STUDY ON THE STRUCTURE OF ESTER ENOLATE COMPLEXES AS MODELS OF THE ACTIVE CENTER.

- B. Schmitt, H. Schlaad, A. H. E. Müller, B. Mathiasch, S. Steiger, H. Weiss, *Macromolecules* **1999**, *32* (25), 8340-8349.
NMR AND QUANTUM-CHEMICAL STUDY ON THE STRUCTURE OF ESTER ENOLATE-ALUMINIUM ALKYL COMPLEXES AS MODELS OF THE ACTIVE CENTER IN THE ANIONIC POLYMERIZATION OF METHACRYLATES IN TOLUENE.
- H. Schlaad, A. H. E. Müller, *Macromolecules* **1998**, *31* (21), 7127-7132.
ANIONIC POLYMERIZATION OF (METH)ACRYLATES IN THE PRESENCE OF TETRAALKYL-AMMONIUM HALIDE-ALUMINIUM ALKYL COMPLEXES IN TOLUENE, 1. KINETIC INVESTIGATIONS WITH METHYL METHACRYLATE.
- B. Schmitt, H. Schlaad, A. H. E. Müller, *Macromolecules* **1998**, *31* (6), 1705-1709.
MECHANISM OF ANIONIC POLYMERIZATION OF (METH)ACRYLATES IN THE PRESENCE OF ALUMINIUM ALKYL, 6. POLYMERIZATION OF PRIMARY AND TERTIARY ACRYLATES.
- H. Schlaad, B. Schmitt, A. H. E. Müller, S. Jüngling, H. Weiss, *Macromolecules* **1998**, *31* (3), 573-577.
MECHANISM OF ANIONIC POLYMERIZATION OF (METH)ACRYLATES IN THE PRESENCE OF ALUMINIUM ALKYL, 5. EFFECT OF LEWIS BASES ON KINETICS AND MOLECULAR WEIGHT DISTRIBUTIONS.
- H. Schlaad, A. H. E. Müller, *Polym. J.* **1996**, *28* (11), 954-959.
MECHANISM OF ANIONIC POLYMERIZATION OF (METH)ACRYLATES IN THE PRESENCE OF ALUMINIUM ALKYL, 4. FORMATION OF A CO-ORDINATIVE POLYMER NETWORK VIA THE LIVING ALUMINATE END GROUP.
- H. Schlaad, A. H. E. Müller, *Macromol. Symp.* **1996**, *107*, 163-176.
EFFECT OF BULKINESS AND LEWIS ACIDITY OF ALUMINIUM COMPOUNDS ON THE ANIONIC POLYMERIZATION OF METHYL METHACRYLATE IN THE PRESENCE OF ALUMINIUM ALKYL.
- H. Schlaad, A. H. E. Müller, H. Kolshorn, R.-P. Krüger, *Polym. Bull.* **1995**, *35* (1-2), 169-176.
MECHANISM OF ANIONIC POLYMERIZATION OF (METH)ACRYLATES IN THE PRESENCE OF ALUMINIUM ALKYL, 3. MALDI-TOF-MS STUDY ON THE VINYL KETONE FORMATION IN THE INITIATION STEP OF METHYL METHACRYLATE WITH *TERT*-BUTYL LITHIUM.
- H. Schlaad, A. H. E. Müller, *Macromol. Rapid Commun.* **1995**, *16* (6), 399-406.
MECHANISM OF ANIONIC POLYMERIZATION OF (METH)ACRYLATES IN THE PRESENCE OF ALUMINIUM ALKYL, 2. KINETIC INVESTIGATIONS WITH METHYL METHACRYLATE IN TOLUENE.
- H. Schlaad, A. H. E. Müller, *Macromol. Symp.* **1995**, *95*, 13-26.
MECHANISM OF ANIONIC POLYMERIZATION OF METHYL METHACRYLATE IN THE PRESENCE OF ALUMINIUM ALKYL.
- H. Schlaad, H. Kolshorn, A. H. E. Müller, *Macromol. Rapid Commun.* **1994**, *15* (6), 517-525.
MECHANISM OF ANIONIC POLYMERIZATION OF (METH)ACRYLATES IN THE PRESENCE OF ALUMINIUM ALKYL, 1. ¹³C NMR STUDIES OF MODEL COMPOUNDS IN TOLUENE.

Reviews

- H. Schlaad, M. Antonietti, *Eur. Phys. J. E* **2003**, *10* (1), 17-23.
BLOCK COPOLYMERS WITH AMINO ACID SEQUENCES: MOLECULAR CHIMERAS OF POLYPEPTIDES AND SYNTHETIC POLYMERS.
- R. Faust, H. Schlaad, in *Applied Polymer Science: 21st Century*, Elsevier Science: Amsterdam, The Netherlands, 2000, pp. 999-1020.
IONIC POLYMERIZATION.
- Y. C. Bae, S. Hadjikyriacou, H. Schlaad, R. Faust, in *Ionic Polymerizations and Related Processes*, NATO ASI Series E, Vol. 359, Kluwer Academic Publishers: Dordrecht, The Netherlands, 1999, pp. 61-73.
CATIONIC MACROMOLECULAR DESIGN USING NON(HOMO)POLYMERIZABLE MONOMERS.

Miscellaneous

- B. G. G. Lohmeijer, H. Schlaad, U. S. Schubert, *Macromol. Symp.* **2003**, *196*, 125-135.
SYNTHESIS AND THERMAL PROPERTIES OF DIBLOCK COPOLYMERS UTILIZING NON-COVALENT INTERACTIONS.
- C. Zhang, H. Schlaad, A. D. Schlüter, *J. Polym. Sci. Part A: Polym. Chem.* **2003**, *41*, 2879-2889.
SYNTHESIS OF AMPHIPHILIC POLY(PARA-PHENYLENE)S BY SUZUKI POLYCONDENSATION.
- S. Roehn, K.-H. Schlaad, H. Schlaad, *5 Programmiersprachen für den C64 genau erklärt*, Luther-Verlag: Gensingen, Germany, 1985.